ROMA TRE
UNIVERSITÀ DEGLI STUDI

SCUOLA DOTTORALE IN SCIENZE MATEMATICHE
E FISICHE

XXIV Ciclo

Multiscale Models in Condensed Matter

Matteo Paoluzzi

Advisor: Antonio DiCarlo

Ph. D. Director: Orlando Ragnisco

Contents

Introduction **4**

1 Inverse Transition **7**

1.1 Scale separation in thermodynamics 7

1.2 The Blume-Capel Model with disorder 15

1.3 Monte Carlo simulations 23

1.3.1 Numerical study of a first-order phase transition 32

1.3.2 Second-order phase transition 34

1.3.3 Thermodynamic first-order phase transition 41

1.3.4 Phase diagrams and inverse freezing 43

1.4 Nature of the SG phase. 48

1.4.1 Equivalence between the site and link overlap distributions . 50

1.4.2 Position Space Four-Spins Correlations 54

1.4.3 Order-parameter distributions across transitions 59

1.5 Conclusions 61

2 Secondary processes in structural glasses **63**

2.1 Structural glasses and time scales 64

2.1.1 A single time scale example: statics and dynamics 65

2.1.2 Multiscale dynamics in glassy systems 68

2.2 Mode coupling theory and $p-$spin models 73

2.2.1 MCT and Schematic Theory 74

2.2.2 The p-spin models 87

2.2.3 Numerical solution for MCT equations 98

2.3 An introduction to secondary processes 102

2.4 The leading spin model for secondary processes 104
2.4.1 Dynamics 108
2.5 Relation between relaxation times 114
2.6 Dynamic scaling equation near plateaus 118
2.7 Conclusions 122

3 Molecular Dynamics and Continuum Mechanics **123**
3.1 Statistical ensembles 124
3.1.1 Liouvillians in MD 133
3.2 Strain and stress 138
3.3 Andersen Dynamics 145
3.4 Parrinello-Rahman method 149
3.5 APR-based multiscale algorithm 152
3.6 Conclusions 157

Conclusions **158**

Acknowledgment **160**

Bibliography **161**

Introduction

Understanding complex, amorphous materials is a typical many-body problem. Statistical mechanics is the main tool which allows us to recover the macroscopic properties of a system starting from a microscopic description. In particular, the equilibrium properties of a system can be computed choosing a suitable model and applying the rules of statistical mechanics.

Moreover, while this approach works well to study a broad class of phenomena, such as the equilibrium properties of a gas or the critical behavior of a substance near a critical point, the situation becomes less clear if we want to study systems whose dynamics involves very many interacting degrees of freedom.

For this reasons it is necessary to develop analytical and numerical techniques able to tackle problems where dynamics evolves over different time scales. In the present work, I will study multiscale problems of three different kinds.

Multiscale Issues in Thermodynamics

The first chapter will present some results obtained studying the thermodynamical properties of a spin-glass model [1, 2, 3]: the Blume-Capel [4, 5] with quenched disorder (BC-random) [6]. BC-random is an Ising-like spin-glass model where the spin variable can take value $\{-1, 0, +1\}$. It is well known that, within the mean-field approximation, this model undergoes an inverse transition between a Spin Glass (SG) and a Paramagnetic (PM) phase [7].

An inverse transition is said to take place when the phase appearing at low temperature resembles a high-temperature phase. In the BC-random, varying the pressure and decreasing the temperature, the spin-glass phase melt into a paramagnet. The reason of this counter-intuitive phenomenon is that a phase

having normally higher entropic content happens to exist in very peculiar patterns, such that its entropy is actually lower than the entropy of the standard *most ordered* phase [8]. From coarse-grained point of view, we can have such kind of scenario if some degrees of freedom, in the low temperature phase, become "neutral".

Multiscale Issues in Dynamics

The second chapter is about secondary processes in glasses and glass formers. The glassy transition takes place when some degrees of freedom evolve over a time-scale much larger than the typical experimental time scale, while a bifurcation of microscopical time scales occurs [9]. In particular, I propose a mean-field theory [10] to describe a glass former which relaxes over three time-scale. I will investigate how dynamic processes active on well-separated time scales in glasses and viscous liquids interact with each other. This study will be done on a model displaying two time-scale bifurcations, once between the fast and the secondary relaxation, other between the secondary and the structural relaxation.

This model is a generalization of the $p-$spin model with quenched disorder [11, 12], which is know to reproduce all the basic features of structural glasses, while its dynamics above the mode coupling temperature is equivalent to the dynamics of schematic mode-coupling theories [13].

Coupling between Continuum Mechanics and Molecular Dynamics

In the third and last chapter, I will try to build a multiscale method for coupling atomistic an continuum degrees of freedom in the framework of molecular dynamics (MD), done in the [1, 2, 3]Andersen-Parrinello-Rahman way [14, 15, 16].

The APR method is based on an extended Lagrangian allowing the MD cell to change both volume and shape during the simulation, its dynamics being governed by an externally applied stress, as well as by the internal particle dynamics. Indeed, the APR formalism allows us to write the equations of motion of a microscopic system interacting with a deformation (tensorial) fields. I am interested in the dynamics of the deforming computational cell, wishing to identify it with a general body element of a Cauchy continuum. On this basis, I plan to construct atomistically informed approximations to a continuum by means of an array of

interacting APR-like cells.

Chapter 1

Inverse Transition

The first chapter of this work is about Inverse Transionts (ITs): a reversible thermodynamic transition occurring between two phases, e. g., solid and liquid, in inverse order with respect to standard transitions. IT can be thought as a multi-scale problem in thermodynamics: IT can take place if some "internal" degrees of freedom of the constituents give contribute to the thermodynamic properties of the system. The internal degrees of freedom are *active* or *inactive* in function of the external thermodynamic parameters.

In particular, I have numerically investigated, through Exchange Monte Carlo simulations, the statics of a spin-glass model, i. e., the Blume-Capel model with quenched disorder and nearest-neighbor, in three dimensions. The phase diagram of the model is characterized by spin-glass to paramagnet phase transitions of both first and second order in the thermodynamic sense. The results presented here have been partially published in [1, 3, 2].

1.1 Scale separation in thermodynamics

It is well know in thermodynamics that, when a first-order phase transition with latent heat and coexistent phases takes place, all the information about the order relationship between the two phases can be obtained from the study of the *Clausius-Clapeyron equation* (CC).

CC can be easily computed by minimizing the intensive Gibbs free-energy

$G(p,T)$ during the transition at the pressure p and temperature T. The Gibbs free energy $G(p,T)$ is the Legendre transform of the free energy $F(T,V)$ done respect to the volume V,

$$\begin{aligned} \tilde{V} &= V(p,T) \\ G(p,T) &= F(T,\tilde{V}) + p\tilde{V} \end{aligned} \tag{1.1}$$

V being the themodinamic variable conjugated to the pressure P.

If the coexistent phases are labelled by $i = 1,2$ and each one involves N_i particles such that $N_1 + N_2$ equals N, the given total number of particles, one has

$$\delta N = \delta(N_1 + N_2) = 0\,. \tag{1.2}$$

Introducing the fraction of particles α_i like

$$\begin{aligned} \alpha_1 &= \frac{N_1}{N} \equiv \alpha \\ \alpha_2 &= \frac{N_2}{N} = 1 - \alpha\,. \end{aligned} \tag{1.3}$$

From the macroscopical point of view the observables are the entropy S, the internal energy U, the volume V and the Gibbs free energy G. We can write the intensive thermodynamic quantities as:

$$\begin{aligned} s &= \frac{S(U,V)}{N} = \alpha s_1(u_1,v_1) + (1-\alpha)s_2(u_2,v_2) \\ u &= \frac{U(\alpha,u_1,u_2)}{N} = \alpha u_1 + (1-\alpha)u_2 \\ v &= \frac{V(\alpha,v_1,v_2)}{N} = \alpha v_1 + (1-\alpha)v_2 \\ g &= \frac{G(p,T)}{N} = \alpha g_1 + (1-\alpha)g_2\,. \end{aligned} \tag{1.4}$$

Imposing thermodynamic equilibrium reads

$$\begin{aligned} ds &= 0 = (s_1 - s_2)d\alpha + \alpha\frac{\partial s_1}{\partial u_1}du_1 + (1-\alpha)\frac{\partial s_2}{\partial u_2}du_2 + \alpha\frac{\partial s_1}{\partial v_1}dv_1 + (1-\alpha)\frac{\partial s_2}{\partial v_2}dv_2 \\ du &= 0 = (u_1 - u_2)d\alpha + \alpha du_1 + (1-\alpha)du_2 \\ dv &= 0 = (v_1 - v_2)d\alpha + \alpha du_1 + (1-\alpha)du_2\,. \end{aligned} \tag{1.5}$$

Through Maxwell relations,

$$\begin{aligned} \left.\frac{\partial s(u,v)}{\partial u}\right|_v &= \frac{1}{T} \\ \left.\frac{\partial s(u,v)}{\partial v}\right|_u &= \frac{p}{T} \end{aligned} \tag{1.6}$$

eqs. (1.1) lead to

$$\begin{aligned} g_1(p,T) &= g_2(p,T) \\ T_1 &= T_2 = T \\ p_1 &= p_2 = p\,. \end{aligned} \tag{1.7}$$

Differentianting $g(p,T)$ with respect to the natural variables (p,T) it follows (cf. 1.1)

$$dg = vdp - sdT \tag{1.8}$$

From the condition for $g_i(T,p)$ one has,

$$\left.\frac{dP}{dT}\right|_{Coex} = \frac{\Delta s}{\Delta v} = \frac{l}{T\Delta v} \tag{1.9}$$

where l is the transitional latent heat. If phase 1 is liquid and phase 2 is solid we can write

$$\left.\frac{dP}{dT}\right|_{Coex} = \frac{s_l - s_s}{v_l - v_s} \tag{1.10}$$

Indeed, the slope of (1.10) gives information about the order of the two coexisting phases. For example, it is known that an indication for the entropy of the superfluid phase in ^{4}He was found through CC equation [17]: since the slope of the CC curve between the solid phase and the superfluid phase is near by zero, the entropy of

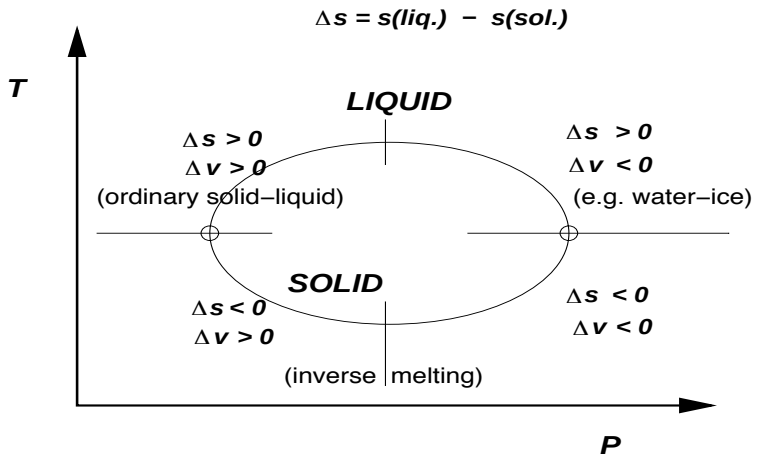

Figure 1.1: Schematic picture of the Clausius-Clapeyron classification of phase transitions.

the superfluid must be of the same order of magnitude that of the solid. This suggested to look for an ordering state in the superfluid phase.

We can classify phase transitions into four kinds (see fig. (1.1)):

1. Ordinary Type I

   At lower temperature there exists a solid phase less entropic and more dense than the liquid phase.

2. Ordinary Type II

   The solid is less entropic, but also less dense than the fluid: specific volume is in the inverted order (e. g., the water-ice transition).

3. Inverse Type I

   At lower temperature, there exists a phase whose symmetries are typical of a high-temperature phase (e. g., a putative cristalline solid that melts as temperature is decreased).

4. Inverse Type II

   The low temperature phase has the symmetry features and the density typical of high temperature phases.

Our attention will be focused on inverse transitions (IT) of type I. The IT is a reversible transformation occurring between phases with entropic contents and symmetries that are in inverse-order relation relative to standard transition. The case, already hypothesized by Tamman [18] more than a century ago, of "ordering in disorder" taking place in a crystal solid that liquefies on cooling is generally termed *inverse melting*. The IT phenomenon includes also the transformations involving amorphous solid —rather than crystal— phases similar to that of a liquid vitrifying upon heating. In this case, the term *inverse freezing* is sometimes used in the literature, when both phases are disordered but the fluid appears to have the least entropic content. The reason for these counterintuitive phenomena is that a phase, usually present only at high temperature, happens to exist also in peculiar patterns such that its entropy is actually less than that of the phase normally considered more ordered.

Inverse transition, in their most generic meaning, have been detected in recent years in a number of different materials and between phases of varied physical nature. The first example —and one of the most documented— is the transition between liquid and crystal phases of helium isotopes ^{3}He and ^{4}He at low temperatures [17]. The transition curve in ^{3}He starts in on 0.315 K at a pressure of 29.3 bar. The coexistence is between normal fluid, i. e., non-superfluid, and body-centered cubic crystal: since ^{3}He is a fermion, the origin of the IT is due to the interaction between spin degrees of freedom. Nuclear spins do not give contribute to the entropy of the liquid phase because they are strongly correlated and oriented. Otherwise, in the solid phase, the spins are relatively free to reorient increasing the entropy. IT takes place in ^{4}He between superfluid liquid and hexagonal-close-packed crystal. The system undergoes a the transition starting in on 0.8 K and 26.2 bar. ^{4}He has no nuclear spin: indeed the nature of the transition is rather different than IT in ^{3}He. In that case, IT is due to the phonon densities of states for the crystal and the liquid phase [19].

A more complex and recent example is the polymer poly(4−methylpentene−1) (P4MP1), in which a crystal polymer melts when the temperature is decreased or the pressure is increased (cfr. fig. (1.2)). By means of exhaustive measurements using differential scanning calorimetry (DSC) and X-ray diffraction, the phase diagram of P4MP1 has been experimentally determined by Rastogi *et al.* [20, 21]

and others [22], showing evidence for both an equilibrium inverse melting between a crystal phase (tetragonal or hexagonal, depending on the pressure) and a fluid phase, and a nonequilibrium IT between the hexagonal crystal and a glassy phase. Raughly speaking, IT in P4MP1 is due to the number of polymer conformations that decreases in the amorphous state.

Another extensively studied instance is a molecular solution in water, composed of $\alpha-$cyclodextrine (αCD) and 4$-$methylpyridine (4MP) mixed in given molecular ratios, investigated by means of neutron scattering, X-ray diffraction, DSC, and rheometric measuraments [23, 24, 25, 26, 27, 28, 29, 30, 31, 32]. The "solid" in this case is a sol-gel porous system formed by an ordered network of molecules of αCD-water-MP filled with liquid 4MP, melting for a decreasing temperature with a constant αCD concentration.

Another important polymeric example is a methyl-cellulose solution in water undergoing a reversible inverse sol-gel transition [33, 34]. Methyl-cellulose is a polymeric chain: it is a hydrophilic polymers containing a few hydrophobic units. The hydrophobic units can interact each other: in order to do it, the polymer must be in an unfolded configuration. From the interaction between hydrophobic units in aqueous media, the polymers can form a network and, consequently, a gel. It is well known [34] that the viscosity of a semi-diluite solution decreases increasing temperature: the system undergoes an IT between clear-gel and turbid-gel.

For such a system, a careful analysis of the behaviour of the microscopic components across the transition has been performed [35]. This turns out to be particularly important for my own modelling effort, as we shall see in the following.

Apart from polymeric and macromolecular substances, in recent years ITs have appeared in many different contexts. Inverse melting from an ordered lattice to a disordered vortex phase takes place, e.g., for the magnetic flux lines in high-temperature supercontuctor [36]. A gas of atoms at zero temperature changes from superfluid to insulator as the lattice potential depth is increased [37]. Furthemore, in the framework of nanosystems, the reversible transition of an isotropic liquid into an ordered cubic phase upon heating has been detected experimentally in ferromagnetic systems of gold nanoparticles [38, 39].

In this work, I stick to definition of IT put forward by Tammann [18]: a temper-

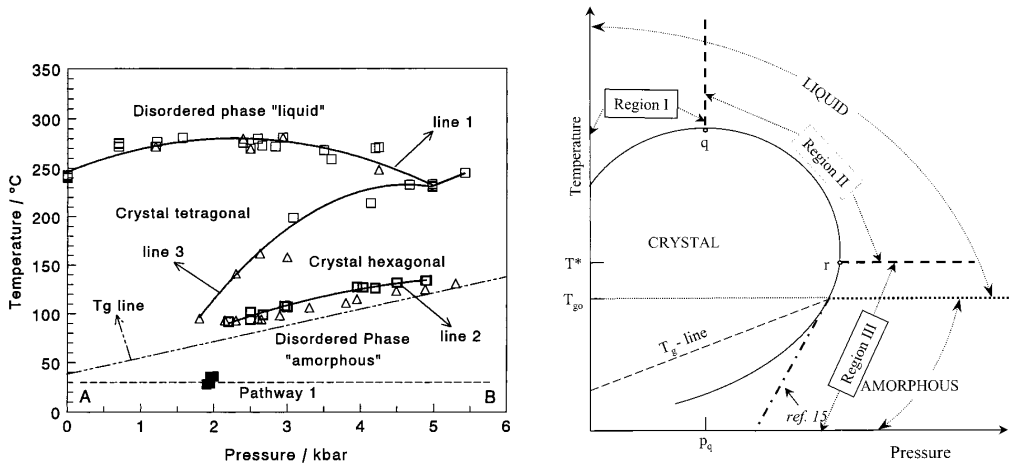

Figure 1.2: Phase diagram of P4MP1 from the original paper of Rastogi *et al.* [20]. Left panel: the phase diagram in the plane p-T obtained by DSC calorimetry. Righ panel: Simplified p-T phase diagram.

ature driven reversible transition at fixed pressure or, more generally, under fixed conditions controlling the interaction strength (such as concentration, chemical potential, or magnetic field) from a solid, high-temperature phase to an isotropic fluid (or a paramagnet, for magnetic systems), low-temperature phase. Generalizing to nonequilibrium systems, one might also call IT those transitions in which an isotropic fluid is dynamically arrested into a glassy state.

A thorough explanation of the fundamental mechanism leading to ITs would require a microscopic analysis of single components and their mutual interactions as temperature goes through the critical point. Due to the complexity of the structure of polymeric chains and macromolecules involved in such transformations, a clear-cut picture of the state of the each components is often not available. For the above-mentioned case of methyl-cellulose, Haque and Morris [35] proposed that chains exist in solution as folded bundles in which hydrophobic methyl groups are packed. As the temperature is raised, the bundles unfold, exposing methyl groups to water molecules and thus causing a large increase in volume and the formation of hydrophobic links, eventually leading to a gel. The polymers in the folded state are thus inactive (or far less active than those in the unfolded state) but are also less entropic than the unfoled ones. As the chains start to unfold because of the thermal noise, they change to an interacting state, thus enforcing bonds with other

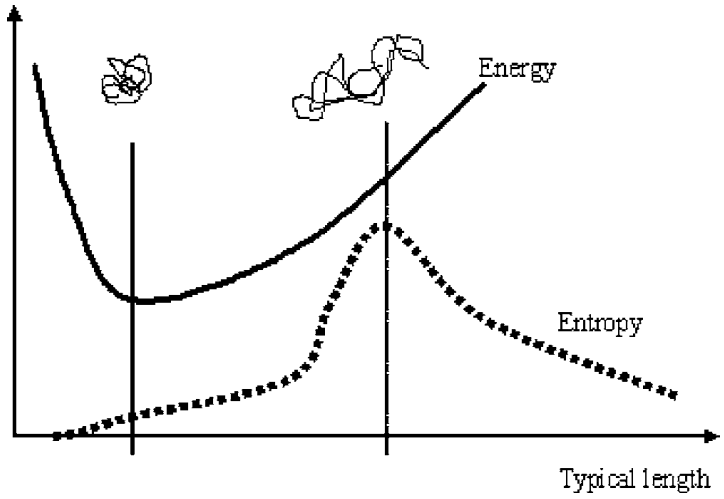

Figure 1.3: Schematic picture of the free-energy landscape of the methyl-cellulose[8, 40]. The unfolded configuration is more interacting and entropic than the folded one.

chains and condensing into a gel (fig.1.3).

Theoretical modelling for ITs is just starting to develop in often uncorrelated steps and consists, at best, in heuristic reproduction of the phenomenon [41, 42, 43, 19, 44, 45, 8, 40, 46, 47, 48, 49, 50]. Many mean field model exist [8, 40, 49, 48, 47]: all of these are lattice gas model with or without disorder. In finite-dimension it has observed an IT in the internally decorated version of the so-called Gaussian core model (CGM)[45]. CGM is a classical many-body model interacting through a pairwise additive Gaussian potential. The standard CGM does not display IT, moreover adding to the particles an internal degrees of freedom it is possible to obtain an IT scenario.

Looking, in particular, at the transition between an amorphous "frozen" phase and a fluid (i. e., paramagnet) phase, recent spin-glass models with spin-1 variables have turned out to effectively represent systems in which the transformation is driven by entropic effects. In these case, inverse freezing has been studied in the mean-field approximation.

In particular, we are interested in IT from the static point of view (i. e., within equilibrium thermodynamics). It is clear that a system can undergoes an IT if some degrees of freedom of the liquid phase (in the low-temperature phase) are

blocked. Indeed, the solid but disordered phase must have a configurational space larger than the configurational space of the liquid. This means that some scales are blocked in the ordered liquids therefore we can think of the statics of an IT like that of a multiscale problem. This point will be clarified in the last section of this chapter.

In the next sections I will describe the static properties of the Blume-Capel (BC) [5, 4] model. In particular, I have studied the thermodynamics of BC with random interactions (a model which will de defined in the next section) in three dimensions by means of a Monte-Carlo simulation.

1.2 The Blume-Capel Model with disorder

The BC model [5, 4] with quenched disorder is a spin-glass model on a three dimensional cubic lattice with bosonic spin-1 variables (i. e., a spin variable s_i can take the values ± 1 and 0). We assume that the interplay between inactive ($s_i = 0$) and interactive ($s_i = \pm 1$) states of a microscopic component is at the core of the hypothesized IT [8]. The random version of the BC model was introduced by Ghatak and Sherrington [6] in order to study the effects of the crystal field in a spin-glass, e. g., $(Ti_{1-x}V_x)O_3$ displays anisotropic spin-glass behavior as a function of x.

The BC-random is defined by the Hamiltonian:

$$\mathcal{H}_J[s] = -\sum_{(ij)} J_{ij} s_i s_j + D \sum_i s_i^2 + K \sum_{(ij)} s_i^2 s_j^2 \, . \tag{1.11}$$

In finite dimension (i, j) denotes an ordered pair of nearest-neighbour sites while. On the contrary, in the mean-field approximation, the sum runs over all pairs of spin which interact with each other through the coupling costant J_{ij}. The parameter K represents the strenght of the biquadratic interaction, i. e., an interaction which does not distinguish the orientation of the spins. The external field D is called *crystal field* or *chemical potential*. For $D > 0$, the state $s_i = 0$ is lower in energy than $s_i = \pm 1$. If all the couplings J_{ij} are fixed at a constant value J, the model undergoes a phase transition between paramagnet and ferromagnet. If the

probability distribution of J_{ij} is fixed, the transition will be between paramagnet and spin-glass.

It is well known that the original BC model (without disorder) undergoes an IT if, and only if, the relative degenaracy of the interacting (± 1) and non-interacting (0) states is larger than one. Schupper and Shnerb [8, 40] suggested that, starting from a minimal model like the BC, in order to obtain an IT we have to introduce a parameter which tunes the entropic content of paramagnect with respect to magnetic phase (i. e., non-interacting and interacting microscopic configurations). Calling k the degeracy of the state $s_i = 0$, and l the degeneracy of the state $s_i = \pm 1$. $r \equiv k/l$ is the relative degeneracy between the states.

$$r = \frac{l}{k} : \begin{cases} s_i = 0, 0, \dots & k - \text{times} \\ s_i = \pm 1, \pm 1, \dots & l - \text{times} \end{cases} \tag{1.12}$$

Imagine to associate the configuration of a polymer to the spin variable: increasing r the configurations accessible to the coil grow and than the interacting configuration becomes entropically advantaged. The entropic advantage for the configuration ± 1 w. r. t. 0 is given by the degeneracy r. We also note that the presence of non interacting sites is favoured by the crystal field D. The order parameter thermodynamically conjugated to cristal field is the density ρ. The external parameter D plays the role of pressure, therefore CC equation in BC model becomes

$$\frac{dD}{dT} = \frac{\Delta s}{\Delta \rho} \tag{1.13}$$

The Blume-Capel model

In the mean field (MF) approximation, the BC Hamiltonian is (where we set the biquadratic interaction due to the coupling K to zero, since it does not play any role in studying the IT [47, 51])

$$\mathcal{H}[s] = -\frac{J}{2N} \sum_{ij} s_i s_j + D \sum_i s_i^2 \,. \tag{1.14}$$

Since the lattice is fully connected, thermodynamics can be easly computed

$$\begin{aligned} \mathcal{Z}_\beta &= \mathrm{Tr}_{[\sigma]} e^{-\beta \mathcal{H}[s]} \\ f(\beta) &= -\lim_{N\to\infty} \frac{1}{\beta N} \log \mathcal{Z}_\beta \,. \end{aligned} \tag{1.15}$$

Introducing the magnetization m and the density ρ one has

$$\begin{aligned} m &= \frac{1}{N}\sum_i s_i \\ \rho &= \frac{1}{N}\sum_i s_i^2 \end{aligned} \tag{1.16}$$

the partition function can be written as follows

$$\begin{aligned} \mathcal{Z}_\beta &= \int dm\, d\rho\, \frac{d\widehat{m}}{2\pi i}\, \frac{d\widehat{\rho}}{2\pi i}\, e^{-N \widehat{f}(m,\rho,\widehat{m},\widehat{\rho})} \\ \widehat{f}(m,\rho,\widehat{m},\widehat{\rho}) &= -\frac{\beta J}{4} m^2 + \beta\rho D - m\widehat{m} - \rho\widehat{\rho} - \log\left[1 + 2e^{-\widehat{\rho}} \cosh \widehat{m}\right] \end{aligned} \tag{1.17}$$

Performing a saddle point approximation the Helmholtz free-energy, i. e., the Landau-Ginzburg free energy, reads

$$f(m,\beta) = \frac{\beta J m^2}{4} - \log\left[1 + 2\, e^{-\beta D}\, \cosh \frac{\beta J}{2} m\right], \tag{1.18}$$

the order parameters satisfie self-consistency equations

$$\begin{aligned} m(\beta, m) &= \frac{2 \sinh \frac{\beta J}{2} m}{e^{\beta D} + 2 \cosh \frac{\beta J}{2} m} \\ \rho(\beta, m) &= \frac{2 \cosh \frac{\beta J}{2} m}{e^{\beta D} + 2 \cosh \frac{\beta J}{2} m} \,. \end{aligned} \tag{1.19}$$

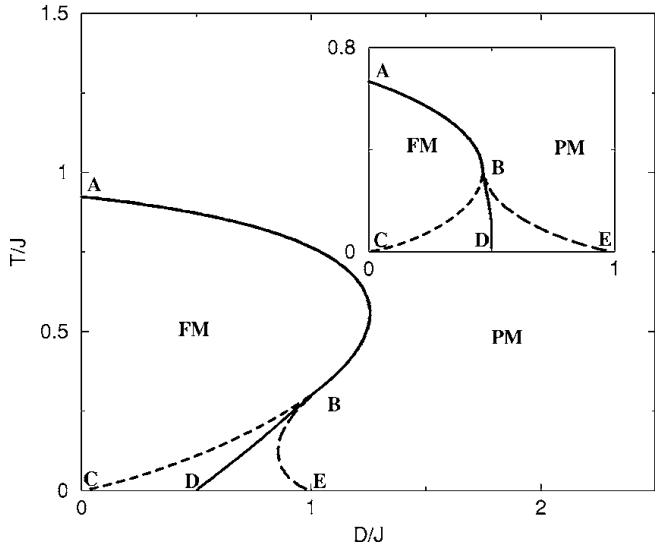

Figure 1.4: BC phase diagram for two values of r. For $r = 1$ (inset) no IT takes place. Otherwise, increasing the relativly entropic content of the interactive states respect the non interacting ones, along the first-order phase-transition line, the system undergoes an IT [8, 40]

Introducing the degeneracy r defined in the previous section, the free energy and the self-consistency equations become

$$\begin{aligned} f(m,\beta) &= \frac{\beta J m^2}{4} - \log\left[1 + 2\,r\,e^{-\beta D}\,\cosh\frac{\beta J}{2}m\right] \\ m(\beta,m) &= \frac{2\,r\,\sinh\frac{\beta J}{2}m}{e^{\beta D} + 2\,r\,\cosh\frac{\beta J}{2}m} \\ \rho(\beta,m) &= \frac{2\,r\,\cosh\frac{\beta J}{2}m}{e^{\beta D} + 2\,r\,\cosh\frac{\beta J}{2}m}\,. \end{aligned} \tag{1.20}$$

the resulting phase diagram is depicted in Fig. (1.4) for two different values of r. We have a second-order phase-transition curve ending in a tricitical point (in fact, the BC model is also called *tricritical Ising model*). From the tricritical point a first-order phase-transition curve originates, together with coexistence of paramagnet (PM) and ferromagnet (FM) phases. If $r = 1$, along the first-order phase transition, no IT takes place. Increasing the relative degeneracy, the slope of the transition lines changes from ordinary to IT. It is important to keep on mind

that IT does not take place for $r < 1$. Moreover, for $r = 1/2$, the BC-model can be mapped onto a lattice-gas model where, two dynamical variables are located in each site, namely, an Ising variable $\sigma_i = \pm 1$ and an occupation number $n_i = 0, 1$.

The Blume-Capel model with disorder

If we wish to reproduce the features of an IT through a simple lattice model with ordered interaction, we have to introduce one more parameter, to allow the slope of the CC curve to vary. Otherwise, introducing quenched disorder in the couplings between the spins, changes the behavior of the first-order transition from ordinary to IT without tuning the degree of degeneracy r [47, 51]. BC-random is defined by the Hamiltonian (1.11), where each coupling constant J_{ij} is extracted from a given probability distribution $P(J_{ij})$, e. g., a Gaussian. Due to the presence of disorder, BC-random is a spin-glass model. The thermodynamics, in the mean-field approximation, can be computed explicitly through the replica trick applying Parisi's replica symmetry breaking theory [52, 53, 54], in order to stabilize the self-consistency solution of the spin-glass (SG) phase. Choosing a Gaussian distribution

$$P(J_{ij}) = \frac{N^{1/2}}{\sqrt{2\pi J^2}} \exp\left(-\frac{J_{ij}^2 N}{2J^2}\right) \tag{1.21}$$

The disorder is *quenched*: we have to average over $P(J_{ij})$ the free energy to compute the thermodynamics:

$$\begin{aligned} \mathcal{Z}_\beta[J] &= \mathrm{Tr}_{[s]} e^{-\beta \mathcal{H}_J[s]} \\ f(\beta) &= -\lim_{N\to\infty} \frac{1}{\beta N} \log \int d\mu(J) \mathcal{Z}_\beta[J] \\ d\mu(J) &\equiv \prod_{ij} dJ_{ij} P(J_{ij})\,. \end{aligned} \tag{1.22}$$

Applying the replica trick to the computation of the thermodynamics, one can recover the quenched free energy as the continuation of the annealed — n-replicated—

partition function down to the unphysical limit $n = 0$, it is[1] [55]

$$\begin{aligned} f(\beta) &= -\lim_{N\to\infty}\lim_{n\to 0}\frac{1}{\beta N n}\partial_n \int d\mu(J)\mathcal{Z}^n[J] \\ \mathcal{Z}^n[J] &= \mathrm{Tr}_{[s_a]} e^{-\beta\sum_a^n \mathcal{H}_J[s_a]} \\ \mathcal{H}_J[s_a] &= -\sum_{ij} J_{ij} s_i^a s_j^a + D\sum_i (s_i^a)^2 \,. \end{aligned} \tag{1.23}$$

The overlap q_{ab} between two replicas labelled by a and b, i.e., a mesure of distance between two configurations, is

$$q_{ab} = \frac{1}{N}\sum_i s_i^a s_i^b \,. \tag{1.24}$$

We can represent q_{ab} through a symmetrical matrix $n\times n$ with zero on the diagonal. An important observable is the overlap distribution $P(q)$, using replicas [55] $P(q)$ reads

$$P(q) = \lim_{n\to 0}\frac{2}{n(n-1)}\sum_{ab}\delta\left(q - q_{ab}\right) \,. \tag{1.25}$$

As we will see in sec. (1.4), through the study of the overlap distribution we can obtain information about the microsopical configuration of the system. For example, in ferromagnetic systems, overlap distribution becomes

$$\begin{aligned} P_{PM}(q) &= \delta(q) \\ P_{FM}(q) &= \frac{1}{2}\delta(q - m^2) + \frac{1}{2}\delta(q + m^2) \end{aligned} \tag{1.26}$$

where PM (FM) means paramagnet (ferromagnet) and m is the magnetization. In a paramagnet it has only one *equilibrium state*: the PM state where $m = 0$. Otherwise, since in an Ising system Z_2 —global spins inversion— symmetry holds, the ferromagnetic phase is characterized by two equilibrium states with $m \neq 0$.

In order to compute the free energy we to made an *Ansatz* about the structure of the matrix $q_a b$. The natural choice is assume that all the replicas are equivalent (RS solution)

$$q_{ab}^{RS} = q_{EA} \quad \forall\, a \neq b \,, \tag{1.27}$$

[1]Some details about replica trick will be discuss in the next chapter.

where q_{EA} is also called *Edwards-Anderson parameter* [56, 57]. RS, in the low –spin-glass– temperature phase, leads to the following overlap distribution

$$P(q) = \frac{1}{2}\delta(q - q_{ED}) + \frac{1}{2}\delta(q + q_{EA}) \tag{1.28}$$

and than RS predicts only two equilibrium states connected by Z_2 symmetry. It is well known that RS is unstable in the SG phase. In order to find a stable solution, we have to break the replica-symmetry. Following the scheme suggested by Parisi [52, 53, 54], and making use of the full-replica-symmetry-breaking-scheme (FRSB), free-energy and self-consistency equations read [51]

$$\begin{aligned}
\beta f &= \frac{\beta}{2}\left(K + \frac{\beta}{2}\right)\rho^2 - \frac{\beta^2}{4}\int_0^1 dx q^2(x) - \beta\varphi(0,0) \\
q(x) &= \int_{-\infty}^{+\infty} dy\, P(x,y)\varphi'(x,y)^2 \\
\rho &= \int_{-\infty}^{+\infty} dy\, P(1,y)\frac{2re^{\Theta}\cosh\beta y}{1 + 2r\cosh\beta y} \\
\Theta &= \frac{\beta^2}{2}\left(\rho - q(1)\right) + \beta K\rho - \beta D
\end{aligned} \tag{1.29}$$

where $\varphi(x,y)$ and $P(x,y)$ solve the partial differential antiparapolic *Parisi equations*

$$\begin{aligned}
\frac{\partial\varphi}{\partial x}(x,y) &= -\frac{dq}{dx}\left[\frac{\partial^2\varphi}{\partial y^2}(x,y) + \beta x\left(\frac{\partial\varphi}{\partial y}(x,y)\right)^2\right], \\
\frac{\partial P}{\partial x}(x,y) &= -\frac{dq}{dx}\left[\frac{\partial^2 P}{\partial y^2}(x,y) - 2\beta x\frac{\partial}{\partial y}\left(P(x,y)\frac{\partial\varphi}{\partial y}(x,y)\right)\right],
\end{aligned} \tag{1.30}$$

with boundary conditions

$$\begin{aligned}
\varphi(1,y) &= \frac{1}{\beta}\log 2\left(1 + 2re^{\Theta}\cosh\beta y\right), \\
P(0,y) &= \delta(y)\,.
\end{aligned} \tag{1.31}$$

As we can see in eqs. (1.29), the overlap becomes a continuous function defined

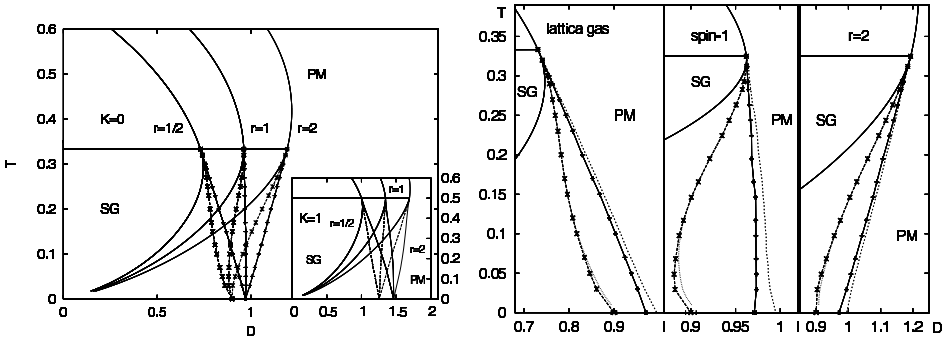

Figure 1.5: Phase diagram of the mean-field BC-random for several values of the relative degeneracy r[47, 51]. For $r \geq 1$ an IT, across the first order phase transition, takes place. For $r = 1/2$ the IT disappears and the first order transition line becomes ordinary.

on $[0, 1]$ and it is related to the overlap distribution as follows [54]

$$\frac{dx(q)}{dq} = P(q) \tag{1.32}$$

where $x(q)$ is the inverse function of $q(x)$. Since $q(x)$ is an increasing and non-vanishing function of x, the overlap distribution is a non-trivial distribution (i. e., not only a sum of Dirac distribution). In particular, a generic expression for $P(q)$ reads

$$\begin{aligned} P(q) &= \frac{1}{2}\widetilde{P}(q) + \frac{1}{2}\widetilde{P}(-q) \\ \widetilde{P}(q) &= x_m \delta(q - q_m) + x_M \delta(x - q_M) + \widehat{P}(q) \\ x_m &= x(q_m) \\ x_M &= x(q_M) \ , \end{aligned} \tag{1.33}$$

where $\widehat{P}(q)$ is a smooth function with support in the interval $q_m < q < q_M$. In sec. (1.4.3) the shape of the overlap distribution across the transition will be discuss.

Other properties of the spin-glass models will be study in the next chapter. The phase diagram is shown in fig. (1.5) for different values of r. As can be seen, the IT scenario holds for $r \geq 1$: therefore the model, along the first order phase transition, undergoes an IT without changing the degeneracy.

1.3 Monte Carlo simulations

In the previous section we have established that BC random, in the mean field approximation, is a minimal model to describe IT. For this reason, I have performed an intensive study of the BC random in three dimensions by means of Monte-Carlo and Parallel-Tempering techniques.

Model and Observables

The BC-random in three dimension is defined by Hamiltonian (1.11). This study is performed by setting $K = 0$. The quenched disorder is bimodal distributed:

$$P(J_{ij}) = \frac{1}{2}\delta(J_{ij} - 1) + \frac{1}{2}\delta(J_{ij} + 1)\,. \tag{1.34}$$

I simulate two real replicas labelled by $i = 1, 2$, i. e., two identical copies of the system with the same realization of the disordered couplings, and define their site and link overlaps, i.e., the order parameters usually characterizing the SG transition, as

$$q_s^{(J)} \equiv \frac{1}{N}\sum_i \langle s_i^{(1)} s_i^{(2)} \rangle\,, \tag{1.35}$$

$$q_l^{(J)} \equiv \frac{1}{ND}\sum_{(jk)} \langle s_j^{(1)} s_k^{(1)} s_j^{(2)} s_k^{(2)} \rangle \tag{1.36}$$

where $\langle \ldots \rangle$ is the thermal average and $D = 3$ is the dimension of the space. If a thermodynamic phase transition occurs, with latent heat, the most significant order parameter that drives the transition is the density ρ of magnetically active ($|s_i| = 1$) sites:

$$\rho^{(J)} = \frac{1}{N}\sum_i \langle s_i^2 \rangle \tag{1.37}$$

The superscript J recalls that the other parameters depend on the particular way in which the disorder is realized ($\{J_{ij}\}$).

Parallel-Tempering

The BC model has been studied via the so-called Parallel Tempering (PT) technique, equivalently called exchange Monte-Carlo, replicating several copies of the system at different values of the temperature and of the external field D. For PT done with respect to the temperature, the swap probability of two copies at temperature T and $T + \Delta T$, where $\beta = 1/T$, is

$$P_{swap}(\Delta\beta) = min\left[1, \exp\left\{\Delta\beta\Delta\mathcal{H}\right\}\right] \tag{1.38}$$

and

$$\Delta\beta = \frac{1}{T + \Delta T} - \frac{1}{T}\,. \tag{1.39}$$

Since the two thermal bath are characterized by two different configurations of the spin variables $[s]$ (at the temperature T) and $[s']$ (at the temperature $T + dT$), $\Delta\mathcal{H}$ reads

$$\Delta\mathcal{H} = \mathcal{H}[s'] - \mathcal{H}[s]. \tag{1.40}$$

Whereas the swap probability in the chemical potential reads

$$P_{swap}(\Delta D) = min\left[1, \exp\left\{\beta\Delta D\Delta\rho\right\}\right]\,. \tag{1.41}$$

We use the latter implementation in trying to identify the IT line in the (T, D) plane. However, since the transition turns out to be first-order in the whole region of inverse freezing, the PT algorithm must be handled with caution. In fact, at transition, $\Delta\rho$ is discontinuous, implying that the $P_{swap}(\Delta D)$ vanishes around the critical point for a given fixed probe ΔD. In order to overcome this problem, I have used a varying ΔD, smaller in the candidate coexistence region and increasingly larger outside it. For very large sizes, thought, this would require too precise an *a-priori* knowledge of the transition curves. Hence, this method could not be applied successfully. On the other hand, finite size scale (FSS) effects appear to be almost nonexistent at the first-order phase transition, so that probes at large size are actually not necessary. The choice of simulation parameters is reported in Tables 1.1 and 1.2 Thermalization has been checked in three ways:

1. I have verified the symmetry of the site-overlap distribution function with

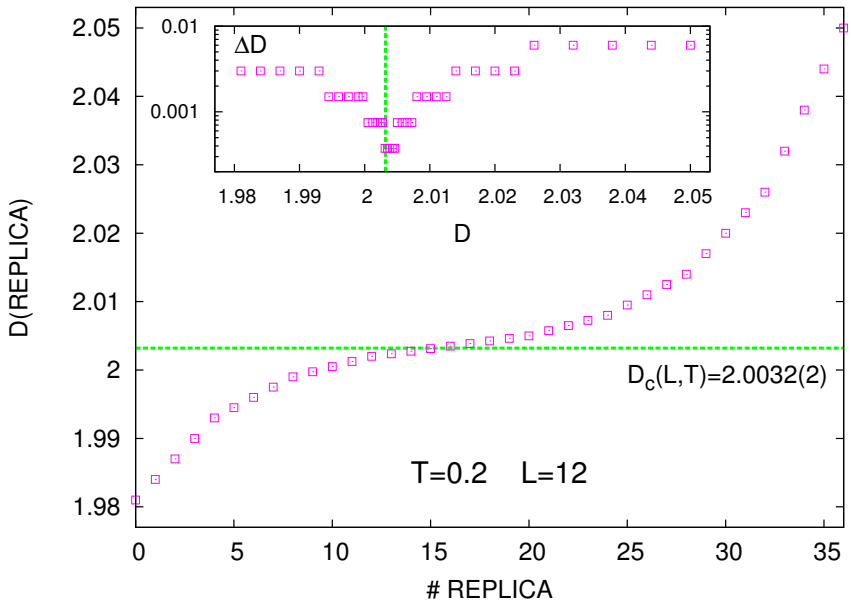

Figure 1.6: Values of the chemical potential D for the replicas in the PT simulation exchanging systems at different D. The parameters refer to the simulated $L = 12$ system at $T = 0.2$. The dashed (green) line is the estimate of the FS critical value $D_c(L, T)$ estimated by means of the equal weight method (cf. Sec. 1.3.1). Inset: Chemical potential intervals ΔD vs. D in log scale for the same instance.

respect to zero $P_J(q_s)$ for single random samples (cf, Fig. 1.7). In absence of an external magnetic field this function has to be symmetric for any choice of $\{J_{ij}\}$ realization.

2. I have checked at the $\log t$ behaviour of the energy. I have considered as thermalized those systems in which at least the last two points coincide to within a set tollerance, cf. Fig. 1.7. This means that at least the second half of the data in MCS can be used for computing statistical ensemble averages.

3. I have checked that of all considered observables (e.g., ξ and χ_{SG}) do not vary on logaritmic time windows on at least two log points.

The simulation has been done on 2000 samples to study the second-order phase transition and on 100 samples to study the first-order phase transition. Since the first-order phase transition is driven by the density —the probability distribution

$D\downarrow$	$L\rightarrow$	6	8	10	12	16	20	24
0.0	T_{in}	0.6	0.6	0.7	0.7	0.85	0.9	1.0
	N_T	37	37	33	33	27	25	21
	MCS	2^{15}	2^{15}	2^{16}	2^{17}	2^{18}	2^{19}	2^{19}
1.0	T_{in}	0.6	0.6	0.7	0.7	0.7	0.8	0.8
	N_T	37	37	33	33	33	29	24
-	MCS	2^{15}	2^{15}	2^{16}	2^{17}	2^{18}	2^{19}	2^{20}
1.75	T_{in}	0.6	0.6	0.6	0.6	0.6	0.6	0.65
	N_T	37	37	33	33	33	20	22
-	MCS	2^{15}	2^{15}	2^{16}	2^{17}	2^{18}	2^{20}	2^{20}
2.0	T_{in}	0.01	0.01	0.025	0.025	0.3	0.4	0.5
	N_T	90	90	36	36	25	21	17
-	MCS	2^{18}	2^{18}	2^{19}	2^{19}	2^{18}	2^{20}	2^{20}

Table 1.1: Simulation parameters of the parallel tempering in temperature: number of samples 2000, Monte Carlo Steps (MCS), number of thermal bath N_T spaced by $\Delta T =, 0.02$ or 0.025.

$T\downarrow$	$L\rightarrow$	6	8	10	12	15
0.2	D_{in}	1.99	1.999	2.00392	1.981	1.981
	ΔD_{in}	0.002	0.0006	0.00027	0.003	0.003
	N_D	21	21	37	37	37
	MCS	2^{15}	2^{17}	2^{18}	2^{20}	2^{20}
0.3	D_{in}	2.0034	2.026	2.0212	2.0256	2.028
	ΔD_{in}	0.002	0.001	0.00037	0.003	0.00025
	N_D	21	21	21	31	31
	MCS	2^{15}	2^{17}	2^{17}	2^{17}	2^{18}
0.4	D_{in}	2.05	2.06	2.057	2.06	2.062
	ΔD_{in}	0.003	0.002	0.0007	0.00085	0.0006
	N_D	21	21	21	31	31
	MCS	2^{15}	2^{17}	2^{17}	2^{17}	2^{18}
0.5	D_{in}	2.06	2.06	2.06	2.026	2.026
	ΔD_{in}	0.01	0.01	0.01	0.008	0.008
	N_D	21	21	21	37	37
	MCS	2^{15}	2^{17}	2^{17}	2^{18}	2^{18}

Table 1.2: Simulation parameters of the parallel tempering in D. Number of disordered samples: 1000

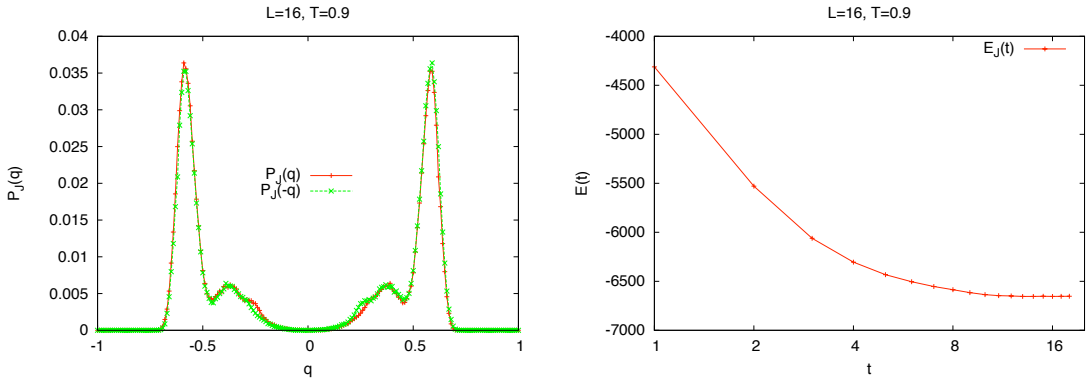

Figure 1.7: Instances of thermalization checks. Left: $P_J(q_s)$ and $P_J(-q_s)$ for an arbitrary sample at $D = 0$, $L = 16$. Right: average energy versus time (in MCS) in log scale.

of the density is self-averaging— the transition curve slightly depends on disorder.

Order parameters distributions

Useful information about the equilibrium properties of the system can be obtained from the following probability distribution functions (PDFs)

$$P(q_s) \equiv \overline{P_J(q_s)} = \overline{\left\langle \delta\left(q_s^{(J)} - \frac{1}{N}\sum_i s_i^{(1)} s_i^{(2)}\right)\right\rangle} \tag{1.42}$$

$$P(q_l) \equiv \overline{P_J(q_l)} = \overline{\left\langle \delta\left(q_l^{(J)} - \frac{1}{ND}\sum_{(jk)} s_j^{(1)} s_k^{(2)} s_j^{(1)} s_k^{(2)}\right)\right\rangle} \tag{1.43}$$

$$P(\rho) \equiv \overline{P_J(\rho)} = \overline{\left\langle \delta\left(\rho^{(J)} - \frac{1}{N}\sum_i s_i^2\right)\right\rangle} \tag{1.44}$$

where $\overline{\ldots}$ denotes the average over quenched disorder. Though the density probability distribution is known to be self-averaging ($\lim_{N\to\infty} P_J(\rho) = \overline{P_J(\rho)}$), this

property does not hold for the overlap distributions $P_J(q_{s,l})$[55], for which

$$P(q_{s,l}) \equiv \overline{P_J(q_{s,l})} \neq \lim_{N\to\infty} P_J^{(N)}(q_{s,l}) \tag{1.45}$$

Four-spin correlation function

In order to infer the details of the critical behaviour from numerical simulations of finite size systems, a fundamental quantity is the four-spin correlation function, defined as

$$C_4(\boldsymbol{r}) \equiv \frac{1}{N}\sum_{\boldsymbol{s}} \overline{\langle s_{\boldsymbol{p}} s_{\boldsymbol{s}+\boldsymbol{r}}\rangle^2} \tag{1.46}$$

under null external magnetic field. It terms of space-dependent overlaps $q_{\boldsymbol{r}} = s_{\boldsymbol{r}}^{(1)} s_{\boldsymbol{r}}^{(2)}$, it can be shown that

$$C_4(\boldsymbol{r}) = \frac{1}{N}\sum_{\boldsymbol{p}} \overline{\langle q_{\boldsymbol{p}} q_{\boldsymbol{p}+\boldsymbol{r}}\rangle_{12}} \tag{1.47}$$

where $\langle\ldots\rangle_{12}$ stays equivalently for the thermal average $\langle\langle\ldots\rangle_1\rangle_2$ or $\langle\langle\ldots\rangle_2\rangle_1$ over the two replicas independently. The information contained in the four-point function can be exploited in different ways to identify the existence of a second order phase transition in systems of finite size.

Correlation lenght and finite size scaling

A conventional way to identify a second-order phase transition is to look at the behaviour of a correlation length-like scaling function defined as

$$\xi^2 \equiv \frac{\int d\mathbf{r}\, r^2 C_4(\mathbf{r})}{\int d\mathbf{r}\, C_4(\boldsymbol{r})} = \left.\frac{\partial \log \hat{C}_4(\boldsymbol{k})}{\partial k^2}\right|_{k^2=0} \tag{1.48}$$

where

$$\widehat{C}_4(\boldsymbol{k}) = \frac{1}{(2\pi)^3}\int d\mathbf{r}\, e^{-i\boldsymbol{k}\cdot\boldsymbol{r}}\, C(\boldsymbol{r})$$

On a 3D cubic lattice, the above defined correlation length becomes [58]:

$$\xi_c^2 = \frac{1}{4\sin^2\frac{k_1}{2}}\left(\frac{\hat{C}_4(\mathbf{0})}{\hat{C}_4(\boldsymbol{k}_1)} - 1\right) \tag{1.49}$$

where $k_1 = |\boldsymbol{k}_1|$, $\boldsymbol{k}_1 \equiv (2\pi/L, 0, 0)$ is the minimum wave-vector of the lattice and $\mathbf{0} = (0, 0, 0)$. In the thermodynamic limit, a second-order transition is characterized by a diverging correlation length, at a critical temperature T_c, whose FSS behaviour is the same as in Eq. (1.49) [59, 60]. In practice, in a finite-size system, we can not mesure an infinite correlation lenght. However, inside the critical region, a remarkable property of critical phenomena survives in finite systems, namely, scale invariance. Measuring the correlation lenght ξ in lattice-unit L, when the system undergoes to a second order phase transition, we can define a size-dependent temperature $T_c(L)$, analogous to temperature where the system is scale-invariant. Obviously, in order to establish $T_c(L)$ we need to compare the behaviour of two systems, whose size is L and L' respectively. Both systems are scale-invariant at the temperature $T_c(L, L')$ if the following relation holds:

$$\left.\frac{\xi(L,T)/L}{\xi(L',T)}\right|_{T_c(L,L')} = 1. \tag{1.50}$$

This temperature depends weackly on the sizes L and L' used. In particular, by increasing the sizes, we can study the asimptotic behaviour of $T_c(L)$[61, 62]

$$T_c(L) = T_c(\infty) + AL^{-1/\nu}, \tag{1.51}$$

where ν is the critical exponent given by the theory of the critical phenomena

$$\xi \sim (T - T_c)^{-\nu}\,. \tag{1.52}$$

Another relevant observable is the SG susceptibility, defined as

$$\chi_{SG} \equiv \frac{1}{N}\overline{\left\langle\left(\sum_i s_i^{(1)} s_i^{(2)}\right)^2\right\rangle}\,. \tag{1.53}$$

Since the overlap between the replicas is defined by the first relation of (1.35), the SG susceptibility reads ($N = L^3$)

$$\chi_{SG} = L^3 \overline{\langle q^2 \rangle} = L^3 \hat{C}_4(\mathbf{0}) \,, \tag{1.54}$$

which diverges at the PM/SG transition as $L \to \infty$. Also for χ_{SG} it is possible to define a critical region where the susceptibilities of system of different size are scale-invariant. In order to do it, we have to introduce another exponent, which are called η. The above can be summarized in the following expressions:

$$\frac{\xi_c}{L} = \bar{\xi}_c \left(\frac{\xi_c}{L} \right) = \bar{\xi}(L^{1/\nu}(T - T_c)) \tag{1.55}$$

$$\chi_{SG} L^{\eta - 2} = \bar{\chi} \left(\frac{\xi_c}{L} \right) = \bar{\chi}(L^{1/\nu}(T - T_c)) \tag{1.56}$$

The values T_c^L at which ξ_c/L at different L cross each other are the FS respective of the critical temperature. Thus, the latter can be estimated by FSS in the $L \to \infty$ limit. A further size-independent scaling function is the so-called Binder parameter:

$$g(L, T) = \frac{1}{2} \left(3 - \frac{q_4}{(q_2)^2} \right) \,, \tag{1.57}$$

where $q_n \equiv \overline{\langle (q^{(J)})^n \rangle}$. It measures the deviation of $P(q)$ from a Gaussian distribution as the SG phase is approached. Since q_4 and q_2^2 scale with L in the same way, g does not depend on L at T_c:

$$g(L, T) = \bar{g}(L^{1/\nu}(T - T_c)). \tag{1.58}$$

Denoting by $O(T, L)$ a generic observable diverging at critical temperature T_c as $L \to \infty$, and considering two sizes L, L' whose scale ratio is $s = L'/L$, the FSS theory predicts that

$$\frac{O(T, sL)}{O(T, L)} = F_O \left(\frac{\xi(L, T)}{L}, s \right) + \mathcal{O}(\xi^{-\omega}, L^{-\omega}) \,, \tag{1.59}$$

where F_O is a universal FSS function and ω is the power of the subleading finite-size corrections. Thus, through the scaling Ansatz (1.59), one introduces a class of universal functions F_O that are size-independent in the critical region. Given two observables O and R displaying scale invariance, F_O may be plotted versus F_R for different values of L: if the data collapse onto a universal scaling function, the scaling Ansatz is verified and the FSS methods can be trusted for a evaluating the critical exponents. I will analyze the behavior of F_ξ, $F_{\chi_{\rm SG}}$ and F_g.

The quotient method

In order to estimate the critical exponents, one can use the quotient method [60], based on the observation that at $T_c^L \equiv T_c^*$, the correlation lengths, mesured in unit of the linear size L, in systems of sizes L and sL are equal:

$$\frac{s\,\xi(T_c^*, L)}{\xi(T_c^*, sL)} = 1. \tag{1.60}$$

For an observable O diverging as t^{x_O} ($t = T/T_c - 1$) in the thermodynamic limit, one has:

$$s^{\frac{x_O}{\nu}} = \frac{O(T_c^*, sL)}{O(T_c^*, L)} + \mathcal{O}(L^{-\omega})\,, \tag{1.61}$$

where the dependence on $\xi^{-\omega}$ in the correction term is neglected because, in the critical region, $\xi_c \gg L$. For a SG we can obtain the exponents ν and η by means of the FSS of the quotients of $\partial_\beta \xi$ and χ_{SG} respectively scaling with the exponents

$$\begin{aligned} x_{\partial_\beta \xi} &= 1 + \nu \\ x_{\chi_{SG}} &= (2 - \eta)\nu\,. \end{aligned}$$

These relations hold if the Ansatz (1.59) is verified [58], i.e., if F_O is a size-independent scaling function for different values of L and sL.

1.3.1 Numerical study of a first-order phase transition

In the first section I have introduced the CC equation which characterizes the behaviour of a first-order phase transition. In the BC-random CC, this reads

$$\frac{dD}{dT} = \frac{s_{PM} - s_{SG}}{\rho_{PM} - \rho_{SG}} = \frac{\Delta s}{\Delta \rho}\,, \tag{1.62}$$

where D plays the role of the pressure. The equilibrium transition curve changes slope at a point where the entropy of the two coexisting phases is equal, $\Delta s = 0$ (Kauzmann locus [63]).

In order to identify a first-order phase transition in a three-dimensional finite-size system from numerical simulation data, four methods to estimate the critical (and spinodal) point will now be introduced.

"Equal weight" estimate

The transition takes place at the point at which the configurations belonging to the SG phase and those belonging to the PM phase have the same statistical weight, i.e., they give equal contribution to the partition function of the single pure phase. Said differently, the free energies of the two coexisting phases are equal. In this statistical mechanical framework, the FS transition curve $D_c(L,T)$ can be obtained as the locus of points where the two phases are equiprobable, i.e., the areas of the two peaks are equal [64]:

$$\int_0^{\rho_0} d\rho\, P(\rho) = \int_{\rho_0}^1 d\rho\, P(\rho) \tag{1.63}$$

where $\rho_0 \in [\rho_{PM} : \rho_{SG}]$ such that $P(\rho) = 0$ (or minimal next to the tricritical point). A way to determine numerically the transition point is, thus, to compare the areas under the peaks of the distributions.

Maxwell "equal distance" estimate

Other two methods to determine a first-order transition in finite system, are based on the Maxwell construction. In the coexistence region, the curve $D(\rho)$ for the system of size L will display a sort of plateau around some $D = D^\star \simeq D_c^L$: in a

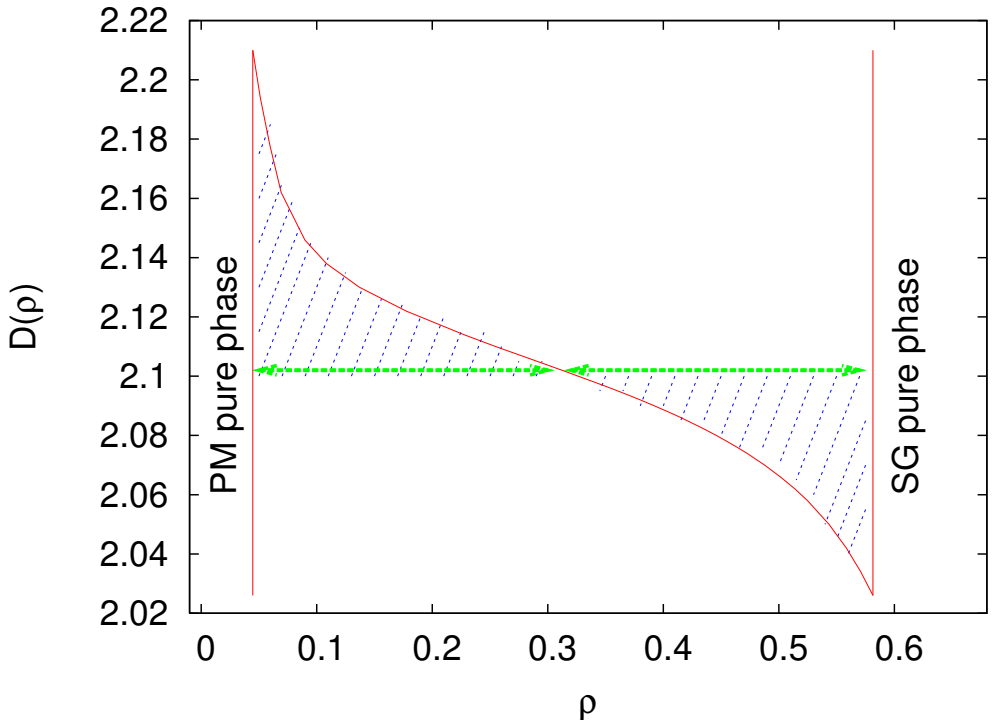

Figure 1.8: Graphical sketch of the equal distance (dashed/green arrows) and equal area methods (dotted/blue areas) for FS systems undergoing first order phase transition for a given instance ($L = 6, T = 0.5$).

very short interval around D, the density changes very rapidly. In the case of a pure state, on the contrary, the $D(\rho)$ curve is much smoother. In order to estimate the critical point we need to extrapolate the behaviour of $D(\rho)$ for the pure phases into the coexistence region. With this aim, I perform two fits based solely on the points outside the spinodal points: for $D < D^{\rm sp}_{\rm SG}$ for the SG phase ($D_{\rm SG}(\rho)$) and $D > D^{\rm sp}_{\rm PM}$ for the PM phase ($D_{\rm PM}(\rho)$). I will call $\rho_{PM,SG}(D)$ the inverse of the curve $D_{PM,SG}(\rho)$ extrapolated from the data points pertaining to the pure PM and SG phases, respectively. The curve $\rho(D)$ will denote the inverse of $D(\rho)$. In this way a Maxwell-like construction in the ρ, D plane at a given temperature may be done to determine the value of D_c as the one with a corresponding $\rho_{\rm ed}$ value along the $D(\rho)$ FS curve that is equally distant from both $\rho_{\rm PM}(D_c)$ and $\rho_{\rm SG}(D_c)$, cf. Fig. 1.8

$$\rho_{\rm ed}(D_c) = 1/2(\rho_{\rm PM}(D_c) + \rho_{\rm SG}(D_c)) \tag{1.64}$$

Maxwell "equal area" estimate

Alternatively, we can determine D_c as the value for which,

$$\int_{D_{\rm SG}}^{D_c} \rho_{\rm PM}(D)dD + \int_{D_c}^{D_{\rm PM}} \rho_{\rm SG}(D)dD = \int_{D_{\rm SG}}^{D_{\rm PM}} \rho(D)dD \tag{1.65}$$

where $D_{\rm SG}$ and $D_{\rm PM}$ are arbitrary, provided that they pertain to the relative pure phases, cf. Fig. 1.8.

Symmetric distribution estimate

Let the skewness of the density probability distribution be defined as

$$\zeta(\langle\rho\rangle) \equiv \frac{\langle(\rho - \langle\rho\rangle)^3\rangle}{\langle(\rho\langle\rho\rangle)^2\rangle^{3/2}}\,. \tag{1.66}$$

In Ref.[65] the critical point was estimated as the point at which the double-peaked distribution is symmetric. Since the skewness of $P(\rho)$ can be computed precisely, this estimate does not suffer, from the arbitrariness of the choice of ρ_0 as in the equal weight method. In the thermodynamic limit, in fact, in the phase-coexistence region, both peaks of $P(\rho)$ should be Dirac distributions and equal weight would be equivalent to a symmetric bimodal distribution. I will show the outcome of this analysis using our system for different cases and compare it with the previous outcomes.

1.3.2 Second-order phase transition

In Fig. 1.9 I present the T-behaviour of ξ/L for different values of $D = 0, 1, 1.75, 2$ and 2.11. In the first four cases curves for different L clearly cross each other, yielding evidence for a non zero T_c^L. From a FSS $T_c^L = T_c^\infty + aL^{-b}$ we can, thus, extrapolate the critical temperature to the thermodynamic limit. The T_c^L crossing points between $L - 2L$ curves are reported on column 3 of Tab.1.3. The FSS estimates are reported in columns 2 and 5 of Tab.1.4, where L/L' pairs are chosen both as $L/2L$ (col. 2) and as contiguous in the series $L = 6, 8, 10, 12, 16, 20, 24$ (col. 5). Analogous, though less precise, estimates can be obtained by studying the

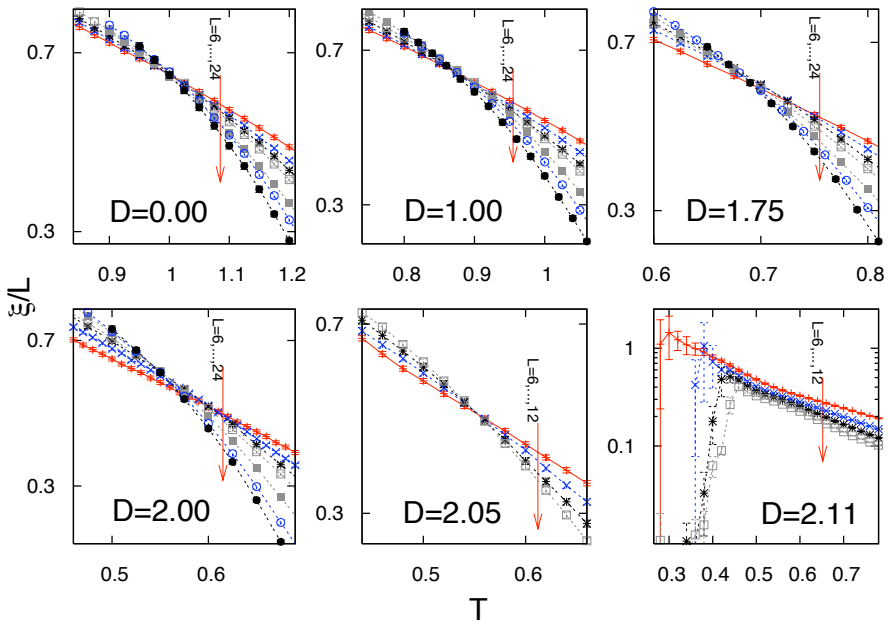

Figure 1.9: Scaling functions ξ_c/L vs. T for different values D. For $D = 0, 1, 1.75, 2$ ($L = 6, 8, 10, 12, 16, 20, 24$) a evidence for a continuous phase transition is found in the region of scale invariance. At $D = 2.11$ ($L = 6, 8, 10, 12$) no crossing is observed and, at low T, $\xi_c/L \to 0$.

behaviour of the Binder cumulant g, (cf. eq. (1.57)). Applying both the quotient and the conventional FSS methods we can, eventually, obtain two estimates for the critical exponents.

Before applying these methods, though, we must check whether cross-over effects in the size due to FS as the chemical potential D is varied. Since we are in presence of a tricritical point, signalled, among others, by the weird behavior of ξ/L at $D = 2.11$, cf. Fig. 1.9, we should control how it influences the results as it is approached along the continuous transition-line, increasing D. In the mean-field approximation, indeed, at the tricritical point the coefficient of the fourth-order term in the SG free energy action goes to zero and the sixth-order term becomes relevant for the critical behaviour, as shown in Ref. [66]. This is a typical be-

D	$L-L'$	$T_c(s)$	$Q_{\partial_\beta\xi}(s)$	$\nu(s)$	$Q_\chi(s)$	$\eta(s)$
0.0	$6-12$	1.02(4)	1.35(1)	2.31(1)	5.1(1)	$-0.34(4)$
	$8-16$	0.99(6)	1.31(2)	2.58(5)	5.1(1)	$-0.36(3)$
	$10-20$	1.0(1)	1.35(4)	2.3(1)	5.2(1)	$-0.39(4)$
	$12-24$	0.98(9)	1.33(2)	2.43(7)	5.1(1)	$-0.35(4)$
	∞	1.01(1)		2.34(3)		$-0.36(1)$
D	$L-L'$	$T_c(s)$	$Q_{\partial_\beta\xi}(s)$	$\nu(s)$	$Q_\chi(s)$	$\eta(s)$
1.0	$6-12$	0.894(9)	1.32(1)	2.51(4)	4.9(3)	$-0.29(9)$
	$8-16$	0.895(9)	1.396(6)	2.08(1)	4.8(4)	$-0.26(1)$
	$10-20$	0.877(9)	1.271(7)	2.89(2)	5.1(5)	$-0.33(1)$
	$12-24$	0.86(1)	1.35(1)	2.29(2)	5.1(5)	$-0.3(1)$
	∞	0.88(1)		2.45(1)		$-0.31(2)$
D	$L-L'$	$T_c(s)$	$Q_{\partial_\beta\xi}(s)$	$\nu(s)$	$Q_\chi(s)$	$\eta(s)$
1.75	$6-12$	0.715(7)	1.41(1)	*	4.7(5)	*
	$8-16$	0.679(9)	1.37(1)	2.12(4)	4.8(5)	$-0.3(1)$
	$10-20$	0.67(1)	1.34(3)	2.4(1)	5.0(6)	$-0.3(1)$
	$12-24$	0.68(1)	1.38(1)	2.11(3)	4.9(5)	$-0.3(1)$
	∞	0.69(1)		2.20(3)		$-0.30(1)$
D	$L-L'$	$T_c(s)$	$Q_{\partial_\beta\xi}(s)$	$\nu(s)$	$Q_\chi(s)$	$\eta(s)$
2.0	$6-12$	0.593(7)	1.59(4)	*	9.5(9)	*
	$8-16$	0.569(8)	1.47(3)	*	18(2)	*
	$10-20$	0.54(1)	1.37(3)	*	16(2)	*
	$12-24$	0.54(1)	1.34(4)	*	10(2)	*
	∞	0.56(1)				

Table 1.3: Critical temperature and exponents are calculated with QM: for $D = 0.00$, $D = 1.00$ and $D = 1.75$, through a FSS analysis of the values of $Q_{\partial_\beta\xi}(s)$ and $Q_\chi(s)$ for $s = L'/L = 2$. Cells with * mean that quotients are computed on sizes too small to significantly represent the asymptotic behavior with L.

haviour of BC-like systems [67, 68], that might hinder the determination of the critical behavior in the neighborhood of the tricritical point for sizes that are not large enough.

To estimate and control FS effects, I use the scaling methods introduced in Sec. 1.3 and compare different universal FSS functions following to the approach first introduced in Ref. [69]. In Fig. 1.10 I plot the Binder parameter g vs. the rescaled correlation length ξ_c/L at all simulated values of the chemical potential D both for a small ($L = 6$, left) and for a large ($L = 20$, right) system. From the

	D	T_c	ν	η	$\xi_c(T_c)/L$	$g(T_c)$
Quotient Method	0.00	1.01(1)	2.34(3)	$-0.36(1)$	~ 0.60	~ 0.79
	1.00	0.88(1)	2.45(1)	$-0.31(2)$	~ 0.66	~ 0.77
	1.75	0.68(2)	2.20(3)*	$-0.30(1)$*	~ 0.61*	~ 0.79
	2.00	0.56(1)	†	†	†	†

	D	T_c	ν	η	$\xi_c(T_c)/L$	$g(T_c)$
Standard FSS	0.00	1.0(1)	2.5(2)	$-0.37(2)$	~ 0.65	~ 0.7
	1.00	0.8(1)	2.6(5)	$-0.31(2)$	~ 0.62	~ 0.8
	1.75	0.6(1)	2.6(6)	$-0.30(4)$	~ 0.61	~ 0.8
	2.00	0.5(1)	2.3(2)	$-0.31(2)$	~ 0.54	~ 0.7

Table 1.4: Critical temperature, exponents and critical values of scaling observables ξ_c/L, g calculated via QM $Q_{\partial\beta\xi}(s, T_c(s))$ and $Q_{\chi_{SG}}(s, T_c(s))$ (cols. 2,3 and 4) and via standard FSS analysis of the behavior of $\log \partial\xi_c(L, T_c(L))/\partial\beta$ and $\log \chi_{SG}(L, T_c(L))$ (cols. 5, 6 and 7). *: estimated through QM without $L = 6$. †: not estimated by QM.

top plot one can easily observe that, as the tricritical value of D is approached, $(2.05 < D_{3c} < 2.11)$ for $L = 6$ the curves do not overlap with each other signaling an apparent lack of universality. At large enough sizes, on the contrary, all curves are superimposed (right plot of Fig. 1.10, $L = 20$), demonstrating that universality holds along the whole continuous transition line. Moreover, because of strong FS effects, a crossover occurs and the analysis limited to (or including also) too small sizes can hinder the prediction of the asymptotic behavior. The same effect is clearly visible in Fig. 1.12 (above), where the size dependence of spin-glass susceptibility at criticality is shown. As D increases towards D_{3c}, there appears to be a crossover in the scaling moving from small to large sizes, which induces wrong asymptotic values of the critical indices. Therefore, I did not make use of the small values of L for $D \simeq D_{3c}$, namely $L = 6$ at $D = 1.75$ and $D = 6, 8, 10$ and 12 at $D = 2$, to interpolate the values of the critical exponents, as they induce a wrong estimate as the limit $L \to \infty$ is performed.

As a visual test, in Fig. 1.11, g vs. ξ_c/L is shown for all D and L values employed for our FSS analysis. If the smallest sizes near the tricritical point are discarded, universality appears quite neatly. In Fig. 1.12 (bottom panel) the universal FSS functions F_ξ are parametrically plotted, $F_{\chi_{\rm SG}}$ and F_g, cf. Sec. 1.3, vs.

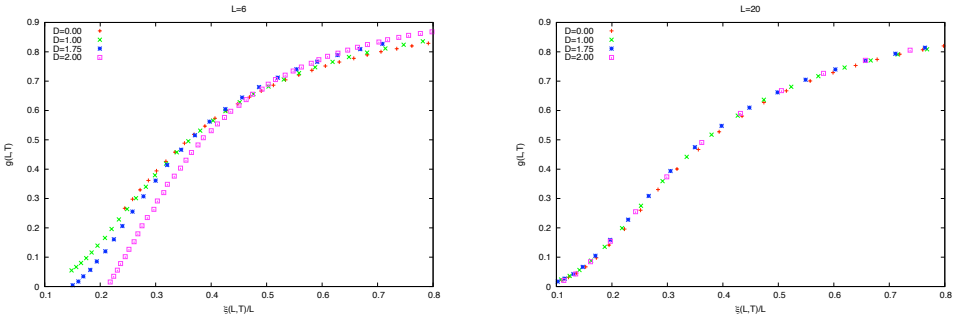

Figure 1.10: Binder parameter $g(L, T_c(L))$ as function of $\frac{\xi(L,T_c(L))}{L}$ in the critical region. Near the tricritiacal point ($D = 2.00$) the effects of finite size is relevant, and one can not use too small sizes to estimate the critical indices.

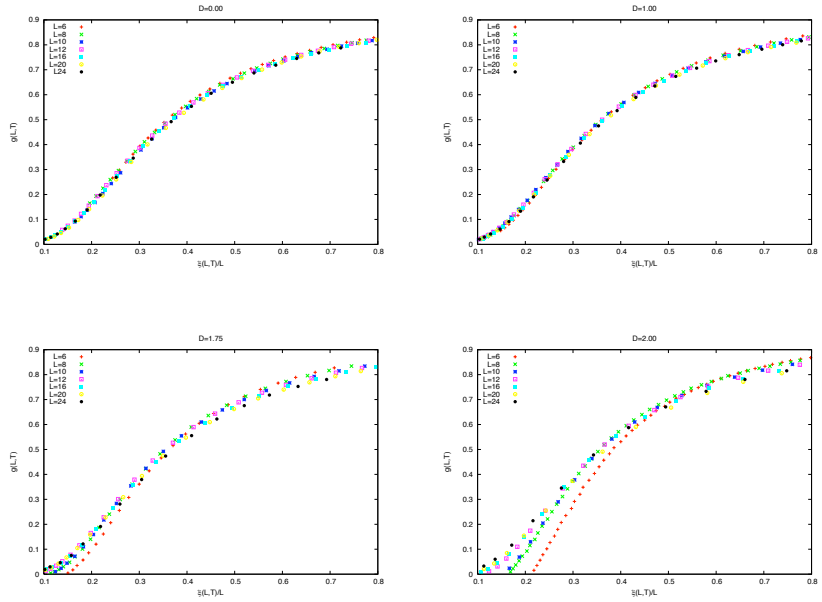

Figure 1.11: Scaling behaviour of $\frac{\chi(2L,T)}{\chi(L,T)}$ and $\frac{\xi(2L,T)}{\xi(L,T)}$ as a function of $\frac{\xi(L,T)}{L}$ for different values of D.

ξ_c/L, as well, for the same simulated systems.

The critical values of the temperature and the exponents η and ν are shown in Tab. 1.4 both for the QM and the canonical FSS methods. Due to the FS cross-over no interpolation was possible with QM at $D = 2$. Only one estimate for

Model	ν	η
SG 3D bd [73]	2.53(8)	-0.384(9)
SG 3D bd [69]	2.22(15)	-0.349(18)
EA 3D [74]	2.39(5)	-0.395(17)
EA 3D [60]	2.15(15)	-0.337(15)
EA 3D [75]	2.00(15)	-0.36(6)

Table 1.5: Critical Indices of EA models in the literature. A complete list can be found in Ref. [74].

the indeces is thus provided. By comparison with estimates of critical exponents summarized in Tab. 1.5, the system appears to be in the same universality class of the Edwards-Anderson model (corresponding to the $D = -\infty$ limit of our model).[60, 70, 71, 72]

In Fig. 1.9 I also plot ξ/L at $D = 2.05$ and $D = 2.11$ for $L = 6, 8, 10, 12$. In the first case, I obtain a $T_c = 0.553(7)$, though no analysis of the critical exponents can be performed because of FS effects. In the latter case, no evidence is found for a second-order phase transition, (cf. Fig. 1.9). As $T \lesssim 0.5$ is approached, moreover, ξ even appears to scale weaker than L. We will see in the following why this comes about.

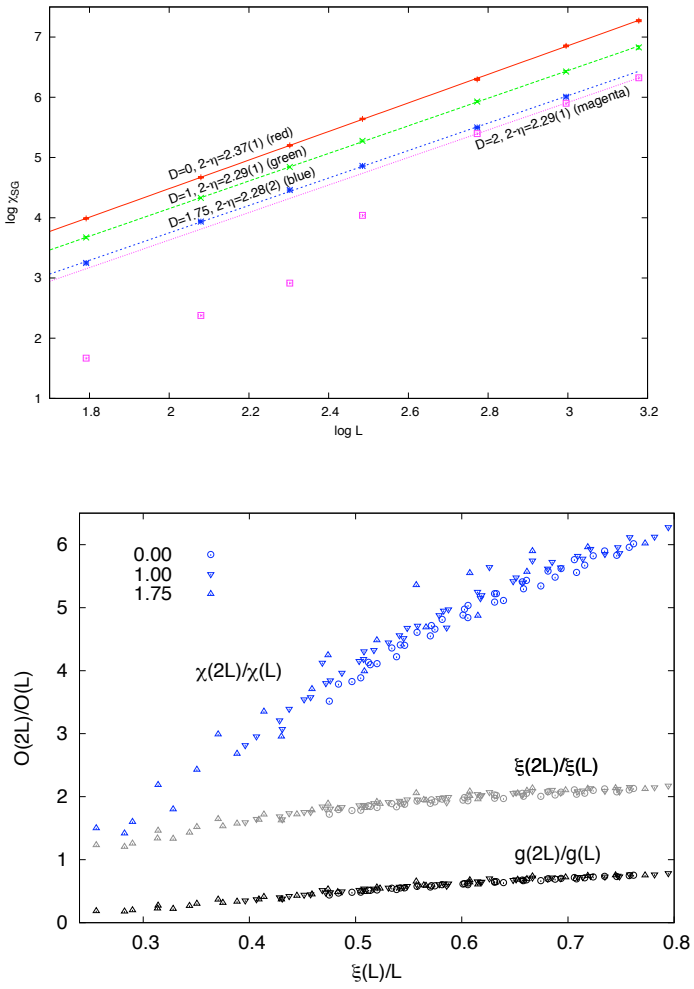

Figure 1.12: For $D = 2.00$ (above), near the tricritical point the quotient method does not yield reliable estimates because of a crossover of the scaling functions in the range of probed sizes. Bottom panel:Scaling behaviour of $F_{\chi_{\rm SG}}$, F_ξ and F_g (top to bottom) vs. $\xi_c(L,T)/L$, cf., respectively, Eqs. (1.3), (1.49), (1.57) and (1.59), at $D = 0, 1$, $L/2L = 6/12, 8/16, 10/20, 12/24$ and at $D = 1.75$, $L/2L = 8/16, 10/20, 12/24$.

1.3.3 Thermodynamic first-order phase transition

Across a second order transition the system undergoes a transformation from a PM pure phase to a SG pure phase. As far as the density distribution $P(\rho)$ is concerned, a pure phase corresponds to a single-peaked distribution. As two peaks appear, the system exists both in PM (low ρ) and SG (high ρ) phases and we are in the neighbourhood of a first-order phase transition. In FS systems the peaks are not Dirac measures, but have finite width becoming sharper and sharper as L increases. At finite L, thus, eq. (1.44) is a good order parameter that drives a first-order transition: when D, T vary, the system undergoes a transition with a discontinuous jump in ρ: the "thermodynamic" average values of ρ are obtained by looking at the peaks of its distribution.

In Fig. 1.13 we show the behaviour of the density distribution through the first-order transition at $T = 0.4$. The FS first-order transition points can be determined with the four methods mentioned in Sec. 1.3.1, as will be shown below. The spinodal lines for a given L are estimated by looking at the values of D at which a secondary peak arises. Since the region of phase coexistence corresponds to an inverse freezing transition, I performed PT simulations at a given finite T, letting D vary. Indeed, in BC-random model, we will see that the first-order transition curve displays a re-entrant behaviour [47, 51] due to the existence of a "fluid" (PM) phase with an entropy lower than that of the spin-glass phase.

For what concerns the estimate of $D_c(T)$ the method of *equal weight* introduced in Sec. 1.3.1, cf. Eq. (1.63) works quite well for data collected at $T \leq 0.4$, because the two peaks are very well separated since their appearence, (cf. Fig. 1.13), and the estimate is robust against reasonable changes of the mid-point ρ_0 (see inset of Fig. 1.13). As T increases towards the tricritical value, however, the PM and SG values of the density approach each other. At $T = 0.5$, cf. Fig. 1.14, we thus have the problem that the density distributions of the two phases overlap also for the largest simulated size. In this case, due to the arbitrary choice of choosing ρ_0, we actually determine the transition point as the D value at which the peaks have the same height. This estimate rough however, gives the same results obtained by fitting the two peaks separately and computing the areas under the interpolating curves. In Tab. 1.6 we report the estimated values of the critical points

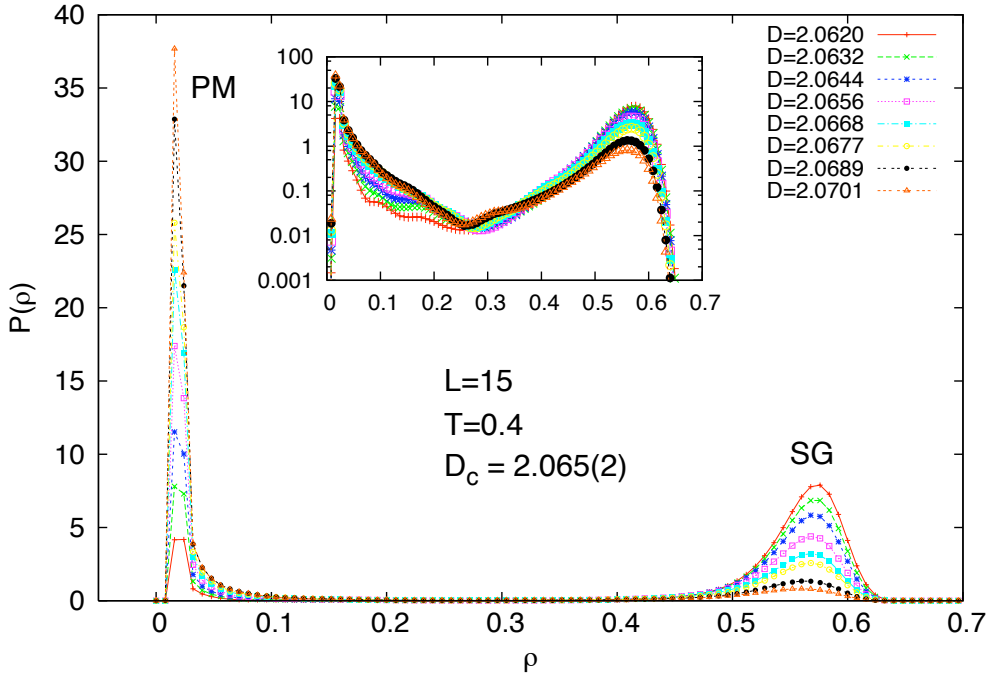

Figure 1.13: Density distribution $P_L(\rho)$, $L = 15$, across the coexistence region at $T = 0.4$: two peaks develop at ρ_{PM} and ρ_{SG}. As D increases the thermodynamically relevant phase (lowest free energy) passes from SG to PM in a first-order phase transition. The dominant phase correpsonds to the one with larger probability, i.e., larger integral of the peak. As the peak at ρ_{SG} vanishes the system is in a purely PM phase. Inset: $P_{15}(\rho)$ on y-Log scale.

obtained by this method for all simulated sizes and temperatures, together with the spinodal points. The spinodals curve are computed through the same methods mentioned above. With a fine-tuning of the external field D, —cf. Tab. (1.6) where the error-bar for the external field is due to the semi-dispersion between two fixed value of D— the spinodal PM (SG) is the first point (D_{sp}, T_{sp}) where a coexsitence of phases appears (ends).

These results can be cross-checked using the methods based on the Maxwell construction, (cf. Sec. 1.3.1). The pure-phase properties $D_{PM,SG}(\rho)$ are interpolated in the coexistence region by a polynomial fitted on those points for which no double peak is present in the distribution $P(\rho)$. At any given L we look at the

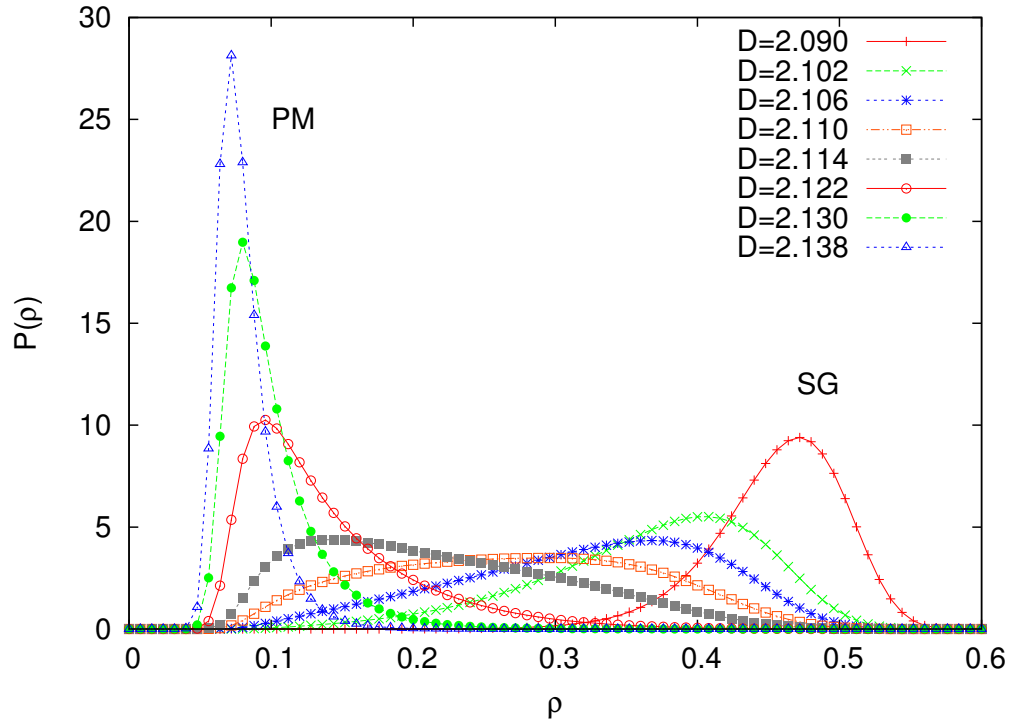

Figure 1.14: $P(\rho)$ in the coexistence region at $T = 0.5$ and $L = 15$. The two peaks are hard tell apart and the coexistence region is rather narrow.

value $D = D_c$, such that (equal distance)

$$\rho_{SG}(D_c) - \rho(D_c) = \rho(D_c) - \rho_{PM}(D_c)$$

and at the value of $D = D_c$ at which the areas between D_c and $D(\rho)$ to the left and to the right of their crossing point are equal, i.e.,

$$\Delta\mathcal{A}(D_c) = \int_0^{\rho(D_c)} d\rho'(D(\rho') - D_c) - \int_{\rho(D_c)}^1 d\rho'(D(\rho') - D_c) = 0. \tag{1.67}$$

1.3.4 Phase diagrams and inverse freezing

Phase diagrams are plotted in Fig.1.15. In the D, T plane we observe a pure SG phase at low T and $D \lesssim 2$. The continuous transition to the pure PM phase

T	D_c	D_{SP}^{PM}	D_{SP}^{SG}
0.2	2.0031(1)	1.9833(2)	2.024(1)
0.3	2.032(3)	2.015(1)	2.043(5)
0.4	2.060(1)	2.046(2)	2.092(5)
0.5	2.106(1)	2.097(4)	2.143(4)

Table 1.6: Results of the first-order phase transition: a fine tuning of the parameters $\{D_i\}$ is needed in order to establish the critical values D_c, D_{SP} and D_{SG}.

T	$D_c[P(\rho)]$	$D_c[\rho_{\rm ed}]$	$D_c[\Delta\mathcal{A}=0)]$	$D_c[\zeta=0]$
0.2	2.0031(1)	2.0033(2)	2.0031(2)	1.991(2)
0.3	2.032(3)	2.031(2)	2.030(1)	2.020(2)
0.4	2.060(1)	2.060(1)	2.058(1)	x
0.5	2.106(1)	2.103(3)	2.102(1)	x

Table 1.7: Evaluation of the first-order critical point with the method of equal weight (col. 2), equal distance (col. 3), equal area (col. 3) and zero skewness.

is denoted by a full line connecting the five numerical estimates of T_c obtained by simulations at $D = 0, 1, 1.75, 2$ and $D = 2.05$. No evidence was found of a continuous phase transition at $D = 2.11$. Beyond $(D, T) = (2.05, 0.53(2))$ a tricritical point is present. Beside changing to a first-order transition, for lower T also a re-entrant behaviour in the $T_c(D)$ line occurs. The hottest first-order point for which we have an estimate is $(D, T) = (2.109(2), 0.5)$. In the top inset of Fig. 1.15(left panel) a detail of the phase coexistence region is plotted (inside the grey-dotted lines). In Fig. 1.15(right panel) we plot the (ρ, T) diagram. Below $T = 0.53(2)$ no pure phase exists with an average ρ in between the dashed-grey curves. The mean-field and the three-dimensions model are compared in Fig. 1.16.

The IF takes place between a SG of high density to an almost empty PM (e.g., at $T = 0.4$, in the coexistence region $D \in [2.046(2) : 2.092(5)]$, $\rho_{SG} \simeq 0.52$ and $\rho_{PM} \simeq 0.03$). The few active sites do not interact with each other but only with inactive neighbours. This induces zero magnetization and overlap. The corresponding PM phase at high T has, instead, higher density (e.g., $\rho_{PM}(D = 2, T = 0.6) = 0.4157(2)$, $\rho_{PM}(D = 2.11, T = 0.6) = 0.596(2)$) and the paramagnetic behavior is brought about by the lack of both magnetic order (zero magnetization) and

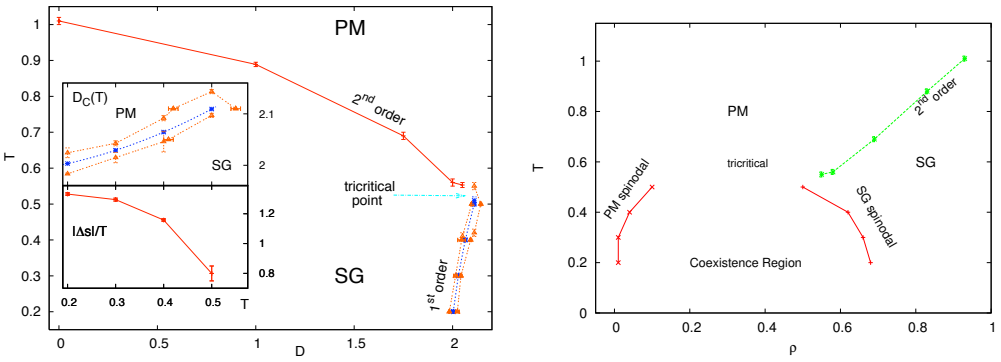

Figure 1.15: Phase diagram in D, T (right panel): a second-order transition and an inverted FOTP occur. In the latter case also the spinodal lines are reported (dashed). Bottom inset: latent heat $|\Delta s|/T$ along the first order line. Top inset: detail of IF region, interpolation of transition line $D_c(\infty, T)$ (dotted), spinodal lines (dashed). The error bars are the FSS of the minimal interval in T and D at each L needed to identify the crossings in ξ_c/L curves (for continuous transitions) or compare the areas under $P_N(\rho)$ for FOPT. Left panel: phase digram in T, ρ plane.

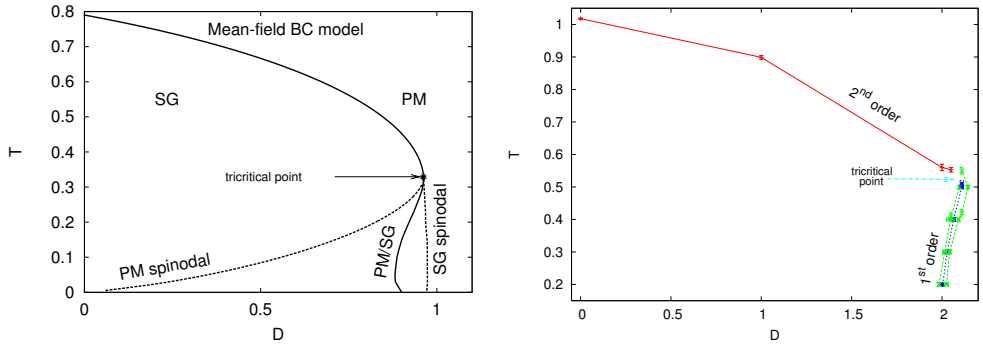

Figure 1.16: Left panel: the phase diagram of the BC model with quenched disorder for the fully-connected lattice with Gaussian distribuited random couplings (MF solution [66, 76]): the Second Order Phase Transition ends in a tricritical point where an Inverse Freezing First Order Phase Transition takes place. The variance of $P(J_{ij})$ in the MF model was $\propto 1/z$, z being the number of sites connected to each spin. In the 3D model, where $z = 6$ (right panel), a bimodal distribution has been chosen with variance 1 rather than $\propto 1/6$.

blocked spin configurations (zero overlap). Using Eq. (1.62), knowing $\Delta\rho$ and the numerical estimate of dD/dT we are able to evaluate the latent heat employed

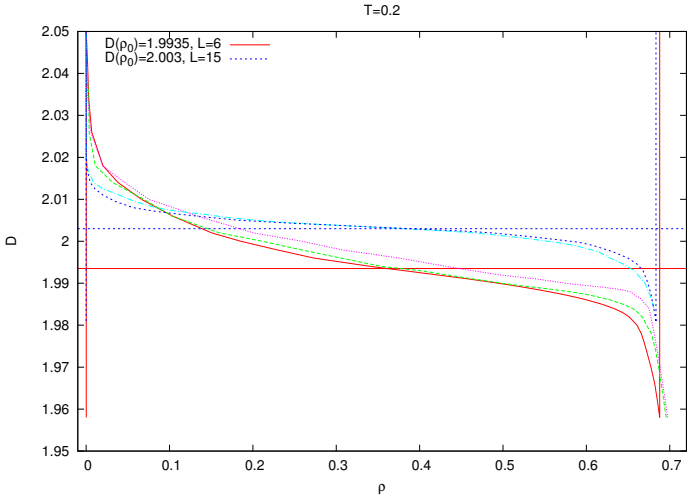

Figure 1.17: Maxwell construction at $T = 0.2$ in the ρ, D plane. $L = 6, 8, 10, 12, 15$ from bottom to top as $\rho \gtrsim 0.6$ (right). The almost vertical curves at small and large density sides are the interpolated pure phase (PM left, SG right) behaviours. As an instance the critical D values for the equal-distance construction are plotted at $L = 6$ (lower horizontal line) and at $L = 15$ (higher horizontal line).

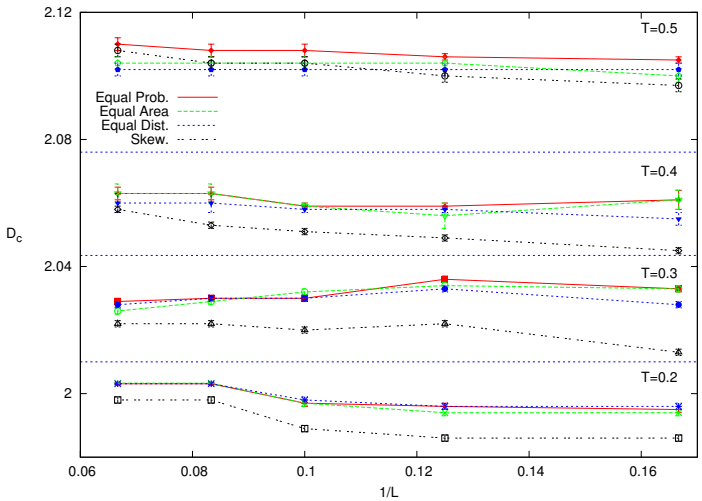

Figure 1.18: Estimates of D_c vs. $1/L$ for $L = 6, 8, 10, 12, 15$ at $T = 0.2, 0.3, 0.4, 0.5$ (bottom up) obtained by the four methods described in Sec. 1.3.1.

in the transition, plotted as a function of the temperature in the bottom inset in Fig. 1.15.

We have a phase doagram quite similar to the MF scenario: in fig. (1.16) the

two phase diagram —three dimensions and mean-field— are shown. The figure can not give a detailed compering because in the MF solution the disorder is Gaussian distribuited: the shape of propability distribution of the disorder changes quantitatively the position of the critical curves. Moreover, as we can see, the coexistence region is very small in three dimension in comparison with MF.

In conclusion, the thermodynamical fluctuations due to the finite dimension do not changes the sign of the slopes of the transition curves. In particular, in three dimension, the first-order phase transition is still an IT.

1.4 Nature of the SG phase.

As we have seen in sec. (1.2), in mean-field the SG phase of the disordered BC model, shows the same features of the Sherrington-Kirkpatrick model [56]. In order to obtain a stable thermodynamics the Full RSB scheme is needed [76, 66]. On the other hand, out of the limit of validity of the mean-field regime, it is still unclear if the properties of SG phase are in agreement with the RSB scenario. Parisi solution predicts a function $q(x)$ as order parameter which leads to a non-trivial distribution $P(q)$ for the overlap. In MF $q(x)$ is fixed self-consistently, and is related to $P(q)$ through the relation

$$\frac{dx(q)}{dq} = P(q) \tag{1.68}$$

The low T, D phase is characterized by a pure spin-glass phase. What this phase consists of in terms of statistical mechanical states is the subject of the following analysis. Three cases are contemplated in the literature in the thermodynamic limit.

Droplet theory: there exists only one SG state (plus its symmetric spin-reversed). Therefore, the overlaps between states in different replicas cannot fluctuate among different disordered samples and the distributions are delta-shaped [77]. The four-spins correlation function in the position space $\mathbf{r} = (x, y, z)$ should tend to a plateau $C_4(|r|) = q_{\mathrm{EA}}^2$, for large enough $|r|$, that becomes larger and larger as T decreases towards T_c [78].

Trivial-Non-Trivial (TNT) scenario: there are many equilibrium states non-trivially organized (i.e., q_s fluctuates from sample to sample), but the excited states are droplet-like (i.e., the q_l overlap, sensitive to interfaces, fluctuates less and less as the size grows). This implies that the distribution $P(q_s)$ is broad and non-trivial, whereas $P(q_l)$ is delta-shaped [79]. Since excitations are trivial, the expected behaviour of $C_4(x, y, z)$ is the same as for the droplet theory.

Replica Symmetry Breaking (RSB) theory: many states characterize the SG phase, with space-filling excitations; both distributions are broad and have a complex structure [52, 55]. The correlation $C_4(x, y, z)$ is expected to decay continuously to zero (the minimum squared overlap for the present system, in absence of an external magnetic field) at all T [80, 81, 82].

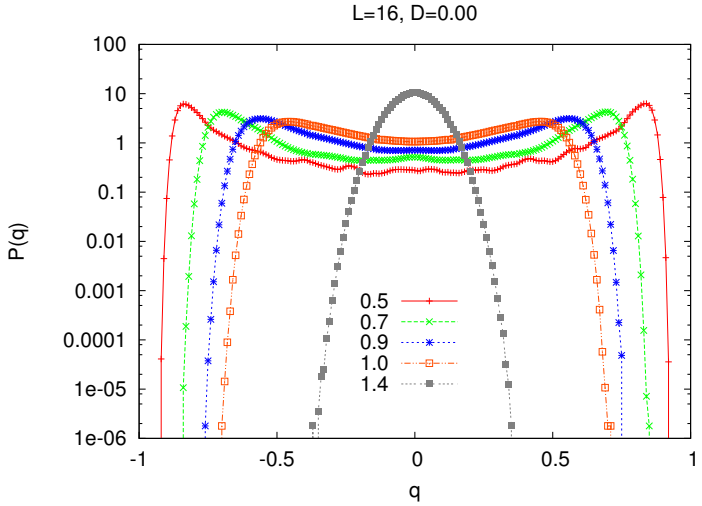

Figure 1.19: Behaviour of the overlap distribution $P(q)$ through the second-order phase transition in the low-temperature phase for $L = 16$.

I will consider first the overlap distribution functions, cf. Eqs. (1.42)-(1.43), since, in the spin glass-phase ($T < T_c$), the site and link overlap distributions — $P(q_s)$ and $P(q_l)$ — can be used as hallmarks to discriminate among different theories for finite-dimensional spin glasses. In the next sectionthe four spin correlation functions will be analyzed.

In order to see whether a finite size $P(q_s)$ is compatible with a trivial distribution in the thermodynamic limit we need to estimate whether, for growing sizes its support shrinks to a single value, the Edwards-Anderson parameter $q_{\rm EA}$ or stays wide. In our case, for a null magnetic field, the support of a non-trivial $P(q_s)$ should range from $q_s = 0$ to $q_{\rm EA}$. In Fig. (1.19) we plot $P(q_s)$ at $D = 0$ and size $L = 16$ for all simulated temperatures: as T decreases $P(q_s)$ moves from a Gaussian to a bimodal distribution. The important issue is, then, whether the continuous part between the two peaks at low T goes to zero or not as L increases. In Fig. (1.20), we plot $P(q_s)$ at the lowest thermalized temperature for $L = 6, 8, 10, 12$ and 16 and, in the inset, we plot the values of $P_L(0)$ displaying no decreasing trend with increasing L in the range of simulated sizes. The states, therrefore, appear to be many and different from each other, since they are found with a finite probability within a non-zero continuous range of overlap values, including $q_s = 0$. Also $P(q_l)$ appears to develop a second peak at small q_l as L increases: this signature becomes

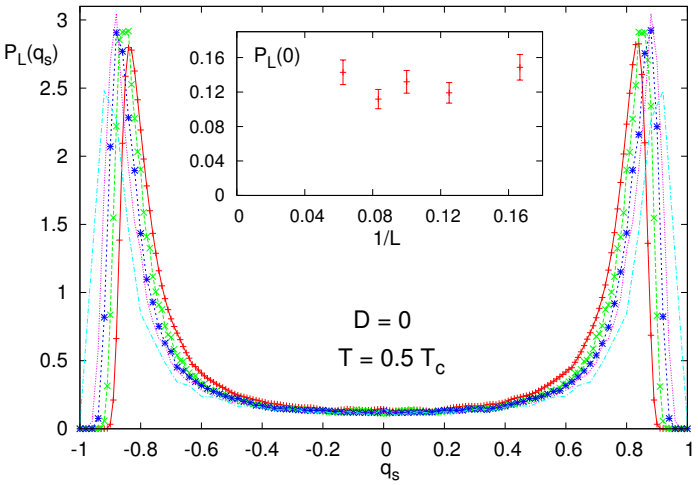

Figure 1.20: Site overlap distribution $P_L(q_s)$ at $T = 0.5$, $D = 0$ for $L = 6, 8, 10, 12, 16$. Inset: $P_L(0)$ vs. $1/L$ does not tend to zero.

clearer and clearer at low temperature, (cf. Fig. 1.21). The analysis of FSS of the variance of $P(q_l)$ might help to better evaluate the breadth of the distribution in the thermodynamic limit. Its behaviour for various sizes is exemplified in the inset of Fig. 1.21 at the lowest thermalized T/T_c for $D = 0$. The variance tends to a small finite value and we cannot make a definitive statement about the finite size $P(q_l)$ tending towards a delta distribution, as conjectured by the TNT scenario in the thermodynamic limit. Moreover, the study of the variance does not yield any indication on the *shape* of the distribution, in particular, on the FSS behavior of the two peaks expected in RSB theory.

1.4.1 Equivalence between the site and link overlap distributions

We can, then, implement a more refined analysis of the pdf data and check whether $P(q_s)$ and $P(q_l)$ are actually equivalent and, thus, if the non-triviality of the former implies the non-triviality of the latter. This can be realized by recalling that in the SK model $q_l = q_s^2$ and by comparing the finite L $P(q_l)$ to the distribution $Q(q_a)$ of

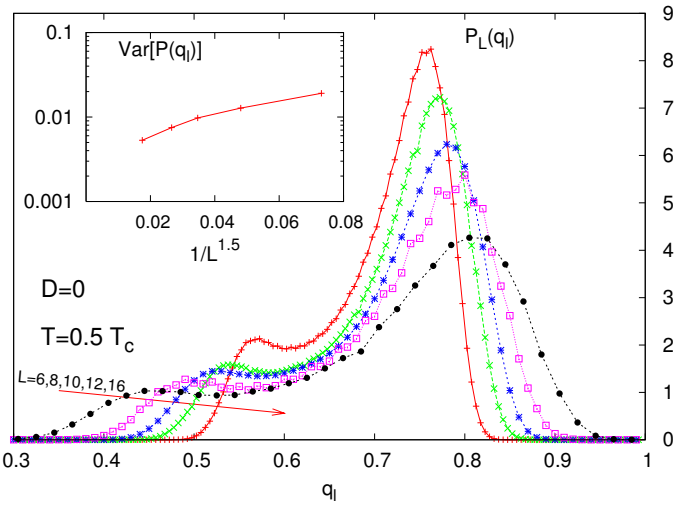

Figure 1.21: Link overlap distribution $P_L(q_l)$ at $T = 0.5$, $D = 0$ for $L = 6, 8, 10, 12, 16$. Inset: Variance vs. $1/L$ tends to a very small value $\sigma^2_{q_l} = 0.0010(7)$ as $L \to \infty$ interpolating with a power-law (1.5(1)).

an auxiliary variable [82]

$$q_a \equiv A + Bq_s^2 + z\sqrt{1 - q_s^2} \tag{1.69}$$

with z a Gaussian random variable of variance σ_z and zero mean, that mimics the presence of fluctuations due to the finite size of the considered systems.

At a given point of the phase diagram D, T and for a given size L, the parameters $A(L)$, $B(L)$ and $\sigma_z(L)$ can be obtained by minimizing the Kullback-Leibler divergence [83] (KLD)

Given two distributions $P(a_i)$ and $Q(a_i)$ of a discrete random variable a_i, KLD is a non-symmetric measure of the difference between P and Q. KLD divergence is defined as

$$D_{\mathrm{KL}}[P, Q] = \sum_i P(a_i) \log \frac{P(a_i)}{Q(a_i)} = S(P) - S(P|Q) \tag{1.70}$$

where $S(P)$ is the entropy of the distribution P and $S(P|Q)$ is called cross entropy of P and Q. Through KLD we can check if the two distributions encoded the same informations.

KLD between $P(q_l)$ and $Q(q_a)$ reads

$$D_{\rm KL}[P,Q] = \sum_{i=1}^{N_{\rm bin}} P(q_i) \log \frac{P(q_i)}{Q(q_i)} \tag{1.71}$$

We will refer to this as "left" KLD. The "right" KLD is the same formula exchanging P and Q, where the symmetrized divergence (sKLD) between $P(q_l)$ and $Q(q_a)$ is defined as:

$$D_{\rm KL}[P,Q] = \frac{1}{2} \sum_{i=1}^{N_{\rm bin}} \left[P(q_i) \log \frac{P(q_i)}{Q(q_i)} + Q(q_i) \log \frac{Q(q_i)}{P(q_i)} \right] \tag{1.72}$$

In Fig. 1.22, we plot the finite size values of A and B parameters. Besides the values of the parameters minimizing the symmetrized KLD, Eq. (1.72) we also plot the values of A and B minimizing the left and the right unsymmetrized KLD's. We observe that, as L increases the spread between different estimates tends to vanish. The infinite size limit of σ_z is always compatible with zero, signaling that FS effects actually tend to vanish as L increases, though with large statistical errors at low temperature, implying that smaller sizes might hinder a correct FSS.

As instances we plot the matching of the two distributions $Q(q_a)$ and $P(q_l)$ in Figs. 1.23 at $T = 0.5 \simeq 0.5 T_c$ and $T = 0.7 \simeq 0.7 T_c$ at size $L = 16$ and $D = 0$. In the insets we plot the size behaviour of A and B from the sKLD for the two specific cases. In the first case, a power-law FSS scaling to $L \to \infty$ gives for B a negative value! In the second case the $L \to \infty$ limit yields a positive value. This observation contrasts with the behaviour, in the bottom panel of Fig. 1.22, of $B(T)$ growing with decreasing T at all fixed sizes. Quite evidently, the low L strong fluctuations strongly bias the interpolation at small T. To show this in a clearer way, in Fig. 1.24 the asymptotic values of both A and B are plotted for all simulated temperatures both from the sKLD and as the average of the extrapolation of the values minimizing the right and left unsymmetrized KLD's. With $A_\infty(T)$ the two estimates appear to be consistent at all temperatures and reproduce the qualitative behaviour detected for all finite L cases, (compare with Fig. 1.22). For $B_\infty(T)$, at low T the two estimates are not consistent anymore. Moreover, $B_\infty(T)$ decreases with T below a certain $T \simeq 0.7$, unlike its finite L counterparts (at least

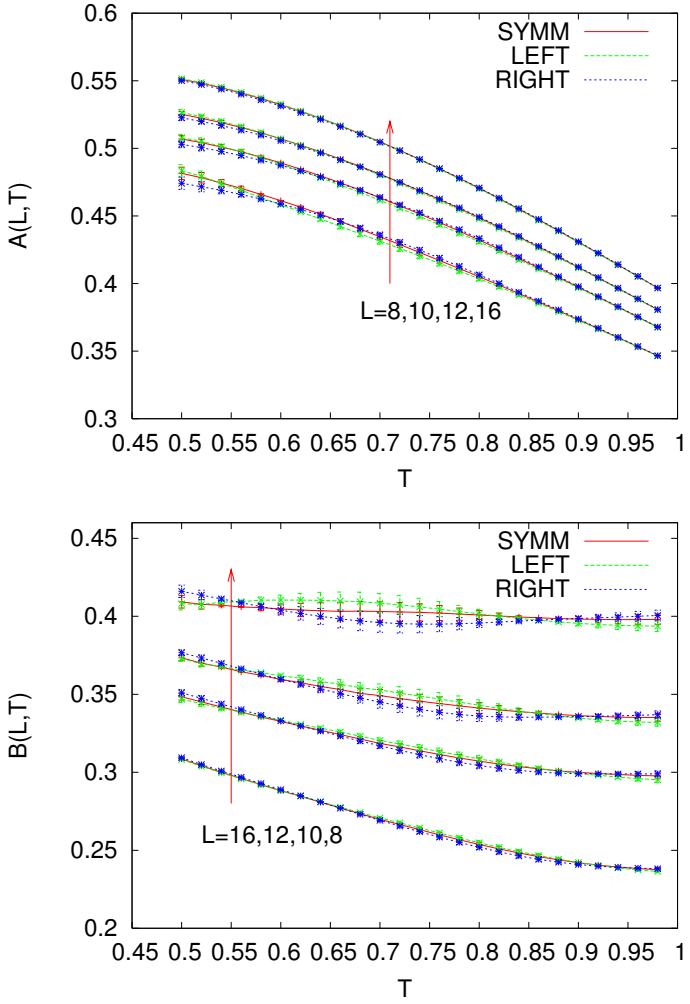

Figure 1.22: Parameter A (top) and B (bottom) of $q_{\rm a}$ vs. T for $L = 8, 10, 12, 16$ as obtained minimizing the left, right and symmetric Kullback-Leibler divergence.

as $L \geq 10$), cf. Fig. 1.22.

We face strong finite-size effects and a crossover between small and large sizes is taking place. However, due to the fact that we cannot easily thermalize larger systems at low temperature, we cannot make any definite statement on the behaviour of $B_\infty(T)$ for very low T. We simply do not have enough reliable points in L at our disposal. The finite size behavior, though, strongly suggests that $Q(q_a)$ and $P(q_l)$ are indeed equivalent even below $T = 0.7$. In any case, the equivalence is proven for $T \geq 0.7$, this implies that not only the equilibrium states but also

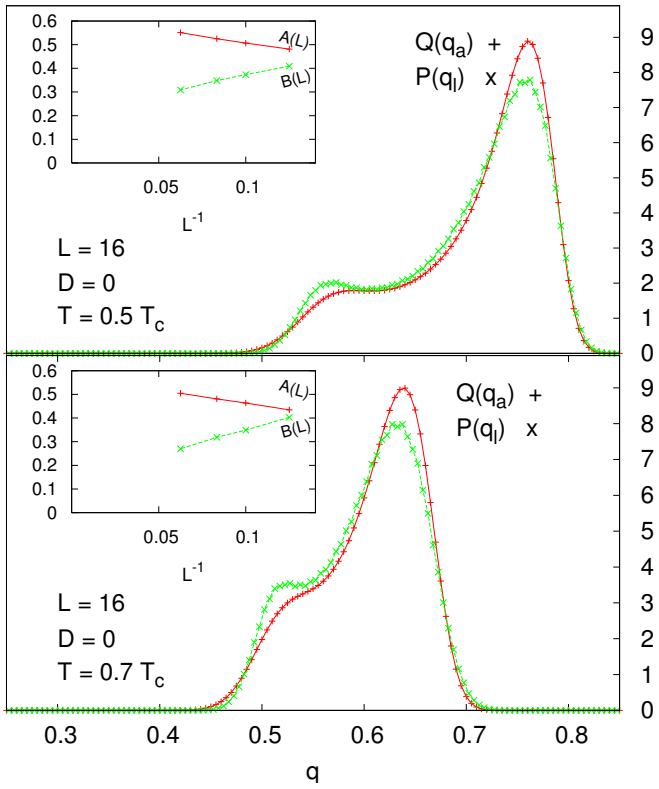

Figure 1.23: The distributions $Q(q_a)$ and $P(q_l)$ at $T = 0.5 \simeq 0.5T_c$ (top) and $T = 0.7 \simeq 0.5T_c$ (bottom), $D = 0$ for an optimal choice of parameters obtained by minimizing sKLD, cf. Eq. (1.72). Inset: FSS behavior of the parameters $A(L)$ and $B(L)$ of the sKLD between $Q(q_a)$ and $P(q_l)$ at $D = 0$ and $T = 0.5 \simeq 0.5T_c$. Sizes are for $L = 6, 8, 10, 12, 16$.

their excitations have a non-trivial distribution, providing evidence in favour of the third scenario considered, the RSB theory, rigorously valid in mean-field systems.

1.4.2 Position Space Four-Spins Correlations

We now investigate the behaviour of the four-spin correlation function, defined in Eq. (1.46), in position space. We recall that the droplet and TNT theories predict that $C_4(x)$ tends to a plateau of height $q_{\rm EA}^2$, [78] whereas the RSB theory predicts a power-law decay $\sim x^{-\alpha}$ for $C_4(x)$ at $T < T_c$[80]. We, thus, have to compare our data with the prediction of one of these hypotheses.

Since we are dealing with small systems, we must first consider possible FS

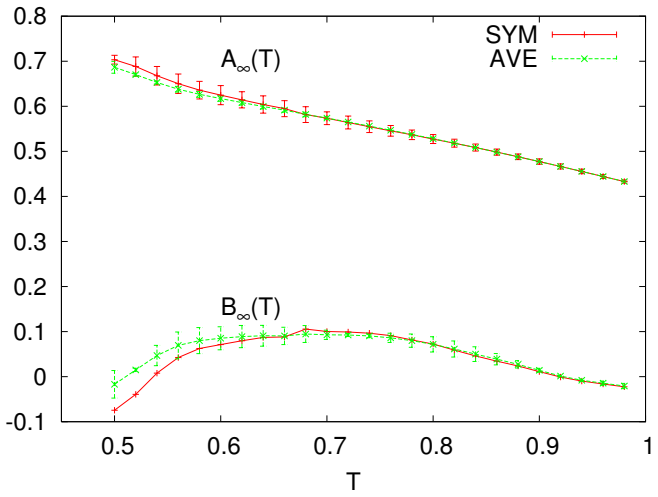

Figure 1.24: FSS limit $L \to \infty$ of A and B parameters vs. T.

effects. Indeed, because of the periodic boundary conditions imposed on the simulated system, the correlation function that we actually measure at a distance x also contains the contribution of correlations at distance $x + kL$, with $k = 1, \ldots, \infty$. The true (yet unknown) correlation function $\mathcal{C}_4(x, y, z)$ is related to the measured one – $C_4(x, y, z)$ – by the relation:

$$C_4(x, y, z) = \sum_{k_x, k_y, k_z}^{0,\infty} \mathcal{C}_4(x + k_x L, y + k_y L, z + k_z L) \tag{1.73}$$

For large distances, when C_4 is small, these extra contribution will strongly bias the estimate of the true $\mathcal{C}_4$ behaviour in space. In particular, correlations at larger distances, of the order $L/2$, will experience relatively stronger systematic errors than $C_4(|r| \ll L)$.

We will now present our results for the case $D = 0$. For temperatures down to the critical region, I simulated lattices whose side length was up to $L = 24$. The largest thermalized size for T down to $0.5T_c$ is, instead, $L = 16$. In Fig. 1.25 we plot the x behavior at $T = 1.5$ in a log-log plot for the sizes $10, 12, 16, 20, 24$. One can observe that FS effects are confined to the last point at $L/2$. The rest of the curves completely superimpose.

At high temperature, correlations are expected to decay exponentially at large

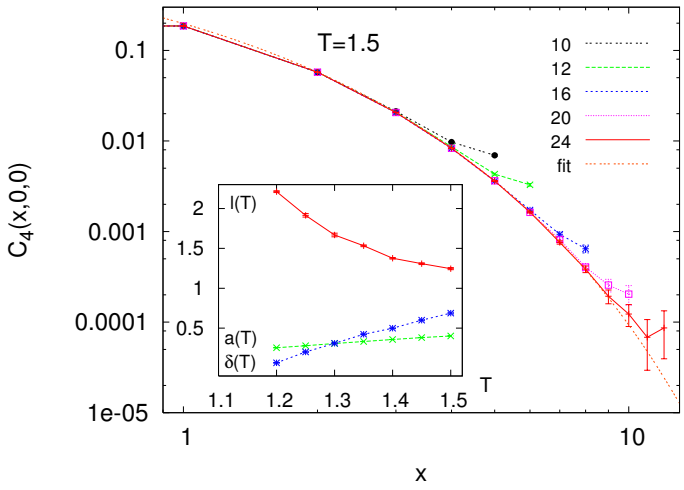

Figure 1.25: Correlation between local overlap for $D = 0$ and sizes $L = 10, 12, 16, 20, 24$, at the largest simulated temperature $T = 1.5$. The fit with Eq. (1.74) is also plotted.

enough distances. As temperature is lowered towards criticality the $C_4(x)$ should become power-law, decaying eventually as $x^{-d+2-\eta}$ at $T = T_c$. We, then, interpolate the four-spin correlation function along the x-axis at criticality with the function:

$$C_4^{\rm fit}(x) = a x^{-\alpha} \left[1 + \left(\frac{x}{\ell} \right)^{-\delta\alpha} e^{\delta x/\ell} \right]^{-1/\delta} \tag{1.74}$$

and equivalently for y and z, due to the isotropy of the system in absence of an external field. This is a function containing a crossover between a short distance power-law decay, $x^{-\alpha}$, and an exponential decay, with characteristic 'correlation' length ℓ. In Fig. 1.25 the function interpolating the $L = 24$ $C_4(x, 0, 0)$ is plotted with $a = 0.402(9)$, $\delta = 0.69(1)$, $\ell = 1.25(1)$ with $\chi^2 = 0.088$. As the temperature decreases the correlation length increases until it becomes too long to be observed in the considered systems. In the inset of Fig. 1.25 we plot the T behavior of ℓ, α and δ until the fit becomes inconsistent, namely for $T \simeq 1.15$.

In Fig. 1.26 we plot the C_4 curves at $T \simeq T_c$ for sizes $L = 10, 12, 16, 20, 24$, as well as the interpolation of the latter with $Ax^{-\alpha}$ (the correlation length is too long to detect the exponential contribution in Eq. (1.74)). The estimated exponent of the interpolating function equals the power at criticality $\alpha = d - 2 + \eta = 0.64(1)$

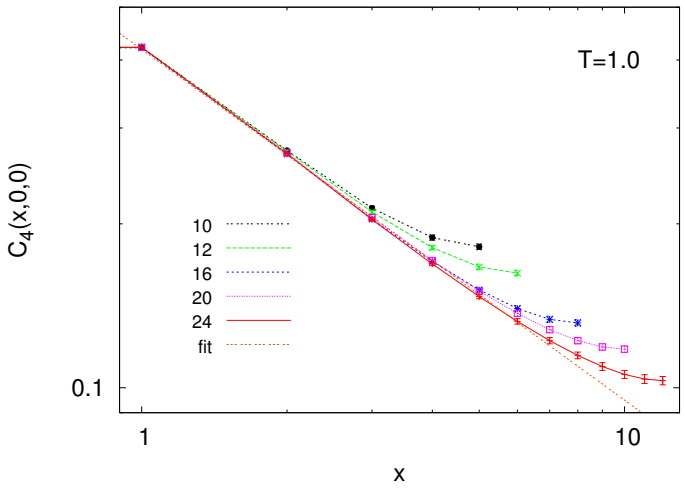

Figure 1.26: Behaviour of $C_4(x)$ at $D = 0$, for $L = 10, 12, 16, 20, 24$ and $T = 1 \simeq T_c$. The interpolation with a simple power-law, $\alpha = 0.64(1)$, is shown for $L = 24$. On shorter systems: $\alpha = 0.64(1), L = 20$ and $\alpha = 0.65(2), L = 16$.

(at crystal field $D = 0$ it was $\eta = 0.36(1)$, cf. Tab. 1.4). At $T = 1$ the interpolated value of α for the $L = 24$ $C_4(x)$ curve is $\alpha = 0.64(1)$, $\alpha = 0.65(2)$ for $L = 16$ and $\alpha = 0.64(1)$ for $L = 20$. FS effects, which how appear to be stronger than in Fig. 1.25, are evident also for $x < L/2$ (only points for $x \leq L/4$ actually stay on the $x^{-\alpha}$ curve).

As $T < 1.2$, approaches T_c (cf. Fig. 1.27), it is impossible to detect a crossover between power-law and exponential decay and the simple power-law decay. The power behavior in T is shown in the inset and compared with the power at criticality, $\alpha = 0.65(1)$.

For lower temperature, Fig. 1.28 shows that the behaviour is power-law until $x \sim L/4$ is reached. At that point, curves deviate upwards as they did at criticality and even at high temperature, (cf. Fig. 1.25). This deviation, however, is an artifact due to the contributions induced by the periodic boundary conditions. On the right side of Fig. 1.28, we show the values of $q^2_{\rm EA}$ at the same temperatures and size of the plotted $C_4(x)$. At all temperatures $C_4(x)$ soon decays below the corresponding value of $q^2_{\rm EA}$. For the sizes simulated, our data are, thus, not consistent with the observation of a plateau at $q^2_{\rm EA}$ in the thermodynamic limit, as predicted by the droplet and TNT theories.

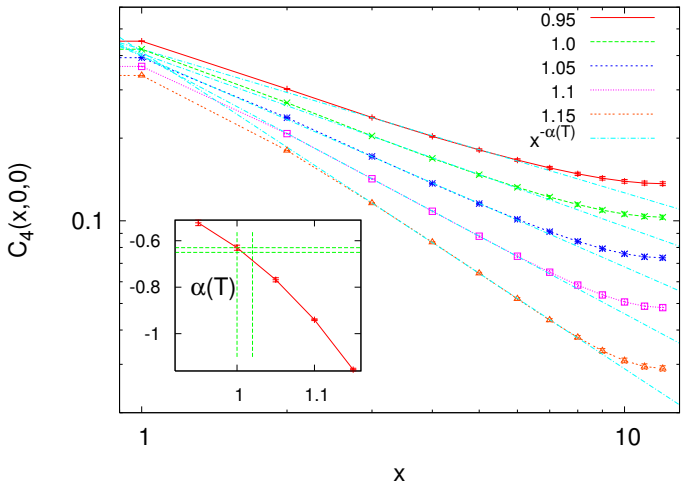

Figure 1.27: Behaviour of $C_4(x)$ for $L = 24$ and $T = 0.95, 1, 1.05, 1, 1.15$. The interpolation with a simple power-law is also shown for $L = 24$. Inset: behaviour of the power α vs. T. Vertical and horizontal dashed lines denote, respectively, the estimates of $-d+2-\eta$ and T_c (with errors: $T_c = 1.01(1)$, $\eta = -0.36(1)$, (cf. Tab. 1.4)).

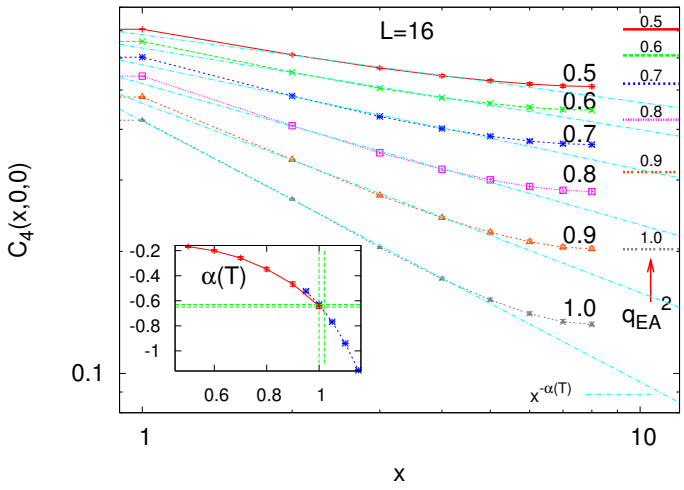

Figure 1.28: Behaviour of $C_4(x)$ for $L = 16$ and $T = 0.5, 0.6, 0.7, 0.8, 0.9.1.0$. The interpolation with a simple power-law is also shown.Values of $q^2_{\rm EA}(T)$ are displayed on the right side. Inset: behavior of the power α vs. T (full line), compared to the $\alpha(T)$ behaviour around criticality for $L = 24$ (dotted line).

1.4.3 Order-parameter distributions across transitions

Fig. (1.29) (left panel) presents the distribution of overlap $P(q)$ for a system of linear size $L = 16$ and $D = 0$. As alredy mentioned, across the second-order phase transition [75] it changes between the PM and SG phase from a Gaussian to a doubly peaked distribution

$$P_{SG}(q) \propto \delta(q - q_{EA}) + \delta(q + q_{EA}) + f(q, L) \,, \tag{1.75}$$

where $f(q, L)$ is a continuous function depending on the size. The right panel shows the behaviour of $P(\rho)$ at fixed values of the crystal field and different temperatures: at low temperature, deep in the SG phase, the average number of active sites is close to one:

$$\lim_{T\to 0} \overline{\langle \rho \rangle} = \int_0^1 d\rho \, P(\rho, T) \, \rho \sim 1 \,. \tag{1.76}$$

The distribution $P_L(\rho)$ does not change shape across this transition.

Beyond the tricritical point, first-order phase transition takes place and the system undergoes a discontinuous transition between an "inactive" PM phase ($\overline{\langle \rho \rangle} \equiv \rho_m \sim 0$) and an "active" SG phase ($\rho_m \neq 0$).

What happens to the overlap pdfs? In the coexistence region, we can write $P(q)$ as the sum of two contributions, i. e.,

$$P(q) = P_{SG}(q) + P_{PM}(q) \,. \tag{1.77}$$

For the PM contribution we have a Gaussian strongly peaked at $q = 0$. The $P_{SG}(q)$ consists of a doubly (trivial) peaked distribution with a continuum (non trivial) part between the two peaks. Fig. (1.30) shows the behaviour of $P(q)$ at different temperatures across the FOPT. In the coexistence region, besides the double peak with a continuous part of the SG phase, a peak in $q = 0$ appears, due to the large number of empty sites.

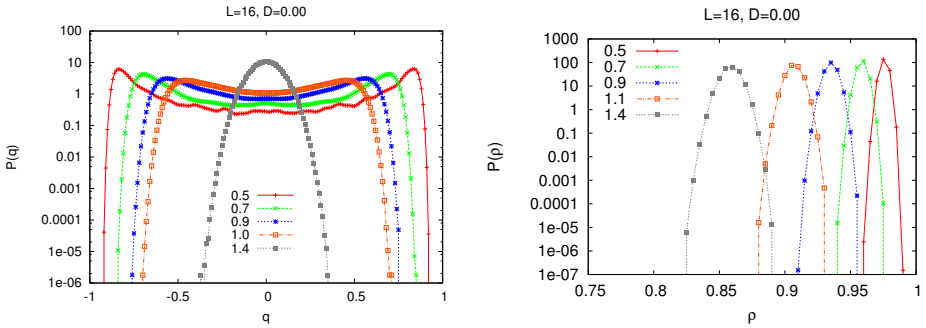

Figure 1.29: $P_L(q)$ and $P_L(\rho)$ for $L = 16$ and $N_J = 1500$ at $D = 0.00$. Across the transition $P(q)$ (left panel) changes continuously from a Gaussian (in the high-temperature phase) to a doubly peaked distribution with a continuum part between the peaks. In this region of the phase diagram the FOPT does not take place: $P(\rho)$ does not change its shape (right panel).

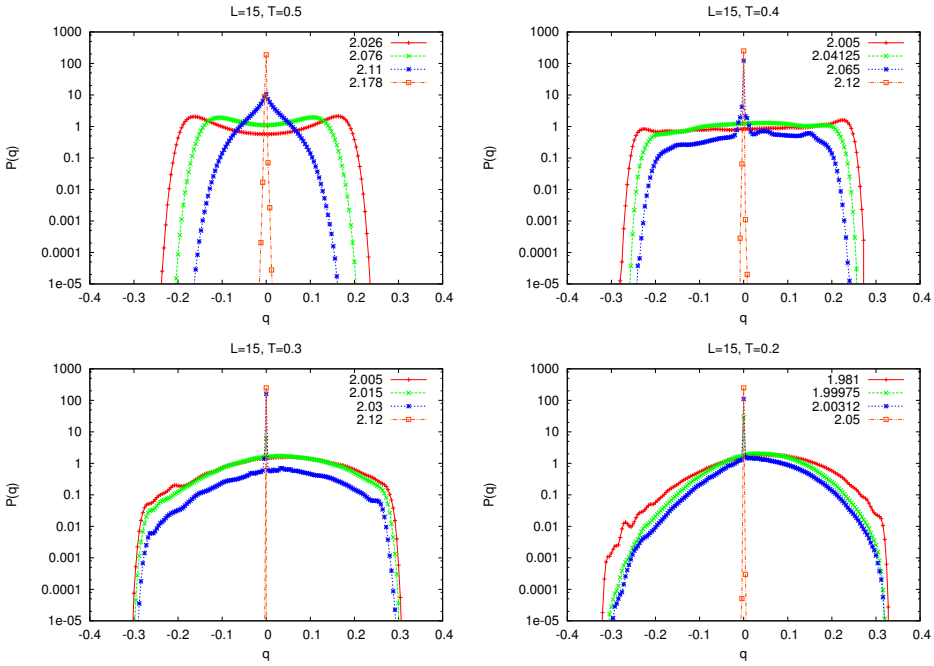

Figure 1.30: $P(q)$ across the FOPT at fixed T and different D values: we have a coexistence region between the phases SG and PM. The PM phase contributes to the $P(q)$ distribution with a Dirac component $q = 0$.

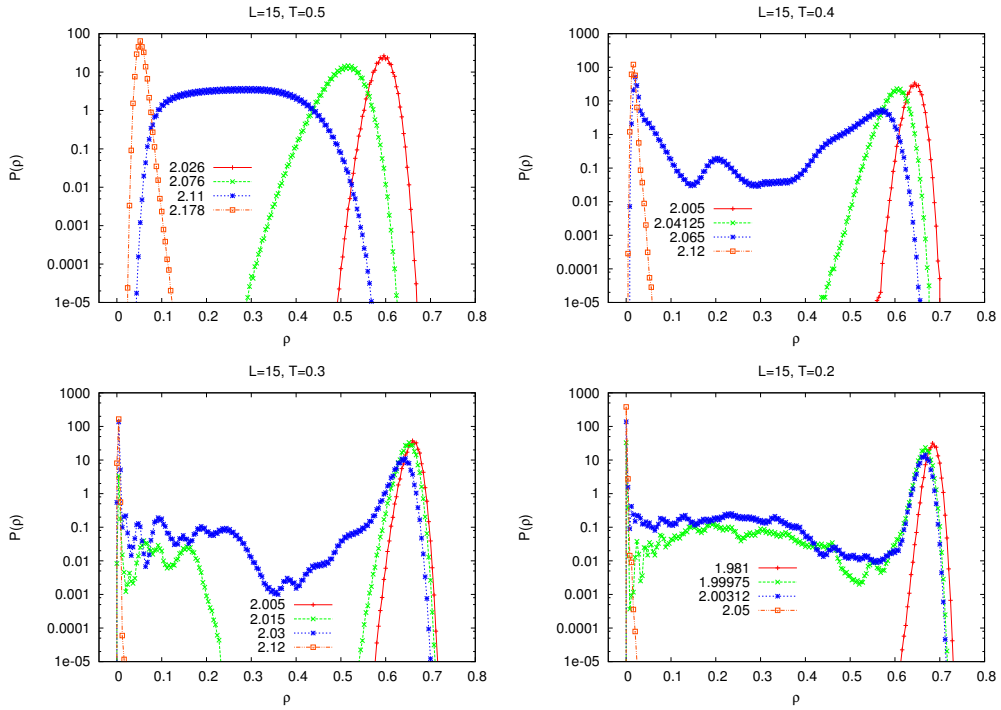

Figure 1.31: $P(\rho)$ during the first-order phase transition: a double peak is the signature of coexistent phases: when the system is in a pure phase, we have a single peak.

1.5 Conclusions

The intensive study of the BC-random in three dimensions has confirmed the phase diagram of the mean-field model. In particular, fluctuations due to finite dimension do not change the slope of the CC equation along the first-order phase transition. Therefore, an IT takes place between a SG phase and a PM phase. The fist-order phase transition is driven by the density: the PM low-temperature phase is less interactive and less entropic of the SG phase and the system undergoes an IT. The IT is first order in the thermodynamic sense, i. e., latent heat is exchanged, and, even though the system is disordered, it is not related to the random first-order transition taking place in structural glasses.

We have also studied the second-order phase transition, carrying out the estimate of critical temperatures and indices by means of parallel tempering sim-

ulations in temperature for different values of the chemical potential D. In this analysis, we have carefully checked FS effects, identified eventual crossovers from small to large size scaling. We verified that for different values of D, the system is always in the same universality class. The outcome is that for all $D < D_{3c}$, the second-order transition belongs to the same universality class of the three dimensional Edward-Anderson model for spin glasses.

We can conclude that, in a disordered system, the neutral component ($s_i = 0$) is sufficient to induce an IT between an active SG phase (characterized by $\rho_m \sim 1$) and an inactive PM phase, i. e., $\rho_m \to 0$. In other terms, the idea of freezed "inner" degrees of freedom which reduces the entropy and energy contribution to the free energy, i. e., as suggested by Schupper and Shnerb [8, 40], provides a good picture able to capture the main features of the IT phenomenon also in three dimensions.

Chapter 2

Secondary processes in structural glasses

In the previous chapter we have studied the static properties of Blume-Capel with quenched disorder. BC model can be thought like a coarse-grained model where, tuning the external parameters, some interacting scales can be given active or inactive.

The statics, i. e., the study of equilibrium thermodynamics, gives information about the fundamental state of a system. In order to study the excitated states we have to perform the dynamics.

In order to investigate the phenomenology of the structural glasses, i. e., real glasses, supercooled liquids, molecular liquids etc.., it is important to build models which show a dynamical arrest. Indeed, all glassy systems are characterized by the increase of viscosity, during a cooling process, leading to the dramatic growing of the relaxation times of the system [84, 85, 86, 9]. The increasing of relaxation times in a glassy system is due to the presence of many metastable states where the system can be trapped, whose number grows exponentially with the size of the system.

From the theoretical point of view, a comprehesive picture to describe the glassy behavior is still missing. At the mean-field level, some spin-glass models seem to heuristically capture the main features of the real glassy system [13, 87, 12, 88]. The study of the equilibrium dynamics of these SG models, exactly solvable without

uncontrolled approximations, leads to the same equation as the Mode Coupling Theory, which was developed, without introducing quenched disorder, to study the ergodicity breaking in the glassformers and supercooled liquid [89].

From the theorytical and the experimental point of view, it is clear that the dynamics of the glassy systems evolves, on at least two different characteristic time scales. In particular, the glassy behaviour is due to the presence of processes which do not reach the equilibrium with the environment, the so-called α processes. For these reasons the equilibrium dynamics is a typical multiscale problem.

2.1 Structural glasses and time scales

Glassy behaviour is a very common feature in many fields of condensed matter and many-body systems [9]. In general, when a bifurcation of microscopical time scales occurs, the degrees of freedom evolving on the slow time scale do not reach equilibrium on the observation time scale, and the system vitrifies.

In the first chapter we have studied the statics (i. e., the thermodynamics) therefore the properties of the free energy ground state. In order to do it we have to thermalize the system at the temperature of the thermal bath: we choose the dynamics (Monte Carlo in the case of the BC-random) which drives the system at the equilibrium. When the system reaches equilibrium we can measure the thermodynamic observables. In the high-temperature phase, far from criticality, the dynamics evolves on a single time scale. The free energy is convex function and the minimum is the macroscopic thermodynamic state. The system fluctuates, according to the Boltzmann measure, between the microscopic configurations belonging to the same macroscopic state. Evidently, we have two relevant time scales: the time scale of the microscpic dynamics τ_α and the time scale τ_O of the observer. If we study the equilibrium properties and we have to thermalize the system, this happens on a time-scale of order $\tau_\alpha \ll \tau_O$.

If the typical time-scale τ_α of the microscopic dynamics grows (i. e., when the memory effects become relevant), the separation between the observer time scale τ_O and τ_α may vanish and even be reversed. In particular, when $\tau_\alpha > \tau_O$ those degrees of freedom wich evolve over characteristic time τ_α are not able to reach the thermodynamic equilibrium, and the system fails to be ergodic.

More in general, as suggested by experiments and numerical simulations, more than τ_α and τ_O it has to take into account: the microscopic dynamics can evolve over several time-scales τ_r and some of the processes can stay away from equilibrium while others can thermalize.

For instance, this happens in supercooled liquid and structural glasses where a bifurcation between two time scales takes place[84]. In particular, we associate to the short time scale the (fast) $\beta-$processes, which thermalize at the temperature of the thermal bath. Whereas, over the long time scale the (slow) $\alpha-$processes evolve, breaking down the ergodicity. In the mean-field (MF) scenario happens at the Mode Coupling Temperature T_{MC}.

2.1.1 A single time scale example: statics and dynamics

Now we try to analyze the meaning of the expression $\tau_\alpha \ll \tau_O$ for a system which reaches the equilibrium. A simple analytically tractable example can be found in the fully connected Ising model

$$\mathcal{H}_I[\sigma] = -\frac{J}{2N}\sum_{ij}\sigma_i\sigma_j. \tag{2.1}$$

The variable σ_i is an Ising spin and it assumes the values -1 and $+1$. The symbol $[\sigma]$ denotes a configuration of N spins σ_i where $i = 1, \ldots, N$ and J is the coupling constant. We introduce the magnetization $m = \frac{1}{N}\sum_i \sigma_i$ which will be determined self-consistently. Since the model is fully connected, the magnetization does not fluctuate and the free energy is

$$f(m,\beta) = \frac{\beta J}{2}m^2 - \log 2\cosh \beta J m \tag{2.2}$$

with $\beta = \frac{1}{k_B T}$, K_B being the Boltzmann constant. The self-consistency relation reads

$$m = \tanh \beta J m\ . \tag{2.3}$$

Since the free energy must be convex in m, we have the condition

$$\frac{\partial^2 f}{\partial m^2} > 0\,. \tag{2.4}$$

It is easy to check that, for the paramagnetic (PM) solution $m = 0$, the thermodynamics is stable for $\beta J < 1$. In the low temperature phase ($\beta J > 1$) we have a spontaneous symmetry breaking which leads to a ferromagnetic phase with $m \neq 0$. Therefore, the microscopic configuration of the system $[\sigma]$ depends on the macrosopic state identified by m.

In the PM phase, the system visits configuration $[\sigma]$, such as $\sum_i \sigma_i = 0$. If the dynamics is driven by a stochastic process (e. g., the MC alghoritm in a numerical simulation or a Langevin equation in a mean-field model), in the high-temperature phase the correlation functions decay exponentially in time. For instance, without loss in generality, we can refer to a Langevin equation, with white noise, for a set of degrees of freedom $[x] = \mathbf{x}$

$$\Gamma_0^{-1} \partial_t x_i(t) = -x_i(t) + \zeta_i(t) \,, \tag{2.5}$$

where the first two momenta of the noise distribution are

$$\langle \zeta_i(t) \rangle_\zeta = 0 \;\; , \;\; \langle \zeta_i(t) \zeta_j(t') \rangle_\zeta = \frac{2\Gamma_0^{-1}}{\beta} \delta_{ij} \delta(t - t') \,, \tag{2.6}$$

where Γ_0^{-1} is the time scale of the microscopic process. Computing the correlation function $C(t, t') = \langle x(t) x(t') \rangle_\zeta$ we have

$$C(t, t') = \frac{\Gamma_0^{-2}}{2\beta} e^{-\Gamma_0 |t - t'|} \overset{|t-t'| \gg \Gamma_0^{-1}}{\longrightarrow} 0 \,. \tag{2.7}$$

The system loses memory of the initial conditions: thermal noise brings it to thermodynamic equilibrium and the time scale of the thermalization is fixed by the microscopic time scale Γ_0^{-1}.

The situation near a second order phase transition is different (e. g., at the PM/FM transition in a Ising model or PM/SG in the BEG-random model, above the tricritical point). From the static point of view, the criticality is revealed by a correlation lenght diverging at the critical temperature. The dynamical counterpart is a characteristic time diverging at the critical point. In such a case, the dynamics is very sensitive to the initial conditions.

Also the mean-field theory of dynamical critical phenomena can be formulated

in terms of a Langevin equation. But, in order to do it, we have to study a Gaussian model for a scalar field

$$\phi = \phi(r,t) \tag{2.8}$$

known to be in the same universality class of the Ising model (called the time-dependent Ginzburg-Landau equation [90]). In this model it is assumed that the "strength" of the noise, i.e., Γ_0 in eq. (2.6), becomes a function of the spatial variable r

$$\partial_t \phi(r,t) = -\int dr'\, \Gamma(r-r') \frac{\delta F}{\delta \phi(r,t)} + \zeta(r,t)\ , \tag{2.9}$$

where F is the Landau free energy and the momenta of the noise distribution $P(\zeta)$ are given by

$$\langle \zeta(r,t) \rangle_\zeta = 0 \ \ , \ \ \langle \zeta(r,t)\zeta(r',t') \rangle_\zeta = \frac{2}{\beta}\Gamma(r-r')\delta(t-t')\,. \tag{2.10}$$

In the Gaussian model the functional dependence of F on ϕ is

$$F = \int dr\ \left(a\phi(r,t)^2 + b(\nabla\phi(r,t))^2 \right), \tag{2.11}$$

where b is a positive constant and $a = (T - T_c)a'$ with a' a positive constant. Since the system is invariant under spatial translation, the problem can be solved in the Fourier space by introducing

$$\tilde{\phi}(k,t) = \int dr\, e^{-ikr}\phi(r,t)\ . \tag{2.12}$$

Finally, integrating out the Gaussian noise, one gets

$$\partial_t \langle \tilde{\phi}(k,t) \rangle = -(2a + bk^2)\tilde{\Gamma}(k)\langle \tilde{\phi}(k,t) \rangle \tag{2.13}$$

where $\langle \tilde{\phi} \rangle$ plays a role analogous to that of the magnetization in the statics of the fully-connected model. The solution of eq. (2.13) is an exponential decay with a characteristic time scale

$$\tau_k = \frac{1}{(2a + bk^2)\tilde{\Gamma}(k)}. \tag{2.14}$$

In the short wave-lenght regime ($k \to 0$), assuming $\tilde{\Gamma}(0)$ finite, the decay time

τ_0 diverges as $(T - T_c)^{-1}$ when approaching the critical temperature T_c. This phenomenon is called *critical slowing down*.

In ordered systems, however, no time scale appears and the divergence of the characteristic time is due to the persistence of the initial condition.

To summarize, the critical properties of statics —though in a simple mean field model (i. e., a coarse-grained model where the only degree of freedom is the order parameter homogenized in space)— have a counter-part in the dynamics towards equilibrium. In particular, the statics shows a critical scenario where the symmetry $[\sigma] \to [-\sigma]$ is spontaneously broken. Therefore, the free-energy landscape, plotted as a function of the order parameter m, under the critical temperature $J/T_c = 1$, displays two minima. The equilibrium dynamics, far from the critical point, is ergodic (i. e., does not depend on the initial condition). In the high-temperature phase the system thermalizes in a time of the order of the microscopic time scale.

2.1.2 Multiscale dynamics in glassy systems

In the example of the fully connected Ising model, the dynamics evolves on a single time scale, defined by the time needed for the system to thermalize at the temperature of the thermal bath. In particular, when the system thermalizes, the correlation function decays to zero. Near a second-order phase transition, the dynamics slows down due to criticality. All the physics of the model can be expressed through the static and the dynamic properties of a single observable: the order parameter.

The order parameter is the slowest degree of freedom of the system [68] and the observable which drives the system across the phase transition. At the leading order in a theory describing a critical phenomena, the order parameter is not affected by the fluctutations due to the finite dimension. As we have seen studying the static properties of the BC-random model, finiteness of dimension changes the details of criticality and, in some cases, may even destroy some general features predicted by the leading (MF) theory.

In general, a material falls in an amorphous phase when some degrees of freedom evolve on a time scale much larger than the time scale of an experiment. In order to study a glassy behaviour, we need models which display more than one single time

scale. Indeed, an evidence of the experiment is a bifurcation between, at least, two types of processes also called α and β processes. Two characteristic time scales τ_α and τ_β are associated with the two processes. The second one (τ_β) is associated with the processes which thermalize with the termal bath or, in general, which reach the equilibrium with the environment. The first one (τ_α), called structural relaxation time, is the time scale which diverges at some temperature called *dynamic* or *mode coupling* temperature. In the next section we will see that spin-glass models allow to define a hierachy of time scales and which different sets of cooperative mechanism lead to a hierarchy of processes.

From the experimental point of view, in order to have a glass, we have to cool a liquid (molecular, polymeric, etc...) fast enough to drive the sample out of the equilibrium. Following a cooling protocol, the typical time scale of the slowest processes increases by many orders of magnitude [9].

In the previous section we have seen how, in an ordered material, it is possible to map the static critical behaviour into dynamics: in particular, from the dynamics we have found a correlation lenght ξ which diverges at the static critical temperature T_c. At the same temperature, the dynamics displays the *critical slowing down* phenomenon. In glassy systems the situation is not clear because, in an experiment, the glassy temperature T_g is a definition and it is not possible equilibrate the system under T_g. In a experiment we can only define T_g in a conventional way such as the temperature at which the viscosity reaches the value of $10^{12}\ Pa\,s$ (cf. left panel in fig.(2.1)).

Actually, some models like spin-glass models predict a precise scenario for the glassy transition. In such models, at the mean-field level, we have a static (thermodynamic) transition to an *ideal glass* at the temperature T_s, called Kauzmann temperature T_K(cf. right panel in fig.(2.1)). Moreover, the dynamics undergoes a kinetic arrest at the temperature T_d. This temperature is defined as the temperature at which the Fluctuation-Dissipation Theorem (FDT) and Time-Translation Invariance (TTI) do not hold anymore. In an experiment, since the sample is blocked, it is not possible to reach the temperature where some models predict a static transition, since it is not possible to equilibrate the system under T_g. Therefore, we are not able to check the validity of some of the scenarios predicted by mean field models. Recently, many works on growing lenght scales have been done

to the purpose of defining an suitable multi-point correlation function (in space and time) which leads to a static lenght scale diverging at the dynamical temperature [91, 92, 93, 94, 95].

Glasses and glass-formers can be divided into two classes: strong and fragile. The classification is based on the behaviour of the relaxation time τ_α as a function of the temperature in a cooling procedure. For strong glasses (e. g., window glasses), characterized by an Arrhenius behaviour, the relaxation time grows exponentially

$$\tau_\alpha = \tau_0 e^{\frac{E}{k_B T}} , \tag{2.15}$$

with k_B the Boltzmann constant. Indeed, the dynamics is dominated by activated processes with a characteristic energy E.

Fragile glasses (e. g., toluene, chlorobenzene), on the contrary, follow a Vogel-Fulcher-Tamman law

$$\tau_\alpha = \tau_0 e^{\frac{DT_0}{T-T_0}} . \tag{2.16}$$

Equation (2.16) suggests a divergence at finite temperature T_0.

The dicotomy Strong/Fragile refers to different mechanisms for the excitations and it is not related to mechanical properties. Therefore, from the point of view of the free-energy landascape, glassy behaviour is due to the presence of many minima, i. e., metastable states, in which the system can be trapped. A glass-to-glass transition corresponds to a transition from a degenerate minimum to another degenerate minimum. In the strong glasses this kind of transition is rare and the minima are separated by high energy barriers. Whereas, in a fragile glass these phenomena are less rare because the phase space is fragmented into a very many basins, and in each basin there is a rich structure of other basins, divided by not too high energy barriers.

Using a simple visco-elastic model [85], it is possible to understand the link between diverging time scale and viscosity. Starting from an elastic solid (e. g., a cube of side L) we can write the relation between deformation and stress applied to a solid like[1]

$$\sigma_{\alpha\beta} = 2Gu_{\alpha\beta} = G\gamma \tag{2.17}$$

[1]The stress and strain tensor will be discussed in the next chapter.

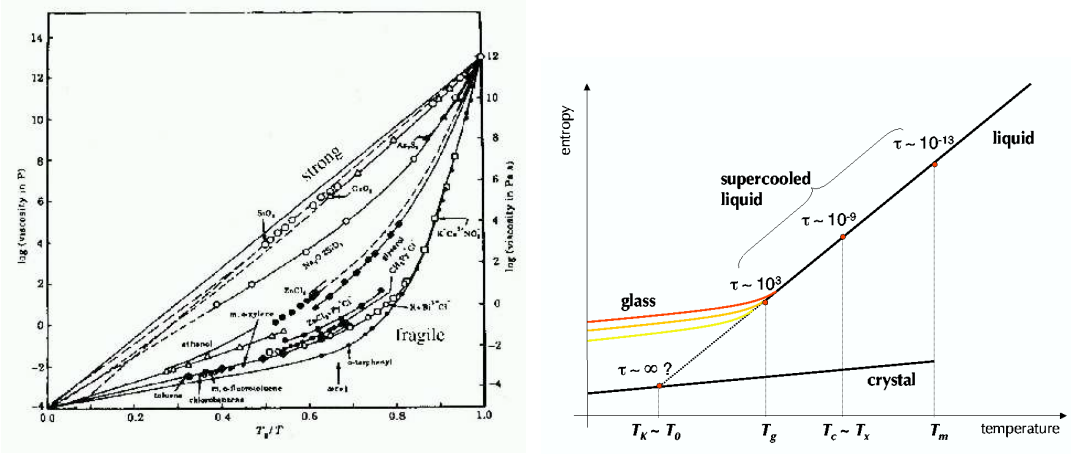

Figure 2.1: Left panel: viscocity as a function of $\frac{T}{T_g}$ for several glass formers [96]. Right panel: typical behavior of the entropy of a supercooled liquid as a function of T [85]. Lowering the temperature, following the spinodal, the characteristic time scale grows and breaks down the ergodicity at T_g. T_K is the Kauzmann temperature where the entropy of supercooled liquid is equal to the entropy of the crystal.

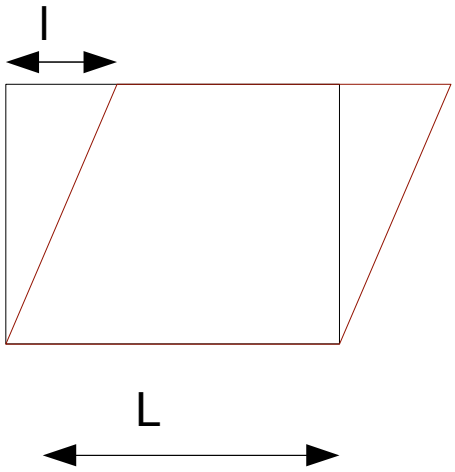

Figure 2.2: Displacement in the direction L due to an external stress.

where the greek indices run over the dimension d of the space. $\sigma_{\alpha\beta}$ is the *stress*

tensor, G is the *shear modulus* and

$$u_{\alpha\beta} \equiv \frac{1}{2}\left(\partial_\beta u_\alpha + \partial_\alpha u_\beta\right) \tag{2.18}$$

is the *strain tensor*, being u_α the displacement in the direction α due to the shear. Since the displacement along α will be proportional (the leading order) to the height along β,

$$u_\alpha = \gamma x_\beta \tag{2.19}$$

calling l the maximum displacement (see Fig. (2.2)), when $x_\beta = L$, defining $\gamma \equiv \frac{l}{L}$ one has

$$u_{\alpha\beta} = \gamma. \tag{2.20}$$

In a solid G will be time-indipendent but in general, for a viscoelastic body, it is time-dependent. In particular, for the Maxwell model [97] of viscoelasticity, it reads

$$G(t) = G_\infty e^{-\frac{t}{\tau_R}} \tag{2.21}$$

where τ_R defines the time scale over which the stress relaxes. Imagine to deform at time t'. The stress tensor at time t will be

$$\sigma_{\alpha\beta} = G(t, t')\gamma \ . \tag{2.22}$$

If the system is time-traslational invariant $G(t, t') = G(t - t')$. In general also the strain can be time dependent, in these cases the variation of $\sigma_{\alpha\beta}$ defined as

$$\delta\sigma_{\alpha\beta}(t) = \sigma_{\alpha\beta}(t) - \sigma_{\alpha\beta}(0) \tag{2.23}$$

whith $\sigma_{\alpha\beta}(0)$ the stress valued at $t_0 = 0$. Assuming $\gamma = \gamma(t)$ and $\dot{\gamma}(t) = const$ and applied at the time $t_0 = 0$.

$$\delta\sigma_{\alpha\beta} = G(t - t')\delta\gamma(t') = G(t - t')\dot{\gamma}(t')dt' \ . \tag{2.24}$$

The total stress $\sigma_{\alpha\beta}$ at the time t will be given by an integration from 0 to t

$$\sigma_{\alpha\beta}(t) = \int_0^t dt'\, G(t,t')\dot{\gamma}(t') = \int_0^t dt'\, G(t-t')\dot{\gamma}(t')\,. \tag{2.25}$$

It follows that

$$\sigma_{\alpha\beta}(t) = \dot{\gamma}\int_0^t d\tau\, G(\tau) = \eta\dot{\gamma}\,, \tag{2.26}$$

where the viscosity η is defined as

$$\eta \equiv \int_0^t d\tau\, G(\tau)\ . \tag{2.27}$$

Viscosity is a macroscopic observable which plays an important role in the study of the mechanical properties of a material. Imagine to have a tagged particle of radius r which moves in a fluid of viscosity η. We can introduce the diffusion coefficient D, according to the Stokes-Einstein relation

$$D = \frac{1}{\beta 6\pi r\eta} \tag{2.28}$$

where r is also called the *hydrodynamic radius*. Indeed, the response of a material to strain is a function of the shear modulus which characterizes the struscture of the material. When a typical time scale diverges the shear modulus does not vanish and the viscosity increases. In particular, even in a simple Maxwell-like model, we can define a set of relaxation. If τ_R is the larger relaxation time of the system, in the Maxwell picture, we have a simple relation between viscosity and relaxation time.

2.2 Mode coupling theory and $p-$spin models

In this section I will try to introduce two independent lines of research —Mode coupling theory and spin glass theory— which lead to the same mean-field scenario for the glassy transition: the so-called *Random First Order Theory* (ROFT) [13]. In the next section we generalize ROFT to study the secondary processes.

2.2.1 MCT and Schematic Theory

As will be shown later, the glassy dynamics of a broad class of mean-field spin-glass models [13, 87] lead to the same equations of a theory meant to describe the glassy behaviour of supecooled liquids and glass formers [89, 98], namely the Mode-Coupling Theory (MCT).

The MCT reproduces some features of glassy materials and it is based on some uncontrolled *a priori* approximation.

In the first part of this section we have studied, in a simple mean-field model, how statical and dynamical properties are related, finding that static criticality has a precise counterpart in the dynamic slowing down. Indeed, information obtained from the statics can be used to build a dynamical theory.

In particular, all the statical information of Hamiltonian system described by

$$\mathcal{H}(\mathbf{p},\mathbf{q}) = \sum_i \frac{\mathbf{p}_i^2}{2m} + \phi(\mathbf{q}) = \sum_i \frac{\mathbf{p}_i^2}{2m} + \sum_{i<j} \varphi(|\mathbf{q_i} - \mathbf{q_j}|) \tag{2.29}$$

is embodied the partition function

$$\mathcal{Z}(\beta, V, N) = \int \prod_i \frac{d\mathbf{p}d\mathbf{q}}{h^{3N}N!} e^{-\beta\mathcal{H}(\mathbf{p},\mathbf{q})} \equiv \int d\mu_{can}(\Gamma) \ , \tag{2.30}$$

where Γ is a shorthand notation for $(\mathbf{p},\mathbf{q})$. With the notation $f(\mathbf{p},\mathbf{q})$ we indicate a function of all the generalized momenta and coordinates $(\mathbf{p_i})_{i=1}^N, (\mathbf{q_i})_{i=1}^N$. In general, the interaction can involve more than two bodies

$$\begin{aligned} \phi(\mathbf{q}) &= \alpha_1 \sum_i \varphi_1(\mathbf{q_i}) + \alpha_2 \sum_{i<j} \varphi_2(\mathbf{q_i},\mathbf{q_j}) + \alpha_3 \sum_{i<j<k} \varphi_3(\mathbf{q_i},\mathbf{q_j},\mathbf{q_k}) + \cdots = \\ &= \sum_{n\leqslant N} \sum_{i_1<i_2<\cdots<i_n} \alpha_n \varphi_{i_n}(\mathbf{q_{i_1}},\ldots,\mathbf{q_{i_n}}) \end{aligned} \tag{2.31}$$

where the α_n are the coupling constants for the n-body interaction. If the system is sufficiently diluted, we can truncate (2.2.1) after the two-body term.

Since the integration over the momenta is Gaussian, all the observables of the system can be expressed in terms of the n-particles density function $\rho(\mathbf{r}_1,\ldots,\mathbf{r}_n)$

(with $n \leqslant N$) [99]

$$\rho(\mathbf{r}_1, \ldots, \mathbf{r}_n) = \int d\mu_{can}(\Gamma) \sum_{i_1 \neq i_2 \neq \cdots \neq i_n} \delta(\mathbf{r}_1 - \mathbf{q}_{i_1}) \cdots \delta(\mathbf{r}_n - \mathbf{q}_{i_n}) \; . \tag{2.32}$$

For instance, the ensemble average of a general observable $\mathcal{O}(q)$ will be

$$\langle \mathcal{O}(q) \rangle = \sum_n \int d\mathbf{r_1} \ldots d\mathbf{r_n} f_n(\mathbf{r_1} \ldots \mathbf{r_n}) \rho(\mathbf{r}_1, \ldots, \mathbf{r}_n) \, , \tag{2.33}$$

where the functions $f_n(\mathbf{r_1} \ldots \mathbf{r_n})$ are defined by the expansion of the observable:

$$\mathcal{O}(q) = \sum_n \sum_{i_1 \neq i_2 \neq \cdots \neq i_n} f_n(\mathbf{q_{i_1}} \ldots \mathbf{q_{i_n}}) \; . \tag{2.34}$$

From the fluctuation of the Fourier transform of the microscopic density (the 1-particle density function)

$$\begin{aligned} \widehat{\rho}(\mathbf{r}, \mathbf{q}) &= \sum_i \delta(\mathbf{r} - \mathbf{q}_i) \\ \tilde{\rho}_{\mathbf{k}}(\mathbf{q}) &= \sum_l e^{-i\mathbf{k}\cdot\mathbf{q}_l} \end{aligned} \tag{2.35}$$

we can build an important observable, namely the structure factor, an ingredient of the MCT. Under the assumption of homegeneous and translationally invariant fluid

$$S(k) \equiv \langle \frac{1}{N} \tilde{\rho}_{-\mathbf{k}}(\mathbf{q}) \tilde{\rho}_{\mathbf{k}}(\mathbf{q}) \rangle = 1 + \rho \int dr e^{-ikr} g(r) \tag{2.36}$$

where $r = |\mathbf{r}|$. In the last equality the radial distribution function $g(r)$ appears. It is defined by the 2-particle density as follows:

$$g(\mathbf{r_1}, \mathbf{r_2}) = \left\langle \frac{\rho(\mathbf{r_1}, \mathbf{r_2}, \mathbf{q_1}, \mathbf{q_2})}{\rho(\mathbf{r_1}, \mathbf{q_1}) \rho(\mathbf{r_2}, \mathbf{q_2})} \right\rangle \; ; \tag{2.37}$$

for a system homogeneous and invariant under spatial translations, it is

$$g(\mathbf{r_1}, \mathbf{r_2}) = g(|\mathbf{r_1} - \mathbf{r_2}|) = g(r) \tag{2.38}$$

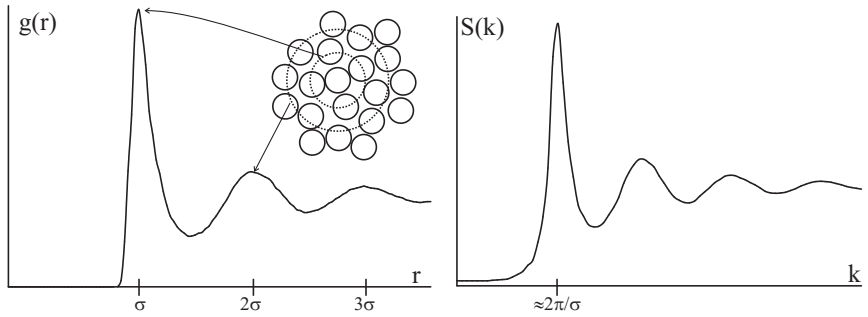

Figure 2.3: Behaviour of the radial distribution function $g(r)$ and the corresponding structure factor $S(k)$ for a simple liquid (σ is the size of the molecules) [100].

and

$$\langle \prod_{i}^{n} \rho(\mathbf{r_i}, \mathbf{q_i}) \rangle = \rho^n \tag{2.39}$$

where $\rho = N/V$. For small values of r, if the interaction potential is repulsive (e.g., soft- or hard-core) on small distances $g(r)$ is vanishing while, for $r \to \infty$, $g(r) \to 1$ because $\rho(\mathbf{r_1}, \mathbf{r_2})$ factorizes into $\rho(\mathbf{r_1})\rho(\mathbf{r_2}) = \rho^2$. For reasons that will be clarified later, we define the function

$$h(r) \equiv g(r) - 1 \tag{2.40}$$

and the *direct correlation function* $c(r)$, related to the $S(k)$ through the Orstein-Zernike (OZ) relation

$$h(r) = c(r) + \rho \int dr'\, c(r - r')h(r')\,. \tag{2.41}$$

OZ in the Fourier space takes the form

$$S(k) = \frac{1}{1 - \rho\hat{c}(k)}\,. \tag{2.42}$$

$S(k)$ can be experimentally measured from the cross-section for scattering of neutrons or X-rays by the fluid as a function of scattering angle. Indeed, we can access to static properties theoretically with the particle density and experimentally by means of the structure factor. Therefore, in order to study the kinetic arrest near the glassy transition, we have to consider the structure factor as a dynamical

variable. To do this we start from the dynanical evolution of a generical observable $\mathcal{O}(t)$ of a Hamiltonian system

$$\frac{d\mathcal{O}(t)}{dt} = \sum_i \left(\frac{\partial \mathcal{O}}{\partial \mathbf{p_i}} \dot{\mathbf{p}}_i + \frac{\partial \mathcal{O}}{\partial \mathbf{q_i}} \dot{\mathbf{q}}_i \right) + \frac{\partial \mathcal{O}}{\partial t}. \tag{2.43}$$

If $\frac{\partial \mathcal{O}}{\partial t} = 0$, defining the Liouvillian operator [98] $i\mathcal{L}$ as

$$i\mathcal{L} \equiv \sum_i \left(\dot{p}_i \frac{\partial}{\partial p_i} + \dot{q}_i \frac{\partial}{\partial q_i} \right) \ , \tag{2.44}$$

from eq.(2.43) it follows that

$$\frac{d\mathcal{O}(t)}{dt} = i\mathcal{L}\mathcal{O}(t)\,. \tag{2.45}$$

We can formally compute the evolution of $\mathcal{O}(t) \equiv \mathcal{O}(\mathbf{p}(t), \mathbf{q}(t))$ as in the form

$$\mathcal{O}(t) = e^{i\mathcal{L}t}\mathcal{O}(0) = U(t)\mathcal{O}(0) \tag{2.46}$$

where we have defined a time-evolution operator

$$U(t) \equiv e^{i\mathcal{L}t}\ . \tag{2.47}$$

We can also write the evolution of the distribution function $\mathcal{P}(\Gamma)$ which defines the measure over the space Γ through the relation

$$d\mu(\Gamma) = \mathcal{P}(\Gamma) d\tilde{\Gamma} \tag{2.48}$$

where $d\tilde{\Gamma} = \prod_i \frac{d\mathbf{p}d\mathbf{q}}{h^{3N}N!}$. Since we assume that the probability distribution does not depend explicitly on time (i. e., we study the equilibrium dynamics allowing the system to reach thermal equilibrium), it follows that

$$\frac{\partial \mathcal{P}(t)}{\partial t} = -i\mathcal{L}t \rightarrow \mathcal{P}(t) = e^{-i\mathcal{L}t}\mathcal{P}(0)\,, \tag{2.49}$$

which is the *Liouville Theorem*. Therefore, an element of the space phase $(\mathbf{p}, \mathbf{q})$

evolves in $(\mathbf{p}(t), \mathbf{q}(t))$ from $(\mathbf{p}(0), \mathbf{q}(0))$ according to eq. (2.46). Since $\mathcal{P}(t)$ evolves according to eq. (2.49), the measure $d\mu(\Gamma)$ will be time-translational invariant:

$$d\mu(\Gamma(t)) = d\mu(\Gamma(0)) \equiv d\mu(\Gamma) \; . \tag{2.50}$$

Since the system is Hamiltonian, it follows that

$$\dot{\mathbf{r}}_i = \frac{\partial \mathcal{H}}{\partial \mathbf{p}_i}(\mathbf{p}, \mathbf{r}) \, , \qquad \dot{\mathbf{p}}_i = -\frac{\partial \mathcal{H}}{\partial \mathbf{r}_i}(\mathbf{p}, \mathbf{r}) \tag{2.51}$$

and the Liouvillian becomes

$$i\mathcal{L} = \frac{1}{m} \sum_i \mathbf{p_i} \cdot \frac{\partial}{\partial \mathbf{q_i}} - \sum_{i \neq j} \frac{\partial \varphi(|\mathbf{q_i} - \mathbf{q_j}|)}{\partial \mathbf{q_i}} \frac{\partial}{\partial \mathbf{p_i}} \, . \tag{2.52}$$

An important role is played by the time-correlation function $C(t, t')_{\mathcal{AB}}$ of the dynamical observables defined as

$$C(t, t')_{\mathcal{AB}} \equiv \langle \mathcal{A}(t) \mathcal{B}^*(t') \rangle \; , \tag{2.53}$$

where the supersription * denotes complex conjugation. If the system is in an ergodic phase, one has that

$$C(t, t')_{\mathcal{AB}} \equiv \langle \mathcal{A}(t) \mathcal{B}^*(t') \rangle = \int d\mu(\Gamma) e^{i\mathcal{L}(t-t')} \mathcal{A}(0) \mathcal{B}^*(0) \, . \tag{2.54}$$

The correlation functions take the form of a scalar product. Indeed, the auto-correlation function is

$$C(t, t')_{\mathcal{OO}} = \langle \mathcal{O}(t) \mathcal{O}^*(t') \rangle = \int d\mu(\Gamma) e^{i\mathcal{L}(t-t')} \mathcal{O}(0) \mathcal{O}^*(0) \tag{2.55}$$

and when $t = t'$

$$C(t, t)_{\mathcal{OO}} = \langle \mathcal{O}(t) \mathcal{O}^*(t) \rangle = \int d\mu(\Gamma) \mathcal{O}(0) \mathcal{O}^*(0) = \langle \mathcal{O}(0) \mathcal{O}^*(0) \rangle \tag{2.56}$$

while, fot $t' = 0$

$$C(t,0)_{\mathcal{OO}} = \int d\mu(\Gamma) e^{i\mathcal{L}t}\mathcal{O}(0)\mathcal{O}^*(0) \equiv C(t)_{\mathcal{O}}. \tag{2.57}$$

In the limit $t \to \infty$, if the system is not only ergodic but also *mixing* since,

$$\lim_{t\to\infty} C(t)_{\mathcal{AB}} = \langle \mathcal{A}(0)\rangle\langle \mathcal{B}^*(0)\rangle \tag{2.58}$$

To describe a system which displays at least two time scales, one has to introduce a projector formalism which allows one to separate slow from fast degrees of freedom [98]. The plain is as follows: correlation functions define a scalar product between the observables; the time evolution of a set of observables $\{\mathcal{A}_i\}$ can be formally computed through the time-evolution anti-hermitian operator $U(t)$. Moreover, the operator $\mathcal{L}$ is a Hermitian operator: a general observable $\mathcal{A}(\mathbf{p},\mathbf{q})$ can be expanded into an infinite set of functions $\varphi_k(\mathbf{p},\mathbf{q})$ in the Hilbert space defined on Γ. Therefore we can associate with each function of the orthonormal set a vector φ_k in the Hilbert space such that

$$\langle \varphi_k|\varphi_l\rangle = \delta_{kl} \tag{2.59}$$

where δ_{kl} is the Kronecker delta symbol. The expansion of an observable will be

$$\mathcal{A}(\mathbf{p},\mathbf{q},t) = \sum_k a_k(t)\varphi_k(\mathbf{p},\mathbf{q}) \tag{2.60}$$

where $a_k(t)$ is

$$a_k(t) = \langle \mathcal{A}|\varphi_k\rangle \tag{2.61}$$

and satisfies the following equation of motion

$$\partial_t a_k(t) = \sum_l \mathcal{L}_{kl} a_k(t) \tag{2.62}$$

where the matrix $\mathcal{L}_{kl}$ is anti-Hermitian and its expression is given by

$$\mathcal{L}_{kl} = \langle \varphi_k|i\mathcal{L}\varphi_l\rangle \ . \tag{2.63}$$

Also an ordered set of dynamical observables $(\mathcal{A}_i)$ is a vector in this Hilbert space. Now, in the space of the observables, we can build a projector $\Pi_{\mathcal{O}}$ which projects the other observables into the space defined by $\mathcal{O}$.

$$\Pi_{\mathcal{O}} = \langle \mathcal{O}| \dots \rangle \langle \mathcal{O}|\mathcal{O}\rangle^{-1} \mathcal{O} \equiv \Pi \,, \tag{2.64}$$

where $\langle \mathcal{O}|\mathcal{O}\rangle \equiv \langle \mathcal{O}\mathcal{O}^*\rangle$. Being $\Pi_{\mathcal{O}}$ a projector, the following properties hold

$$\begin{aligned} \Pi\mathcal{O} &= \langle \mathcal{O}|\mathcal{O}\rangle \langle \mathcal{O}|\mathcal{O}\rangle^{-1} \mathcal{O} = \Pi^2 \mathcal{O} = \mathcal{O} \\ \Pi\Pi\mathcal{A} &= \Pi^2 \mathcal{A} = \Pi\mathcal{A} \,. \end{aligned} \tag{2.65}$$

Defining $\mathcal{Q} \equiv (1 - \Pi)$

$$\begin{aligned} (1-\Pi)(\Pi\mathcal{A}) &\equiv \mathcal{Q}\Pi\mathcal{A} = \Pi\mathcal{Q}\mathcal{A} = 0 \\ \mathcal{Q}\mathcal{Q}\mathcal{A} &= \mathcal{Q}\mathcal{A} \,. \end{aligned} \tag{2.66}$$

Therefore, the projector $\mathcal{Q}$ defines the subspace orthogonal to Π.

Because we want to know what happens when the dynamics evolves over separated time scales, we have to study the dynamics of a general observable $\mathcal{O}(t)$ in its space during the time-evolution due to the operator $U(t) = e^{i\mathcal{L}t}$. In general, the observable can be a multiplet of observables suitably chosen. Indeed, the projector operators allow us to study a subset $\{\mathcal{O}_i\}$ in the space of the observables $(\mathcal{A}_i)$. In order to simplify the notation, we define a relevant observable $\mathcal{O}$ and we want to write an evolution equation for $\mathcal{O}(t)$.

Starting from (2.45) and (2.46) we can write the following operatorial integro-differential equation for $\mathcal{O}$

$$\begin{aligned} \partial_t \mathcal{O}(t) &= i\Omega\mathcal{O}(t) - \int_0^t dt' K(t')\, \mathcal{O}(t-t') + f(t) \\ f(t) &\equiv e^{i\mathcal{Q}\mathcal{L}t}\, \mathcal{Q} i\mathcal{L}\, \mathcal{O}(0) \\ K(t) &\equiv \langle f|f(t)\rangle \langle \mathcal{O}|\mathcal{O}\rangle^{-1} \\ i\Omega &\equiv \langle \mathcal{O}|i\mathcal{L}\mathcal{O}\rangle \langle \mathcal{O}|\mathcal{O}\rangle^{-1} \,. \end{aligned} \tag{2.67}$$

To obtain (2.67) we have written the time-evolution operator as

$$\begin{aligned} e^{i\mathcal{L}t} &= e^{i\mathcal{L}t}M(t) + e^{i\mathcal{Q}\mathcal{L}t}\,, \\ M(t) &= i\int_0^t dt'\, e^{-i\mathcal{L}t'}\,\mathcal{Q}\mathcal{L}\, e^{i\mathcal{Q}\mathcal{L}t'}\,, \\ M(0) &= 0\,. \end{aligned} \tag{2.68}$$

The expression for $M(i)$ is obtained by differentianting with respect the time of the first equation of (2.68). Using the identity

$$i\mathcal{L} = \Pi i\mathcal{L} + (1-\Pi)i\mathcal{L} = \Pi i\mathcal{L} + \mathcal{Q}i\mathcal{L} \tag{2.69}$$

we can compute

$$\begin{aligned} e^{i\mathcal{L}t}(1-\Pi)i\mathcal{L}\mathcal{O} &= e^{i\mathcal{L}t}i\mathcal{L}\mathcal{O} - e^{i\mathcal{L}t}\Pi i\mathcal{L}\mathcal{O} = \\ &= \partial_t\mathcal{O}(t) - \langle\mathcal{O}|i\mathcal{L}\mathcal{O}\rangle\langle\mathcal{O}|\mathcal{O}\rangle^{-1}\mathcal{O}(t) = \\ &= \partial_t\mathcal{O}(t) - i\Omega\mathcal{O}(t)\,. \end{aligned} \tag{2.70}$$

The action of (2.70) on the operatorial identity (2.68) leads to the following equation:

$$\begin{aligned} f(t) &+ \int_0^t dt'\, e^{i\mathcal{L}t-t'}\langle\mathcal{O}|i\mathcal{L}f(t')\rangle\langle\mathcal{O}|\mathcal{O}\rangle^{-1}\mathcal{O} = \\ &= f(t) + \int_0^t dt'\,\langle\mathcal{O}|i\mathcal{L}f(t')\rangle\langle\mathcal{O}|\mathcal{O}\rangle^{-1}\mathcal{O}(t-t')\,, \end{aligned} \tag{2.71}$$

where we have introduced the noise term

$$f(t) \equiv e^{i(1-\Pi)\mathcal{L}t}(1-\Pi)i\mathcal{L}\mathcal{O}\,. \tag{2.72}$$

Using the anti-Hermitian property of the inner product and the fact that $\langle\mathcal{O}|f(t)\rangle = 0$, we can define a kernel $K(t)$ as

$$\begin{aligned} \langle\mathcal{O}|i\mathcal{L}f(t)\rangle\langle\mathcal{O}|\mathcal{O}\rangle^{-1} &= -\langle\mathcal{O}i\mathcal{L}|f(t)\rangle\langle\mathcal{O}|\mathcal{O}\rangle^{-1} = \\ &= -\langle f|f(t)\rangle\langle\mathcal{O}|\mathcal{O}\rangle^{-1} \equiv -K(t) \end{aligned} \tag{2.73}$$

and finally obtain the expression (2.67).

We can generalize the above results for a vector observable $\mathcal{O}(t)$. Projecting along $\mathcal{O}(0)$ we obtain

$$\partial_t \mathbf{C}(t) = i\mathbf{\Omega} \cdot \mathbf{C}(t) - \int_0^t dt' \, \mathbf{K}(t')\mathbf{C}(t-t') \; , \tag{2.74}$$

where we used the relation $\langle \mathcal{O}|f(t)\rangle = 0$.

Obviously, eq. (2.74), also called *Generalized Langevin Equation* (GLE) [101], is just an alias of the operatorial evolution equation which has the formal solution $\mathcal{O}(t) = U(t)\mathcal{O}(0)$. Through eq. (2.74), it is clear the role played by the other degrees of freedom on the relevant observable. In particular, while the linear term in the r.h.s of (2.74) depends only by the evolution of $\mathbf{C}(t)$, the memory term $\mathbf{K}(t)$ encodes, through the noise term $f(t)$, the effects of the other degrees of freedom on $\mathcal{O}$.

Since the most general features of the glassy systems is the decoupling of two time scales, it is natural to try to study GLE when $\mathbf{C}(t)$ is a vector of slow variables and the noise term $f(t)$ is due to fast degrees of freedom. The most important correlation function for a fluid and supercooled-liquid is the density-fluctuation function (i. e., the *intermediate scattering function*) defined as

$$F(\mathbf{k},t) = \frac{1}{N}\langle \tilde{\rho}_{-\mathbf{k}}(\mathbf{q},t)\tilde{\rho}_{\mathbf{k}}(\mathbf{q},0)\rangle = \frac{1}{N}\sum_{l,m}\langle e^{i\mathbf{k}\cdot\mathbf{q}_l(0)}e^{-i\mathbf{k}\cdot\mathbf{q}_m(t)}\rangle \tag{2.75}$$

where we have introduced the Fourier transform of the time-dependent local density

$$\widehat{\rho}(\mathbf{r},\mathbf{q},t) = \sum_i \delta(\mathbf{r}-\mathbf{q}_i(t)) \tag{2.76}$$

and

$$\tilde{\rho}_{\mathbf{k}}(\mathbf{q},t) = \sum_l e^{-i\mathbf{k}\cdot\mathbf{q}_l(t)} \; . \tag{2.77}$$

We note that for $t = 0$ it is $F(\mathbf{k},0) = S(k)$.

From hydrodynamics it is known that the slow observables [102] are the local

density fluctuations and the longitudinal velocities:

$$\mathcal{O} = \left(\delta\tilde{\rho}_{\mathbf{k}}(\mathbf{q},t)\,,\, j^L_{\mathbf{k}}(\mathbf{p},\mathbf{q},t)\right) \tag{2.78}$$

where $\delta\tilde{\rho}_{\mathbf{k}}(\mathbf{q},t)$ is the local fluctuation of the density

$$\delta\tilde{\rho}_{\mathbf{k}}(\mathbf{q},t) = \tilde{\rho}_{\mathbf{k}}(\mathbf{q},t) - (2\pi)^3\rho\delta(k)\,, \tag{2.79}$$

where $k = |\mathbf{k}|$. The longitudinal velocity is given by the following expression

$$j^L_{\mathbf{k}}(\mathbf{p},\mathbf{q},t) = \frac{1}{m}\sum_i \frac{\mathbf{k}}{k}\cdot\mathbf{p_i}\, e^{-i\mathbf{k}\cdot\mathbf{q_i}} \tag{2.80}$$

Finally, we can replace the previous definition of $F(\mathbf{k},t)$ with the following one:

$$F(\mathbf{k},t) \equiv \langle\delta\tilde{\rho}_{-\mathbf{k}}(\mathbf{q},t)\delta\tilde{\rho}_{\mathbf{k}}(\mathbf{q},0)\rangle \tag{2.81}$$

where we have replaced the local density with its fluctuation. In order to simplify the notation, since the thermal averages are done on the generalized coordinates and momenta $(\mathbf{p},\mathbf{q})$, we write

$$\langle\mathcal{O}_{\mathbf{k}}(\mathbf{p},\mathbf{q},t)\rangle = \langle\mathcal{O}_{\mathbf{k}}(t)\rangle\ . \tag{2.82}$$

The matrix elements of $\mathbf{C}(t)$ will be

$$\mathbf{C}_{\mathbf{k}}(t) = \begin{bmatrix} \langle\delta\tilde{\rho}_{-\mathbf{k}}\delta\tilde{\rho}_{\mathbf{k}}(t)\rangle & \langle\delta\tilde{\rho}_{-\mathbf{k}}j^L_{\mathbf{k}}(t)\rangle \\ \langle j^L_{-\mathbf{k}}\delta\tilde{\rho}_{\mathbf{k}}(t)\rangle & \langle j^L_{-\mathbf{k}}j^L_{\mathbf{k}}(t)\rangle \end{bmatrix}\,, \tag{2.83}$$

since $\langle\sum_i \mathbf{p}^2/2m\rangle = 2/\beta$, using the general property

$$\langle\mathcal{A}\dot{\mathcal{A}}\rangle = 0 \tag{2.84}$$

and defining the following function

$$\mathcal{K}_{\mathbf{k}} \equiv \left[\frac{dj^L_{\mathbf{k}}}{dt} - i\frac{k\,\delta\tilde{\rho}_{\mathbf{k}}}{\beta m S(k)}\right] \tag{2.85}$$

we can write

$$\mathbf{K}_{\mathbf{k}}(t) = \begin{bmatrix} 0 & 0 \\ 0 & \langle \mathcal{K}_{-\mathbf{k}} \mathcal{K}_{\mathbf{k}}(t) \rangle \end{bmatrix} , \tag{2.86}$$

and rewrite eq. (2.74) in terms of the choosen observable[2]

$$\frac{d^2 F(\mathbf{k},t)}{dt^2} + \frac{k^2 F(\mathbf{k},t)}{\beta m S(k)} + \frac{\beta m}{N} \int_0^t dt' \, \langle \mathcal{K}_{-\mathbf{k}} \mathcal{K}_{\mathbf{k}}(t') \rangle \frac{dF(\mathbf{k}, t-t')}{dt} = 0 \, . \tag{2.87}$$

The equation obtained is still exact for the dynamics of $F(\mathbf{k},t)$.

Now, in order to solve in closed form eq. (2.87), several approximations have to be introduced. Eq. (2.85) contains the time-derivative of the current, proportional to the gradient of the interaction potential. Using the formalism of density distribution functions, the potential can be expressed in terms of density fluctuations in the Fourier space. Therefore, it is useful to introduce the projector Π_2 over the density pairs

$$\Pi_2 = \sum_{\mathbf{k_1 k_2 k_3 k_4}} \langle \mathcal{O}_{\mathbf{k_3 k_4}} | \dots \rangle \langle \mathcal{O}_{\mathbf{k_1 k_2}} | \mathcal{O}_{\mathbf{k_3 k_4}} \rangle^{-1} \mathcal{O}_{\mathbf{k_1 k_2}} \tag{2.88}$$

and then factorize all the four-point density terms into products of two-point density correlation. In particular, choosing $\mathcal{O} = \delta\tilde{\rho}_{\mathbf{k_1}} \delta\tilde{\rho}_{\mathbf{k_2}}$, one has

$$\begin{aligned} \Pi_2 \, \mathcal{K}_{\mathbf{k}} &= \sum_{\mathbf{k_1 k_2}} V_{\mathbf{k}}(\mathbf{k_2}, \mathbf{k_1}) \delta\tilde{\rho}_{\mathbf{k_1}} \delta\tilde{\rho}_{\mathbf{k_2}} \\ V_{\mathbf{k}}(\mathbf{k_2}, \mathbf{k_1}) &\equiv \sum_{\mathbf{k_3 k_4}} \langle \delta\tilde{\rho}_{\mathbf{k_1}} \delta\tilde{\rho}_{\mathbf{k_2}} | \mathcal{K}_{\mathbf{k}} \rangle \langle \delta\tilde{\rho}_{\mathbf{k_1}} \delta\tilde{\rho}_{\mathbf{k_2}} | \delta\tilde{\rho}_{\mathbf{k_3}} \delta\tilde{\rho}_{\mathbf{k_4}} \rangle^{-1} \, . \end{aligned} \tag{2.89}$$

Through the projector Π_2 the memory kernel $\mathcal{K}_k$ can be factorized as follows

$$\mathcal{K}_k \sim \langle \delta\tilde{\rho} \delta\tilde{\rho} \rangle \langle \delta\tilde{\rho} \delta\tilde{\rho} \rangle \propto \sum_{k_1} F(k_1, t) F(k - k_1, t) \tag{2.90}$$

Without entering into details on the approximations, which can be found in [89, 86, 100, 102], one is able to write a close equation for $F(\mathbf{k},t)$. In particular the

[2]For a detailed derivation of the MCT see[89, 86, 100, 102]

vertex function in MCT is given by

$$\begin{aligned} V_{\mathbf{k_1},\mathbf{k_2}-\mathbf{k_1}} &= \frac{i\frac{\mathbf{k_2}}{k2}}{2\beta m N}\cdot\left\{\frac{\mathbf{k_1}}{S(k_1)}+\frac{\mathbf{k_2}-\mathbf{k_1}}{S(k_2-k_1)}-\mathbf{k_2}\right\}= \\ &= \frac{i\rho\frac{\mathbf{k_2}}{k2}}{2\beta m N}\cdot\left\{\mathbf{k_1}c(k_1)+(\mathbf{k_2}-\mathbf{k_1})\,c(k_2-k_1)\right\} \end{aligned} \tag{2.91}$$

and the MCT equation for the *intermediate scattering function* is

$$\begin{aligned} \frac{d^2F(k,t)}{dt^2} &+ \frac{k^2F(k,t)}{\beta m S(k)}+\int_0^t dt'\,K(k,t-t')\frac{dF(k,t')}{dt'}=0 \\ K(k,t-t) &\equiv \frac{\rho}{16\pi^3 m\beta}\int d\mathbf{k_1}\,|V_{\mathbf{k}-\mathbf{k_1},\mathbf{k_1}}|^2\,F(k_1,t)F(k_1-k,t) \end{aligned} \tag{2.92}$$

Therefore, MCT gives a closed set of integro-differential equations for the density correlator $F(k,t)$. In particular, this is possible if we approximate the memory kernel (i. e., *the vertex function* V_{k_1,k_2-k_1}) of the exact (untractable) theory with a polynomial of density correlators. In order to study how $F(k,t)$ depends on the wave number k, one needs to fix the *static structure factor* (or, equivalently, the *direct correlation function* $c(k)$) as an input parameter of the theory.

In order to study the phenomenology predicted by the MCT, it is sufficient to study the limit $k\to k_0$, where k_0 is the position of the peak of $S(k)$. We can thus define the function

$$\phi(t)\equiv F(0,t)\,. \tag{2.93}$$

Indeed, numerical computations of the MCT equation, show [103] that the main contribution comes from the peak of $S(k)$ (cfr. fig(2.2.1)), so we can approximate

$$S(k)\sim\delta(k-k_0)\,. \tag{2.94}$$

Moreover, for a broad class of glassy systems we can replace the second time derivative of $\phi(t)$ with a first time derivative (e. i., we are interested by the Aristotelic regime). The theory obtained through these assumptions is called schematic theory (ST) [100] and the equation (2.92) becomes

$$\dot\phi(t)+\omega^2\phi(t)+\gamma\int_0^t dt'\,\phi^2(t-t')\dot\phi(t')=0 \tag{2.95}$$

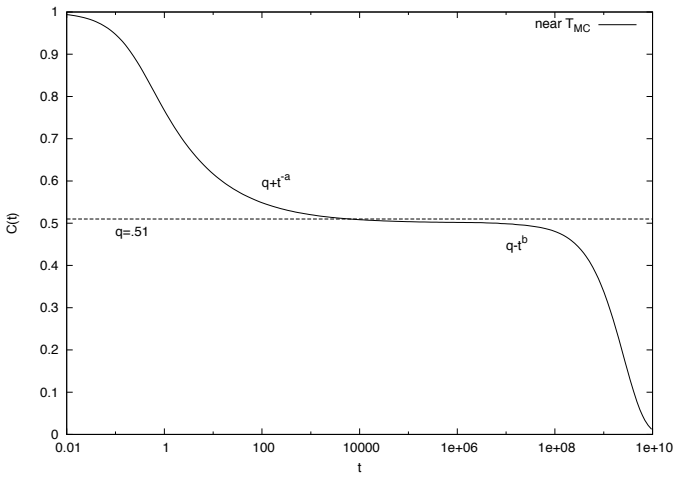

Figure 2.4: Intermediate Scattering Function in a Schematic Model near T_{MC} with ϕ^2 kernel.

where ω and γ are parameters of the model.

In a ST a more general memory kernel can appear such as a polynomial of degree q. Through a suitable (i. e., phenomenological) choice of the memory kernel, it is possible to build different MCT models. We have introduced the ST because the dynamical equations of a class of spin-glass model leads to the same equations of the ST.

Figure (2.4) shows the solution of eq. (2.95), for the memory kernel $\phi(t)^2$, obtained through numerical integration, near T_{MC}. We can see a double step relaxation: the first relaxation to the value $q = 0.51$ is due to the β process that reaches equilibrium with the environment. The plateau, extending for five decades in time, is due to the α processes which break the ergodicity at T_{MC}. In particular, at the Mode Coupling temperature one has

$$\lim_{t\to\infty} \phi(t) = q \tag{2.96}$$

When the solution develops a plateau it is possible to evalutate analytically the behaviour of $\phi(t)$ approaching to and departing from q[89], obtaining the MCT

exponents

$$\begin{aligned} \phi(t) &\sim q + At^{-a} \text{ for } \phi \to q^{+} \\ \phi(t) &\sim q + Bt^{b} \text{ for } \phi \to q^{-} \\ \frac{\Gamma(1-a)^2}{\Gamma(1-2a)} &= \frac{\Gamma(1+b)^2}{\Gamma(1+2b)} = \bar{m}\,. \end{aligned} \tag{2.97}$$

The last expression of (2.97) will be generalized in the last section of this chapter for $\phi(t)$ which displays a multistep relaxation.

Finally, it is possible to compute how the characteristcal time scale τ_α diverges at T_{MC}, finding the follows relations

$$\begin{aligned} \tau_\alpha &\sim (T - T_{MC})^{-\gamma} \\ \gamma &= \frac{1}{2a} + \frac{1}{2b} \end{aligned} \tag{2.98}$$

The scaling properties (2.97) are a remarkable result of the MCT. We do not analyse successes and failures of MCT because a broad literature about this subject already exists (see [100] for a review). We will examine a class of models that can be exactly solved in MF and which leads to a dynamical equation formally equivalent to eq. (2.95) of the ST.

2.2.2 The p-spin models

Thermodynamics and dynamics of spin glass models —at mean-field level— can be exactly computed without uncontrolled approximation. The dynamics can be solve without *replica trick* and leads to the same equation of MCT-ST.

Replica Theory

In the previous chapter, we have studied the static properties of spin-glasses in finite dimensions. Now we briefly discuss the general properties of spin glass models. These are lattice models, defined through a Hamiltonian $\mathcal{H}[\sigma; J]$, where the couplings between the spin variables are chosen randomly with a suitable distribution $P(J)$. Quenched disorder means that the integration over the couplings is done after the thermal average, and therefore, after the calculation of the partition

function. In fact, thermodynamics is defined as follows [55]:

$$\begin{aligned} \mathcal{Z}_\beta[J] &= \mathrm{Tr}_\sigma e^{-\beta\mathcal{H}[\sigma;J]} \\ f(\beta;J) &= -\lim_{N\to\infty}\frac{1}{\beta N}\log\mathcal{Z}_\beta[J] \\ f(\beta) &= -\lim_{N\to\infty}\frac{1}{\beta N}\int d\mu(J)\log\mathcal{Z}_\beta[J] \equiv \overline{f(\beta;J)} \\ d\mu(J) &\equiv \prod_{ij} dJ_{ij}\,P(J_{ij})\,. \end{aligned} \tag{2.99}$$

The overbar $\overline{\cdots}$ denotes average over the disorder. The prototype SG model is the Edwards-Anderson Model [57]: an Ising-like model with *quenched disorder*

$$\mathcal{H}_{EA}[\sigma;J] = -\sum_{(i,j)} J_{ij}\sigma_i\sigma_j\ ,\quad \sigma_i = \pm 1\,. \tag{2.100}$$

where the bracket means that the sum is extended to nearest-neighbours sites. Several choices for $P(J)$ are possible. In analytical treatments, the Gaussian measure

$$P(J_{ij}) = \frac{1}{\sqrt{2\pi z J^2}}\exp\left(-\frac{(J_{ij}-J_0)^2 z}{2J^2}\right) \tag{2.101}$$

is often used, where z is the coordination number, i. e., the number of nearest-neighbours. Another choice, often used in numerical simulations, is the bimodal distribution

$$P(J_{ij}) = p\delta\left(J_{ij}-J\right) + (1-p)\delta\left(J_{ij}+J\right)\ ,\quad 0\le p\le 1, \tag{2.102}$$

p being the concentration of ferromagnetic bonds.

The statistical mechanics of (2.100) is analitically computable at the mean-field level (when the space dimension is large enough for the thermodynamic fluctuations to be neglected).

The mean-field approximation of the EA model is the Sherrington-Kirkpatrick Model (SK) [56]

$$\mathcal{H}_{SK}[\sigma;J] = -\frac{1}{N}\sum_{i<j} J_{ij}\sigma_i\sigma_j\ ,\quad \sigma_i = \pm 1\,. \tag{2.103}$$

We can generalize the SK model by extending the interaction from binary to n-ary [11].

$$\mathcal{H}[\sigma;J] = -\sum_{t=1,\dots,n}\sum_{i_1<\dots<i_t} J^{(t)}_{i_1\dots i_t}\sigma_{i_1}\dots\sigma_{i_t}\,. \tag{2.104}$$

To obtain models with many-body interaction which are analytically soluble, we change hard to soft spins, by imposing a global spherical constraint [12]:

$$\sum_i \sigma_i^2 = N\,. \tag{2.105}$$

In the MF models, in order to have a stable thermodynamics, the probability distribution of the random couplings has the following momenta (choosing a zero mean)

$$\begin{aligned}\overline{\left(J^{(n)}_{i_1\dots i_n}\right)} &= 0 \\ \overline{\left(J^{(n)}_{i_1\dots i_n}\right)^2} &= \frac{J^2 t!}{2N^{t-1}}\,,\quad i_1<\dots<i_t\,.\end{aligned} \tag{2.106}$$

The statics can be computed exactly. Since we have to compute the average of a logarithm, we introduce replica in order to change the quenched average to an annealed average over the replicated partition function

$$f(\beta) = -\lim_{N\to\infty}\lim_{n\to 0}\frac{1}{\beta N n}\partial_n\overline{Z^n} = -\lim_{N\to\infty}\lim_{n\to 0}\frac{1}{\beta N n}\log\overline{Z^n}\,. \tag{2.107}$$

In order to perform the computation, we need to exchange the order of the limits $N\to\infty$ and $n\to 0$. Indeed, to solve the MF, we have to perform a saddle-point approximation which is exact in the thermodynamic limit. Although *a priori unwarranted*, the trick works and leads to the right thermodynamically stable solution [104, 105, 106, 107].

For the p-spin model [12], obtained by (2.104) as follows

$$\mathcal{H}_p[\sigma;J] = -\sum_{t=1,\dots,n}\delta_{tp}\sum_{i_1<\dots<i_t} J^{(t)}_{i_1\dots i_t}\sigma_{i_1}\dots\sigma_{i_t} = -\sum_{i_1<\dots<i_p} J^{(p)}_{i_1\dots i_p}\sigma_{i_1}\dots\sigma_{i_p} \tag{2.108}$$

the replicated average partition function is

$$\overline{\mathcal{Z}_\beta^n} = const. \int \mathcal{D}\mathbf{Q} \, \exp\left(N\phi(\mathbf{Q})\right) \tag{2.109}$$

$$\phi(\mathbf{Q}) = \frac{\beta^2 J^2}{4} \sum_{ab} Q_{ab}^p - \log\det Q_{ab} \tag{2.110}$$

$$\mathcal{D}\mathbf{Q} \equiv \prod_{ab} dQ_{ab} \tag{2.111}$$

where $\mathbf{Q}$ is a symmetric $n \times n$ matrix, called overlap matrix, with 1 all entries in the main diagonal equal to 1 (due to the spherical constraint). The saddle point gives a self-consistency relation for $\mathbf{Q}$. However, in order to obtain the thermodynamics, an *Ansatz* is needed for the structure of the matrix $\mathbf{Q}$.

The natural choice is the Replica Symmetric *ansatz*:

$$Q_{ab} = (1-q)\delta_{ab} + q \,, \tag{2.112}$$

which leads to a phase transition at T^* between a PM phase and a SG phase. Moreover, in the low temperature phase the solution is unstable. A stable solution can be found applying a Replica Symmetry Breaking scheme at the matrix $\mathbf{Q}$.

In particular, following the scheme suggested by Parisi [52, 53, 54], it is possible to prove that a stable solution for the p-spin models can be found by imposing a $1-$RSB structure to the overlap matrix [12]. Breaking the RS structure means to parametrize $\mathbf{Q}$ through, at least, two parameters q_0 and q_1 which destroy the invariance under permutation of the RS *ansatz*. In order to preserve the invariance with respect to a sub group of permutations, the matrix may be divided into a diagonal block, where the overlap value is q_0, and an out-of-diagonal block where it is q_1. Clearly, we have to introduce one more parameter, say $m < n$ or *breaking point*, the size of the diagonal block. All these parameters will be fixed self-consistently by the MF equations. In this scheme the matrix becomes

$$Q_{ab} = q_0 + (q_1 - q_0)\epsilon_{ab}^m + (1-q_1)\delta_{ab} \tag{2.113}$$

where the matrix ϵ is defined as

$$\epsilon_{ab}^{m} = \begin{cases} 1 & \text{if } a \text{ and } b \text{ are in the diagonal block} \\ 0 & \text{otherwise} \end{cases} \tag{2.114}$$

In a spin-glass model we can build a precise link between the structure of the matrix $\mathbf{Q}$ and the structure of the space phase [55]. In particular the following relation holds

$$P(q) = \lim_{n\to 0} \frac{1}{\frac{n(n-1)}{2}} \sum_{ab} \delta(Q_{ab} - q) \tag{2.115}$$

where $P(q)$ is the distribution of the overlap, numerically computable via the evolution of two identical copies of the systems, by measuring the codistance between two real replicas. The behaviour of $P(q)$ in a finite-size system for a short-range interaction, was shown in the previous chapter (cf. section 1.4). In particular, the BC-random, at the mean-field level is solved by a Full-RSB.

If a system displays a $1-$RSB scheme, the overlap distribution will show a double peak:

$$P_{1-\mathrm{RSB}}(q) = m\delta(q - q_0) + (1 - m)\delta(q - q_1)\,. \tag{2.116}$$

Without an external field the first peak will be at $q_0 = 0$, and the second at $q_1 \neq 0$. The weight of each peak is proportional to the parameter m. This structure of $P(q)$ means that the space phase is partitioned into disconnected region. The overlap mesure if, taken two configurations of the system in the amorphous phase, they are in the same basin or in two different basins. The temperature where this happens is the static temperature T_c, also called T_K because the thermodynamics transition is a Kauzmann-like transition, i. e., a supercooled liquid changes into an ideal glass phase. Note that the T_c obtained from the $1-$RSB scheme is smaller than the RS one T^*.

The $p + s-$model is defined by the Hamiltonian

$$\begin{aligned} \mathcal{H}[\sigma, J_p, J_s] &= \mathcal{H}_s[\sigma; J_s] + \mathcal{H}_p[\sigma; J_p] \qquad (2.117) \\ \mathcal{H}_t[\sigma; J] &= -\sum_{t=1,\ldots,n} \delta_{tp} \sum_{i_1<\cdots<i_t} J^{(t)}_{i_1\ldots i_t}\sigma_{i_1}\ldots\sigma_{i_t} = -\sum_{i_1<\cdots<i_p} J^{(p)}_{i_1\ldots i_p}\sigma_{i_1}\ldots\sigma_{i_p}\,, \end{aligned}$$

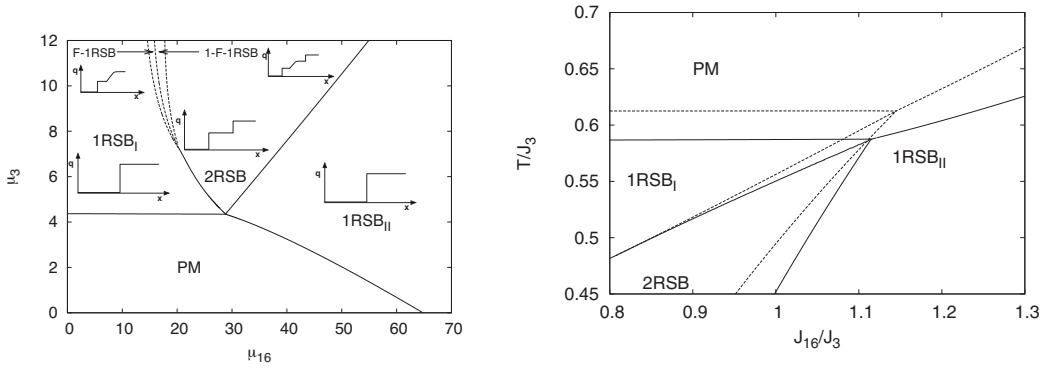

Figure 2.5: Left panel: static phase diagram of the spherical $3 + 16$ spin glass model. Between two 1-RSB regions it has a 2-RSB glass [108]. Right panel: phase diagram in T/J_3-J_{16}/J_3 plane.

the replicated free energy reads [108]

$$\begin{aligned} \phi(\mathbf{Q}) &= \frac{1}{2p}\sum_{ab} Q_{ab}^p + \frac{1}{2s}\sum_{ab} Q_{ab}^s - \log\det Q_{ab} \qquad (2.118) \\ \mu_t &= \frac{t\beta^2 J_t^2}{2}\,. \end{aligned}$$

The nature of the low-temperature glassy phase, i. e., the number of replica symmetry breaking, depends on s and p. For a fixed $s > 2$ the critical value of p to have a 2-RSB phase is given by the following equation

$$(p^2 + p + s^2 + s - 3sp)^2 - ps(p-2)(s-2) = 0\,. \qquad (2.119)$$

The corresponding phase diagram for $s = 3$ and $p = 16$ is shown in fig. (2.2.2). As we will see in the next section, near the region where a 2-RSB solution holds, the dynamics evolves on three well-separated time scales.

Equilibrium dynamics

For the SGM we can compute also the *equilibrium dynamics*: the dynamics that brings the system to the equilibrium with the environment. This can be done

through a Langevin equation where also the quenched degrees of freedom appear:

$$\begin{aligned} \Gamma_0^{-1}\partial_t\sigma_i(t) &= -\frac{\delta\mathcal{H}[\sigma;J]}{\delta\sigma_i(t)} + \zeta_i(t) \\ \langle\zeta_i(t)\rangle &= 0\,, \qquad \langle\zeta_i(t)\zeta_j(t')\rangle = \frac{\Gamma_0^{-1}}{2\beta}\delta_{ij}\delta(t-t') \equiv D_{ij}(t,t')\,. \end{aligned} \tag{2.120}$$

With no loss in generality, we may fix the microscopic time scale Γ_0^{-1} equal to 1. The spherical constraint can be encoded in the Hamiltonian through a time-dependent Lagrange multiplier $r(t)$. The Lagrange multiplier allows the spin to fluctuate continuously from $-\infty$ to $+\infty$ in a hypersphere of radius $\sqrt{N}$. The constraint is satisfied at any time t. We are interested in the case $p > 2$, where a general Hamiltonian takes the form

$$\mathcal{H}[\sigma;J] = -\sum_{t=3,\dots,n}\sum_{i_1<\dots<i_t} J^{(t)}_{i_1\dots i_t}\sigma_{i_1}\dots\sigma_{i_t} + \frac{r(t)}{2}\sum_i \sigma_i^2\,. \tag{2.121}$$

The main observables are the correlation function $C(t,t')$ and the response function $G(t,t')$, where the perturbation is applied at $t\prime < t$.

$$C(t,t') = \overline{\langle\sigma(t)\sigma(t')\rangle} \tag{2.122}$$

$$G(t,t') = \frac{\delta\overline{\langle\sigma(t)\rangle}}{\delta\beta h(t')}\,, \qquad t > t'\,. \tag{2.123}$$

Since we study the equilibrium dynamics, the Fluctuation-Dissipation Theorem holds and gives a relation between correlation and response:

$$G(t,t') = \theta(t-t')\partial_{t'}C(t,t') \tag{2.124}$$

where $\theta(t)$ is the Heaviside distribution. Defining the probability distribution $P(\sigma_i,t;\sigma_i,0)$ for a path $\sigma_i(0) \to \sigma_i(t)$, according to the Martin-Siggia-Rose-de Dominicis-Peliti path-integral formulation [109, 110]:

$$\begin{aligned} P(\sigma_i,t;\sigma_i,0) &= \langle\delta\left(\sigma_i(t)-\sigma(0)\right)\rangle_\zeta = \int \mathcal{D}\zeta(t)e^{\zeta D^{-1}\zeta}\delta\left(\sigma_i(t)-\sigma(0)\right) \\ \zeta D^{-1}\zeta &\equiv \int_0^t dt'dt''\,\zeta(t')_i D^{-1}_{ij}(t',t'')\zeta(t''_j) \end{aligned} \tag{2.125}$$

In this formulation the average over disorder can be computed using the identity

$$1 = \int \mathcal{D}\sigma(t)\, P(\sigma_i, t; \sigma_i, 0) \equiv Z_J \,. \tag{2.126}$$

Since the noise is Gaussian, introducing a set of response fields which play the role of a Lagrange multiplier $\hat{\sigma}_i(t)$, we can write

$$\begin{aligned} Z_J &= \int \mathcal{D}\sigma(t)\mathcal{D}\hat{\sigma}(t)\, e^{S[\sigma,\hat{\sigma}]} \\ S\left[\sigma,\hat{\sigma}\right] &= -\frac{1}{2}\int_0^t dt'dt''\, \hat{\sigma}(t')_k D_{kl}(t',t'')\hat{\sigma}_l(t'') + i\int_0^t dt'\, \hat{\sigma}_k(t')\mathcal{L}_J \\ \mathcal{L}_J &\equiv \partial_t\sigma_k(t) + \frac{\delta\mathcal{H}[\sigma;J]}{\delta\sigma_k(t)} \,. \end{aligned} \tag{2.127}$$

From eq. (2.127) it follows that we can study the equilibium dynamics by averaging over the disorder without introducting replicas.

Averaging over the disorder involves several indipendent averages over the set of quenched variables $J_t \to J^t_{i_1\ldots i_t}$. Each of these variables, according to the first two momenta chosen in (2.106) are Gauss distributed

$$\overline{\mathcal{A}_J} = \int d\mu(J)\, \mathcal{A}_J = \int \prod_{t=1}^{n} d\mu(J_t)\mathcal{A}_J \,. \tag{2.128}$$

We can then factorize the terms which contain differents coupling in eq. (2.127): in particular, we can use the well-known results about the dynamics of the p-spin models [88].

If we have only one interaction between p-bodies one has

$$\begin{aligned} \mathcal{L}_J &= \frac{p}{p!}\sum_{i1,\ldots,i_{p-1}} J^p_{i_1,\ldots,i_p}\sigma_{i_1}\ldots\sigma_{i_{p-1}} + \mathcal{L}_0 \\ \mathcal{L}_0 &\equiv (\partial_t - r(t))\,\sigma_i \,. \end{aligned} \tag{2.129}$$

After the integration over the Gaussian disorder, we can perform a saddle-point approximation which allows us to write an effective Langevin equation for the single spin. The noise of the new Langevin equation is no longer delta-correlated

[111]

$$\begin{aligned}
\partial_t \sigma(t) &= r(t)\sigma(t) + \int_0^t dt'\, \mathcal{K}(t,t')\sigma(t') + \xi(t) \\
\langle \xi(t) \rangle &= 0\,, \quad \langle \xi(t)\xi(t') \rangle = 2\delta(t-t') + \Lambda(t,t') \\
\Lambda(t,t') &\equiv \Lambda\left[C(t,t')\right] = \mu_p C(t,t')^{p-1}\,, \quad \mu_p \equiv \frac{(\beta J^{(p)})^2 p}{2} \\
\mathcal{K}(t,t') &\equiv \mathcal{K}[C(t,t'), G(t,t')] = \frac{\delta\Lambda\left[C(t,t')\right]}{\delta C(t,t')} G(t,t')\,.
\end{aligned} \tag{2.130}$$

Since we are interested in the equilibrium dynamics, we assume the validity of FDT and time translational invariance (TTI). Using the spherical constraint, we can write a self-consistency equation for the correlation function:

$$\begin{aligned}
\frac{dC}{dt}(t) &= -\int_0^t dt'\, K(t)\dot{C}(t') - C(t) \\
K(t) &\equiv \mu_p C(t)^{p-2}\,.
\end{aligned} \tag{2.131}$$

It is clear that eq. (2.131) is equivalent to the MCT equation (2.95) in the schematic theoryv[13]. In particular, the equations of the schematic theory are recovered for $p = 3$.

Studying eq. (2.131), we find a critical temperature where the ergodicity is broken: it is the temperature where TTI and FDT fail. When ergodicity breaks down, $C(t)$ develops a plateau at the value $q_d = .51\ldots$. The temperature where this happens, after tuning the parameters, is the same of the MCT. Moreover, in the p-spin model we have two critical temperature: at the first one, the T_d or T_{MC} temperature, the dynamics is arrested, the second one, the static temperature $T_c < T_d$, is the temperature where a true thermodynamic transition takes place.

We can straightforwardly generalize the dynamic equations to the case with different many-body interactions by using the kernel

$$K(t) = \sum_{s=3}^{n} \mu_s C(t)^{s-2} \tag{2.132}$$

In the study of the equilibrium dynamics of a spin system, Sompolinsky [112] suggested that these models reach equilibrium through a sequence of characteristics

time scales (τ_r) all of them diverging at the thermodynamic limit. In particular, supposing to have R time scales with $\tau_r > \tau_s$ with $r > s$, it holds $\tau_r/\tau_s \to \infty$ when $N \to \infty$. At the same time, the shorter time scale τ_s with $s < r$ relax to equilibrium. The Sompolinsky solution brings to the right static solution only in models which display a Full Replica Symmetry Breaking solution, e. g., SK model or Blume-Capel with quenched disorder. Indeed, if a model is solved by a finite number of RSB (e. g., p-spin models) the Sompolinsky solution is actually not correct. However, it is possible to prove that, assuming the Sompolinsky's picture for the hierarchy of time sectors, but following the calculation of Crisanti-Horner-Sommers (CHS) [88], it is possible to solve the dynamics via the same procedure used for the static calculation with the RSB scheme.

In particular, if a model displays an r-steps RSB then the dynamics evolves over $r + 1$ time sectors. From the point of view of the solution of the equation for the correlation $C(t)$, it means that exists a region of the phase diagram where $C(t)$ displays r plateaus. Choosing a suitable path in the phase diagram we send to infinity one or more of these plateau.

Configurational Entropy

Another object which can be exactly computed in the MF-SG models is the Complexity Σ, also called Configurational Entropy.

In structural glasses the Configurational Entropy is the excess between the entropy of the liquid and that of the crystalline phase

$$S_{exc} = \Delta S = S_{liq} - S_{cry}\,. \tag{2.133}$$

As we have seen in the previous section, the behaviour of the excess entropy, as a function of temperature, can be extrapolated by the experiment below T_g.

In particular, the curve obtained by extrapolation seems to show that S_{exc} vanishes linearly at some finite temperature T_K called Kauzmann temperature [63]. If it were possible to bring a sample of supercooled-liquid following some *equilibrium protocol* down to T_K, the liquid would undergo a thermodynamic transition to an ideal glass. This is due to the fact that, below T_K, the entropy of the glass is lower than the entropy of the crystal.

In a mean-field model the configurational entropy is a true state function and can be computed via a Legendre transformation of the replicated free energy Φ with respect to the single-state free energy f[84]

$$\Sigma(f,T) = \min_m \left[-\beta m \Phi(m,T) - \beta m f\right] \tag{2.134}$$

where m is the breaking point of the RSB calculation.

We can see it also from another point of view[113]. The complexity is related to the number of metastable states of the system. Imagine to compute the partition function of a system in which ergodicity can be broken and the phase space separates into many components or states. In each state the Boltzmann measure can be different from zero:

$$\begin{aligned} \mathcal{Z} &= \mathrm{Tr}_\sigma e^{-\beta\mathcal{H}[\sigma]} = \sum_\alpha^{\mathcal{N}} \mathrm{Tr}_{\sigma_\alpha} e^{-\beta\mathcal{H}[\sigma_\alpha]} = \\ &= \sum_\alpha^{\mathcal{N}} e^{-\beta N f_\alpha} = \sum_\alpha^{\mathcal{N}} \int df\, \delta(f-f_\alpha) e^{-\beta N f}\,. \end{aligned} \tag{2.135}$$

Introducing the number of states with free energy equal to f_α,

$$\mathcal{N}(f) = \sum_\alpha \delta(f-f_\alpha) \tag{2.136}$$

it is known [cita] that this number grows exponentially with the size of the system

$$\mathcal{N}(f) = e^{N\Sigma(f)} \tag{2.137}$$

where $\Sigma(f)$ is the complexity of the states with free energy f. Inserting (2.137) into (2.135)

$$\mathcal{Z} = e^{-\beta F_{eq}(\beta,N)} = \int df\, e^{-\beta N(f - T\Sigma(f))} \tag{2.138}$$

since the integrand in (2.2.2) is exponentially large in the size of the system, it may perform a saddle-point approxiamtion:

$$F_{eq}(\beta,N) = \min_f \left[f - T\Sigma(f)\right] \tag{2.139}$$

In the p-spin models the dynamic transition takes place when a non vanishing configurational entropy appears and the system can be trapped in an exponentially large number of metastable states. Between T_d and T_c, at a high *threshold* free energy very many (exponentially many with the size) metastable states occur between a threshold free energy and a lower free energy f_0, that depends on temperature such that

$$\Sigma(F,T) > 0\,, \tag{2.140}$$

for $f \in [f_0, f_K]$. As $T \searrow T_c$ the lower free energy at which Σ is non-vanishing goes to the global free energy minimum, and $\Sigma(T) \searrow 0$. Indeed, $\Sigma(T)$ is the complexity of the lowest lying (in free energy) dynamically relevant metastable states.

2.2.3 Numerical solution for MCT equations

In this section, we want to illustrate the algorithm used to numerically solve the MCT equations. The method implemented is well known [114]. Since we have already studied schematic models, we discuss only the case indipendent from the wave number $\mathbf{k}$. However, the algorithm can be straightforwardly generalized to the $\mathbf{k}-$dependent case.

The equation to solve has the form

$$\begin{aligned} \dot{\phi}(t) &+ \omega^2\phi(t) + I(t) = 0 \\ I(t) &\equiv \int_0^t dt'\, K(t-t')\dot{\phi}(t') \end{aligned} \tag{2.141}$$

the memory kernel can be integrated by parts as follows

$$\begin{aligned} I(t) &= K\left(t-\frac{t}{2}\right)\phi\left(\frac{t}{2}\right) - K(t)\phi(0) - \int_0^{\frac{t}{2}} dt'\, \dot{K}(t-t')\phi(t') + \\ &- \int_0^{t-\frac{t}{2}} dt'\, K(t-t')\dot{\phi}(t')\,. \end{aligned} \tag{2.142}$$

Now we have to discretize the problem, defining the times $t_i = i\delta$ with $i = 0, 1, \ldots$.

$$\begin{aligned} \dot{\phi}_i &+ \omega^2\phi_i + I_i = 0 \qquad (2.143)\\ I_i &= K_{i-\frac{i}{2}}\phi_{\frac{i}{2}} - \phi_0 K_i - \sum_{j=1}^{\frac{i}{2}} \int_{t_{j-1}}^{t_j} dt'\, \dot{K}(t-t')\phi(t') + \\ &- \sum_{j=1}^{i-\frac{i}{2}} \int_{t_{j-1}}^{t_j} dt'\, K(t-t')\dot{\phi}(t') \end{aligned}$$

where $\frac{i}{2}$ is the maximum integer small than the real number $\frac{t}{2}$. To calculate the integrals in (2.143) we use the following identity

$$\begin{aligned} \int_{t_{j-1}}^{t_j} dt'\, \dot{A}(t')B(t') &= (A(t_j) - A(t_{j-1}))\, dB + O(\delta^3) \qquad (2.144)\\ dB &\equiv \frac{1}{\delta}\int_{t_{j-1}}^{t_j} dt'\, B(t')\,. \end{aligned}$$

In order to simplify the notation, we introduce the following symbols

$$S_{l,m}^{\pm,\pm k}(A, dB) \equiv \sum_{j=l}^{m} \pm\, (A_{k\pm j+1} - A_{k\pm j})\, dB_j \qquad (2.145)$$

using (2.144) and (2.145), the integral becomes

$$I_i = K_{i-\frac{i}{2}}\phi_{\frac{i}{2}} - \phi_0 K_i - S_{1,\frac{i}{2}}^{-,-i}(K, d\phi) - S_{1,i-\frac{i}{2}}^{-,-i}(\phi, dK)\,. \qquad (2.146)$$

To approximate numerically the first derivative $\dot{\phi}_i$ we adopt the expression

$$\dot{\phi}_i = \frac{1}{2\delta}\phi_{i-2} - \frac{2}{\delta}\phi_{i-1} + \frac{3}{2\delta}\phi_i \qquad (2.147)$$

and we can finally write

$$\begin{aligned} \phi_i &= \frac{(1-d\phi_1)}{\alpha}K_i + \frac{b_i}{\alpha} \\ \alpha &\equiv \frac{3}{2\delta} + \omega^2 + dK_1 \\ b_i &\equiv -\Sigma^{-,-i}_{2,\frac{i}{2}}(K, d\phi) - \Sigma^{-,-i}_{2,i-\frac{i}{2}}(\phi, dK) - K_{i-\frac{i}{2}}\phi_{\frac{i}{2}} + \phi_{i-1}dK_1 - K_{i-1}d\phi_1 \end{aligned} \tag{2.148}$$

In MCT the memory kernel $K(t)$ is polynomial in $\phi(t)$. So eq. (2.148) takes the form

$$\phi_i = \frac{K_i(\phi_i)}{\alpha} + \frac{b_i}{\alpha}\,. \tag{2.149}$$

Indeed, for any time $t_i = \delta i$, we have to find by iteration a solution of (2.149). This means that, at each time i, we have to iterate n times eq. (2.149) until

$$\phi_i^{(n+1)} - \phi_i^{(n)} < \epsilon \tag{2.150}$$

for a initially selected ϵ indipendent of n.

Since near the glassy transition the dynamics evolves in a plateau over very long time, some tricks are needed in order to implement a numerical algorithm that solves the self-consistency equation. The algorithm used is based on a procedure of decimation and doubling of the integration step δ. This procedure saves memory and is able to explore many time decades.

1. Choosing $\delta N_t \ll 1$, where N_t is such that $t_{max} = \delta N_t$, we expand eq. (2.141) up to $t_{max}/2 \ll 1$. From the short time expansion, we evalutate ϕ_i with $i = 0, \ldots, \frac{N_t}{2} - 1$.

2. Through eq. (2.149), we compute the solution from $t_{max}/2$ to t_{max} by solving self-consistently the equation for ϕ_i.

3. Once the solution is obtained up to t_{max}, we decimate by half the number of

points N_t with the following prescriptions

$$\begin{aligned}
&(K_{2i}, \phi_{2i}) \to (K_i, \phi_i) \\
&\frac{1}{2}\left(dK_{2i} + dK_{2i-1}, d\phi_{2i} + d\phi_{2i-1}\right) \to (dK_i, d\phi_i)\ , \quad 1 \leq i \leq \frac{N_t}{4} \\
&\frac{1}{6}\left(dK_{2i} + 4dK_{2i-1} + dK_{2i-2}, d\phi_{2i} + 4d\phi_{2i-1} + d\phi_{2i-2}\right) \to (dK_i, d\phi_i)\ , \quad \frac{N_t}{4} \leq i \leq \frac{N_t}{2}\,.
\end{aligned} \tag{2.151}$$

4. Go back to 2. repeating the procedure with $\delta_{new} = 2\delta$.

Since to study a multi-step relaxation we need to solve MCT equation on very long times, we have chosen $\delta_{in} = 10^{-10}$, $N_t = 10^3$ repeating the decimation procedure up to $N_{dec} = 100$.

In order to study the spectrum of $\phi(t)$ defined through the Fourier Transform

$$\widehat{\phi}(\omega) = \frac{1}{2\pi}\int_{-\infty}^{+\infty} dt\, e^{-i\omega t}\phi(t) \tag{2.152}$$

I have used a Fast Fourier Transform (FFT) algorithm. Discretizing time and frequencies one has

$$\widehat{\phi}_\omega = \sum_{k=0}^{N-1} \phi_k e^{-i\frac{2\pi}{N}\omega k} \tag{2.153}$$

If t_{max} is the support of $\phi(t)$, the minimum frequency of $\widehat{\phi}(\omega)$ is

$$\omega_{min} = \frac{2\pi}{t_{max}}, \tag{2.154}$$

in order to solve ω_{min} we need of

$$N = \frac{\omega_{max} t_{max}}{\pi} \tag{2.155}$$

number of points. Since $\phi(t)$ varies on a huge time scale, i. e., t_{max} can be $\sim 10^{16}$, while the fast processes thermalize in a time of order ~ 1 we need of $N \sim 10^{18}$ to observe both processes. Therefore, FFT has been done on increasing time windows with $N \sim 10^6$ defined on a varying time sector $0 < T < t_{max}$.

2.3 An introduction to secondary processes

Secondary processes[10] in supercooled liquids and glasses are related to complicated local, non- cooperative (or not fully cooperative) dynamics. They occur on time scales much slower than cage rattling, but much faster than structural relaxation. Their existence was first pointed out in the sixties from the experimental observation of a second peak in dielectric loss spectra at a frequency, $\nu_\beta \sim 1/\tau_\beta$, higher than the frequency $\nu_\alpha \sim 1/\tau_\alpha$ of the peak known to represent the structural α relaxation. This so-called β-peak was recorded in glycerol, propyleneglycol, n-propane, various polymeric substances and made similar liquids composed of rigid molecules. Johari and Goldstein eventually conjectured that such processes — now known as Johari-Goldstein (JG) — originate from the same complicated frustrated interactions leading to the glass transition [115, 116, 117].

Also in cases where the spectral density of response losses does not show a neat second peak, secondary processes can be active and produce anomalies at high frequency. This feature of the susceptibility loss part is called "excess wing" and was initially observed as a separate phenomenon [118]. Actually, classifications exist in terms of glass formers displaying excess wings and substances showing well defined β-peaks [119, 120, 121]. However, more recent investigations provided evidence supporting the idea that the excess wing is not an indipendent dynamic process, but rather a manifestation of a JG process [122][123]. That tuning proper thermodynamic parameters (temperature, pressure, concentration, ...) the latter can emerge out of the former (or, viceversa, a secondary peak can change into an excess wing). Cummins [124] e. g., suggests that the relevant parameter may be the rotation — translation coupling constant which grows as density increases, and is larger for liquid glass former made of elongated, strongly anisotropic molecules. Also theoretical attempts have been carried out in this direction as, for instance, in the framework of Mode Coupling Theory (MCT). The relaxation of reorientational correlation and rotation-translation coupling in liquids composed of strongly anisotropic molecules appears to be logarithmic in time [125]. In fig. (2.3) the dielectric loss spectra of benzophenone for various temperatures is shown. It is possible to distinguish α relaxation peaks and excess wings.

A comprehensive picture is not yet been established and many questions are

open. For instance, the dependence on temperature and pressure (or concentration) of characteristic time scales of JG processes, or the possibility that seconday processes might hide a certain degree of cooperativeness [126], or the persistence of β processes also below the glass transition temperature T_g [124]. A very interesting question is whther there is a straightforward connection, and in case which one, between processes evolving at different time scales. Or, in other terms, whether one might deduce the long-time behaviour of the α relaxation from the behaviours of the fast small-amplitude cage dynamics (γ processes) and of the (slower) secondary processes.

In glasses, and glass-formers, where α and JG β peaks can be clearly resolved in frequency (e.g., 4-polybutadiene, toluene [127] [128] or sorbitol [129]), one can describe the system in terms of a scenario where two time-scale bifurcations speed up as temperature is lowered and processes consequently evolve on three "well separate" time sectors. A multistep relaxation mechanism over three separated time scales has been numerically simulated in high density gel [130].

The generalization consists in coupling the dynamical variable "spin" (playing, e.g., the role of a density fluctuation, or a component of molecular orientation) with other spins in two different ways: as a part of a group of s variables and as a part of a group of p variables. Variables in each group interact among themselves through random multi-body interaction of zero mean and mean square strength of magnitude $\sim J_s$ and J_p, respectively. As one of these two interaction mechanisms (e.g., p-body interaction) involves more dynamical variables than the other (e.g., s-body interaction), this triggers a mixture of strong and weak cooperativeness that can be varied by an external control parameter (e.g, J_p/J_s).

Our aim is to provide a model to interpolate between different resolutions of secondary processes and support the idea that excess wings and secondary peaks are both manifestations of "intermediate" (slow, yet thermalized) processes between cage rattling and structural relaxation. Relying on the results about correlation functions and spectral densities we can argue on the possible relation between processes evolving on different time scales and their characteristic times, τ_α, τ_β and τ_γ.

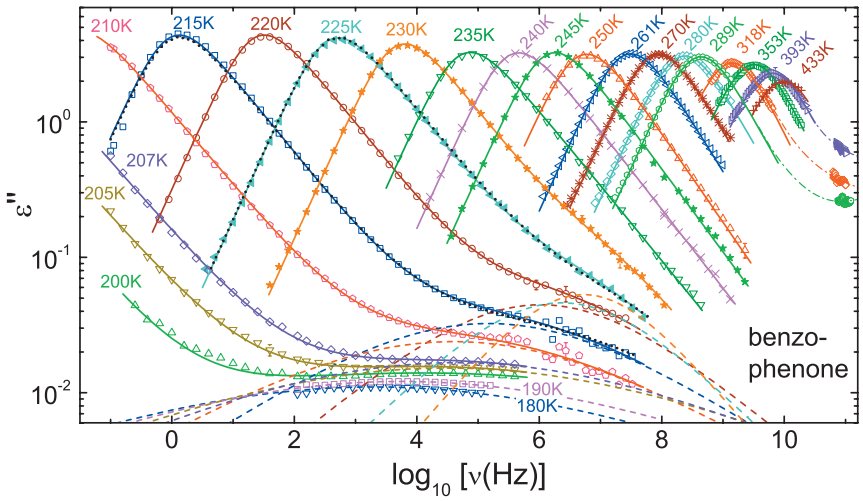

Figure 2.6: Frequency-dependent dieletric loss of benzophenone (BZP) for various temperatures [131]

2.4 The leading spin model for secondary processes

The model we will consider is a spherical $s+p$-spin interaction model:

$$\mathcal{H} = \sum_{i_1<\ldots<i_s} J^{(s)}_{i_1\ldots i_s}\sigma_{i_1}\cdots\sigma_{i_s} + \sum_{i_1<\ldots<i_p} J^{(p)}_{i_1\ldots i_p}\sigma_{i_1}\cdots\sigma_{i_p} \tag{2.156}$$

where $J^{(t)}_{i_1\ldots i_t}$ $(t=s,p)$ are uncorrelated, zero mean, Gaussian variables of variance

$$\frac{J_t^2 t!}{2N^{t-1}} \tag{2.157}$$

and σ_i are N "spherical spins" obeying the constraint

$$\sum_i \sigma_i^2 = N\,. \tag{2.158}$$

Since every spin interacts very slightly:

$$J_t \sim \frac{1}{N^{(t-1)/2}} \tag{2.159}$$

with every other one, for this system the mean-field approximation is exact. We will consider the case in which each spin interact with the rest of the system in two different ways: in *small* groups (of s elements) and in *large* group (of p elements). If $p-s$ is large enough, standard MCT provides evidence for glass-to-glass transitions beyond the validity of time translational invariance [132], which is a fundamental assumption for MCT. The theories developed for quenched disordered systems, allow to the computation of the stable solutions corresponding to the glassy phases below the dynamic transition and the identification of the nature of the processes going on in each glassy phase. Eventually, it can be shown that the model thermodynamics displays three distinct glass phases below the line of dynamic arrest, one of which consists of processes thermalized at three completely separate time scales [108][133]. Starting from these considerations dynamic equations are obtained, reducing to those of schematic MCT above the mode coupling temperature T_d.

The glass phase with double bifurcation of time scales can be obtained in the s-p spherical spin model under a certain condition on the values of s and p, namely for a given s, p that solve the equaltion

$$(p^2 + s^2 + p + s - 3ps)^2 - ps(p-2)(s-2) = 0. \tag{2.160}$$

as it has been shown in Ref. [108]. Some example of "threshold" couples (s, p) to obtain a double bifurcation are $(3, 8)$, $(4, 11)$ or $(5, 16)$. The larger $p - s$, the broader the region of phase diagram where a double bifurcation can be found.

The external thermodynamic parameters are the temperature and the relative weight of the two interaction terms (big to small) in the Hamiltonian. In unit of J_s: T/J_s and J_p/J_s. These are related to the usual mode-coupling parameters so that the memory kernel of the dynamic equation takes the mode-coupling form

$$\mathcal{K}(\phi) = \mu_s \phi^{s-1} + \mu_p \phi^{p-1} \tag{2.161}$$

$$\mu_p = p\beta^2 J_p^2/2 \tag{2.162}$$

$$\mu_s = s\beta^2 J_s^2/2 \tag{2.163}$$

We stress that as $p-s$ is large, and $s > 2$, the theory we are considering yields qualitatively different results from schematic MCTs with, e.g., $s = 2$ and $p = 3$

[125, 134]. Indeed, in schematic MCT with linear and quadratic terms in the kernel a clear separation of time scales is unfeasible and the (possible) thermodynamic glassy phase can only speed up the bifurcation time scales, as discussed in Refs. [135, 136, 132, 133].

The strong three-level separation we study can, then, be softened and adapted to less defined structures than the two peaks (e.g., the excess wing), by tuning the external parameters temperature and J_p/J_s, or by choosing s, p model instances with smaller $p - s$.

The model was initially developed to study the nature of polyamorphism and amorphous-to-amorphous transitions. On the static front, the analysis can be carried out within the framework of the RSB theory, leading to the identification of low temperature glass phases of different kinds [108]. Below the Kauzmann-like transition line $T(J_p/J_s)$, the model displays both "one-step" RSB solutions, known to reproduce all the basic properties of structural glasses [137], and a physically consistent "two-step" solution [108].

Above the Kauzmann transition line, the thermodynamically stable phase is the fluid paramagnetic phase, but excited glassy metastable states are present in large number, growing exponentially with the size N of the system. The configurational entropy of the system is thus extensive. Because barriers between minima of the free energy landscape separating local glassy minima grow as some positive power of N in the mean-field approximation, "metastable" states have actually an infinite life time in the thermodynamic limit and ergodicity breaking occurs as soon as an extensive configurational entropy appears. The highest temperature at which this happens is known as *dynamic* [88], *arrest* [137] or *Mode Coupling* [89] temperature. We shall denote it by T_d. As the temperature is lowered down to T_d the spin-spin time correlation function (analog to the correlation between density fluctuations) develops a plateau that, eventually, extends to infinite time as $T = T_d$, signaling the ergodicity breaking.

In Fig. 2.7 we display the $(T/J_s, J_p/J_s)$ phase diagram for $s = 3$ and $p = 16$. We will use this specific case throughout this thesis, for which strong discrimination of the secondary processes is easily realizable in a relative wide region of the phase diagram. The dynamic and thermodynamic properties of such an instance below the dynamic transition are discussed in Ref. [138].

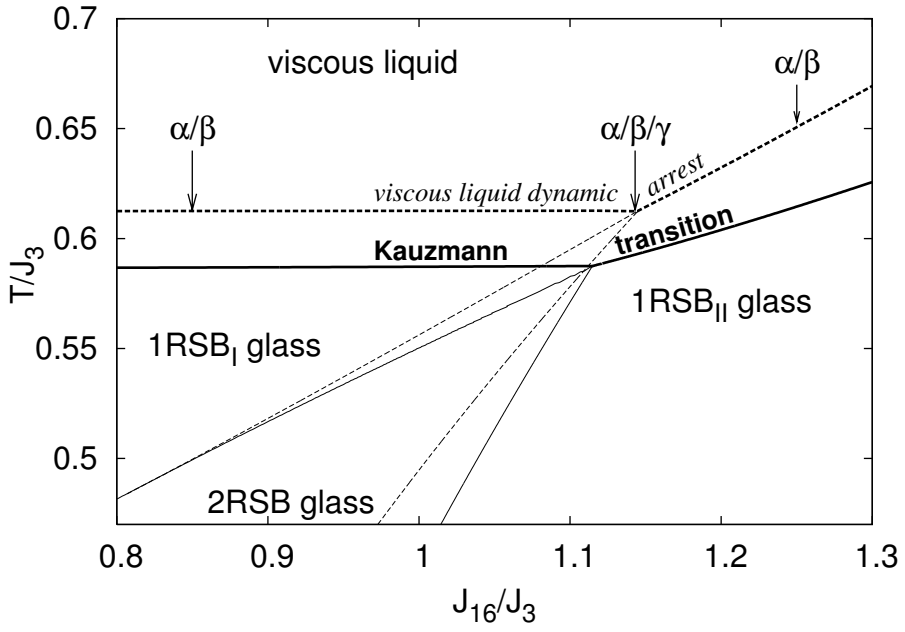

Figure 2.7: Phase diagram of the $s = 3$, $p = 16$ spherical spin model. Dynanical transition lines are dashed, while thermodynamical transition lines beneath are full. 1RSB_I stays for a glass with a single time scale bifurcation with relatively low nonergodicity factor for the time correlation function. 1RSB_{II} glass stays for a glass with a single time scale bifurcation with higher nonergodicity factor. The 2RSB displays two bifurcations and two possible correlation values in the arrested state.

Since the dynamic counterpart of a RSB is known to be a time scale bifurcation [112, 139], Eq. (2.156) provides a leading model to probe the behaviour of characteristic time scales in presence of secondary processes and the different mechanisms in which they can arise starting from high temperature and cooling down the system.

2.4.1 Dynamics

The relaxational dynamics of the system is described by the Langevin equation

$$\begin{aligned} \Gamma_0^{-1}\frac{\partial\sigma_k(t)}{\partial t} &= -\frac{\delta\mathcal{H}[\{\sigma\}]}{\delta\sigma_k(t)} + \eta_k(t) \\ \langle\eta_k(t)\eta_n(t')\rangle &= 2k_BT\Gamma_0^{-1}\delta_{kn}\delta(t-t') \end{aligned} \tag{2.164}$$

where η_k is the thermal white noise and Γ_0^{-1} is the microscopic time scale. Using a Martin-Siggia-Rose path-integral formalism one can reduce the equations of motion to a single variable ($\sigma(t)$) formulation [109, 110]. The fundamental observables to study the onset of a slowing down of the dynamics are the time correlation between the spin variable at time t' and time $t > t'$ and the response function to a small perturbative field h. For our system, they are defined as

$$C(t,t') = \overline{\langle\sigma(t)\sigma(t')\rangle} \tag{2.165}$$

$$G(t,t') = \frac{\delta\overline{\langle\sigma(t)\rangle}}{\delta\beta h(t')}; \qquad t > t' \tag{2.166}$$

where the overbar denotes average over quenched disorder, whereas brackets stay for average over different trajectories (thermal average). For temperature above T_d the time translational invariance (TTI) holds and the response and correlation functions are related by the Fluctuation - Dissipation Theorem (FDT):

$$G(t-t') = \theta(t-t')\partial_{t'}C(t-t') \tag{2.167}$$

The dynamical equation of the correlation function takes the form

$$\Gamma_0^{-1}\frac{\partial C(t)}{\partial t} + \bar{r}C(t) + \int_0^t dt'\Lambda[C(t-t')]\frac{\partial C(t')}{\partial t'} = \bar{r} - 1 \tag{2.168}$$

with initial condition $C(0) = 1$, and

$$\bar{r} = r - \Lambda[C(0)] \tag{2.169}$$

The parameter r is the "bare mass" [140], that for the spherical model is related to the Lagrange multiplier used to enforce the spherical constraint [88]. The value of

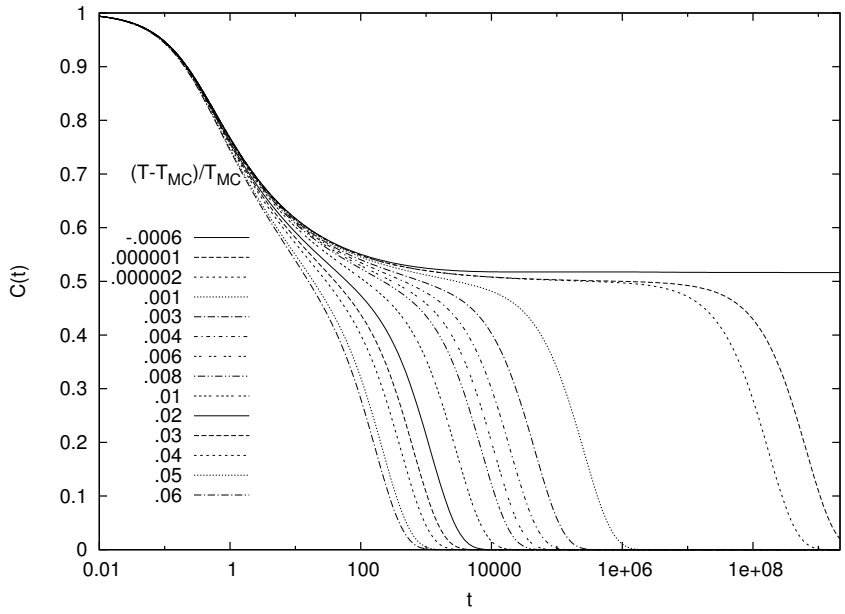

Figure 2.8: Correlation function vs. time on log scale at fixed temperature for the $s = 3$-spin model ($J_p = 0$).

$\bar{r}$ depends on the temperature, and $J_{s,p}$; however, in the high temperature phase it equals 1, so that the r.h.s. of (2.168) vanishes.

The function $\Lambda(t) = \Lambda[C(t)]$ is the memory kernel. In the specific case of our model, it has the functional form

$$\Lambda(q) = \mu_s q^{s-1} + \mu_p q^{p-1} \tag{2.170}$$

(compare with eq. (2.161)). In fact, the evolution of the correlation function is described by a dynamical equation equivalent to that of schematic mode-coupling theories, in which second time derivative term in MC equations is replaced by the first [141, 89].

For $J_s = 0$ the usual spherical p-spin model [88] is recovered. In this model, above T_d the correlation function has the shape plotted in Fig. 2.8, with one plateau developing for a long time.

Cooling down the system and increasing J_s along certain paths in the phase diagram approaching the tricritical point, the time-correlation function develops *two* plateaus at different correlation values, cf. Figs. 2.9, 2.10 and 2.11.

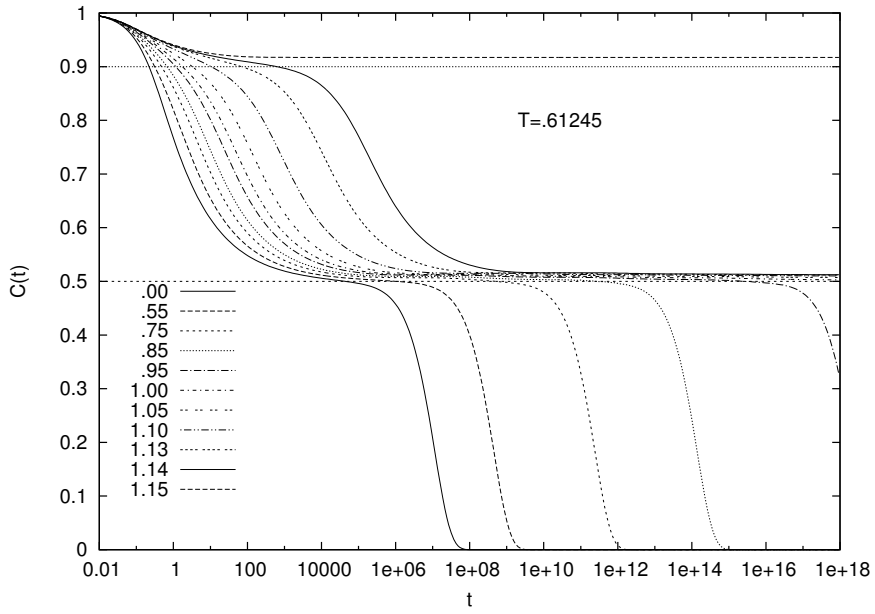

Figure 2.9: Correlation function vs. time on log scale at fixed $T/J_s = 0.61245$ with $s = 3$ and $p = 16$ increasing J_{16} from zero to $J_{16}/J_3 = 1.145$ such that $T_d(J_{16}/J_3) = 0.61245$.

As mentioned above we will denote by γ the fastest relaxation (also referred to as β_{fast} [142]), by β the secondary Johari-Goldstein relaxation (β_{JG}) and by α the structural relaxation. In Fig. 2.10 we display the behaviour of $C(t)$ when approaching the tricritical point from high temperature along a $T(J_p)$ line normal to the dynamic transition line with the 1RSB_{II} glass. Changing path, cf. Fig. 2.11 the qualitative behaviour is the same (though quantitative differences may be sizeable). A first plateau, q_1, occurs for $t \gtrsim t_\gamma$ and a second one, $q_2 < q_1$, on the characteristic time-scale at which the secondary relaxation occurs ($t \gtrsim t_\beta$). We now study the behaviour in T of characteristic relaxation times for processes on different time scales and their functional interrelation.

Near each plateau q_k the dynamical equation (2.168) predicts a power law behaviour of $C(t)$:

$$C(t) - q_\kappa \sim t^{-a_\kappa}, \tag{2.171}$$

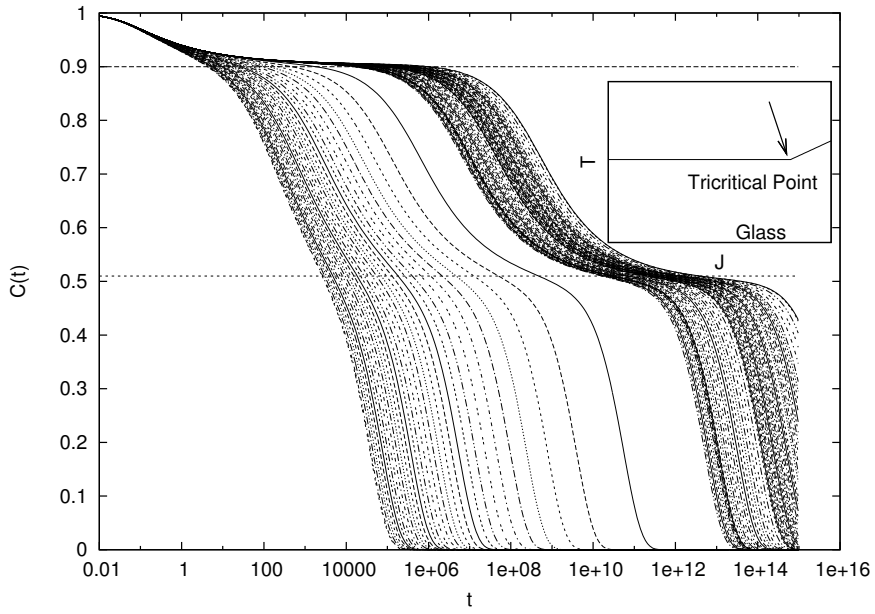

Figure 2.10: Correlation function vs. time on log scale in a cooling procedure in the $T/J_s, J_p/J_s$ phase diagram with $s = 3$ and $p = 16$ along a path normal to the right hand side fluid/glass dynamic transition line, ending at the tricritical point $(0.61234, 1.1446)$.

for $C(t) \gtrsim q_k$, and the von Schweidler law:

$$C(t) - q_\kappa \sim -t^{b_\kappa} \tag{2.172}$$

for $C(t) \lesssim q_\kappa$. We can now expand the dynamical equation (2.168) about the plateaus in powers of

$$\phi(t) = C(t) - q_\kappa \,, \tag{2.173}$$

with $\phi \ll 1$. To this aim, a suitable rescaled time $\tau = t/t_\kappa$, is introduced, where t_κ diverges at the critical point, and a relative rescaling function $g_\kappa(\tau)$, such that $\phi(t) \sim g_\kappa(\tau)\sqrt{\bar{r}(q) - \bar{r}}$, cf. next section. Eventually the scaling equation

$$(1 - \overline{m}_\kappa) g_\kappa^2(\tau) + \int_0^\tau d\tau' \, [g_\kappa(\tau - \tau') - g_\kappa(\tau)] \, \frac{\partial g_\kappa(\tau')}{\partial \tau'} = -1 \tag{2.174}$$

is obtained. The parameter $\overline{m}_k$, also called "exponent parameter" λ in MCT, is

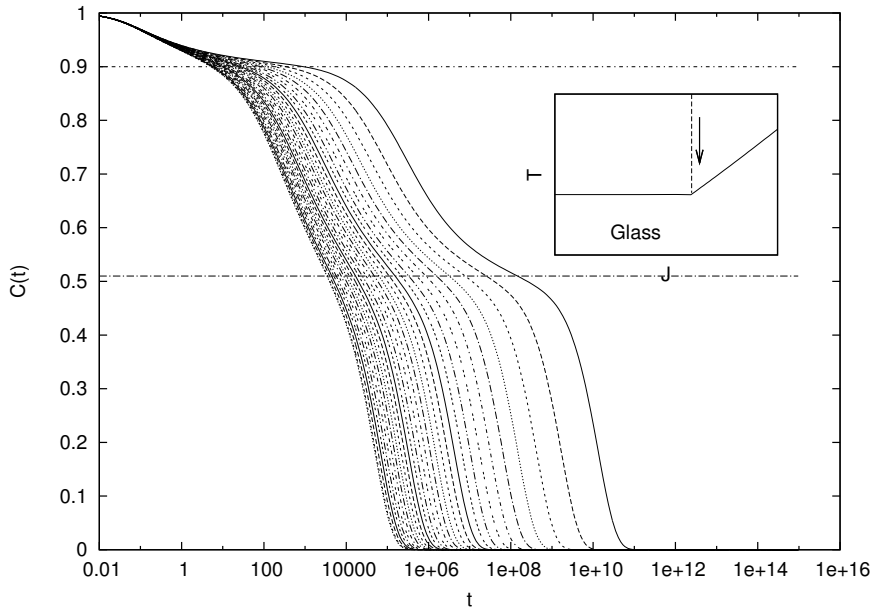

Figure 2.11: Correlation function vs. time on log scale in a cooling procedure in the $T/J_s, J_p/J_s$ phase diagram with $s = 3$ and $p = 16$ along the constant $J_{16} = 0.1446$ line, i.e. path normal to the left hand side fluid/glass dynamic transition line ending at the tricritical point.

given exactly by

$$\overline{m}_\kappa = \frac{(1-q_\kappa)^3}{2}\Lambda''(q_\kappa) \tag{2.175}$$

where the plateau correlations q_k are obtained from the self-consistency equations for the asymptotic dynamic solution for the 2RSB glass [138]. Inserting the expressions (2.171)-(2.172) of $g_k(t)$ into Eq. (2.174) one obtains the following relation:

$$\overline{m}_\kappa = \frac{\Gamma^2(1-a_\kappa)}{\Gamma(1-2a_\kappa)}; \quad 0 < a_\kappa < 1/2 \tag{2.176}$$

and

$$\overline{m}_\kappa = \frac{\Gamma^2(1+b_\kappa)}{\Gamma(1+2b_\kappa)}; \quad 0 < b_\kappa < 1 \tag{2.177}$$

The analysis of the exponents for the two plateaus as the tricritical point is approached along the path normal to the high J_{16} dynamic transition line is reported in Table 2.1. The approach to the tricritical point is not unique and the estimate of the exponents is usually very sensitive in the MCT. This can possible because

Table 2.1: Mode-coupling theory exponents of power-law relaxation to and from high and low plateau in correlation.

a_1	b_1	$\bar{m}_1$	a_1 (th)	b_1 (th)	$\bar{m}_1$ (th)
0.38(1)	0.89(1)	0.54(1)	0.38797	0.95045	0.5252
a_2	b_2	$\bar{m}_2$	a_2 (th)	b_2 (th)	$\bar{m}_2$ (th)
0.302(3)	0.55(1)	0.754 (6)	0.30441	0.55738	0.7505

for the mismatch between numerically interpolated and theoretically evalutated exponents, (cf., eq. (2.175)).

Moving to the frequency domain, the susceptibility loss, related to the spectral densities by the Fluctuation-Dissipation Theorem, since TTI holds one has

$$G(t) = -\frac{1}{T}\partial_t C(t) \tag{2.178}$$

performing the Fourier Transform of $G(t)$ reads

$$\widetilde{G}(\omega) = 1 + \omega\widetilde{C}(\omega) = \chi'(\omega) + i\chi''(\omega). \tag{2.179}$$

The loss spectra χ'' is related to the spectrum of $C(t)$ through

$$\chi''(\omega) = \frac{\omega}{2T}S(\omega) \tag{2.180}$$

near the tricritical point displays two peaks, analogously to the dielectric loss in materials for which JG processes have been detected, cf., e.g., [129, 127, 128, 143].

The development of the secondary peak is plotted in figs. (2.12,2.4.1,2.4.1,2.15) as the tricritical point is approached in the T, J_p diagram. For small contribution from the p interaction only the α peak is visible near the transition of dynamic arrest. As the p-body interaction increases in strength and the tricritical point is approached a secondary β peak arises.

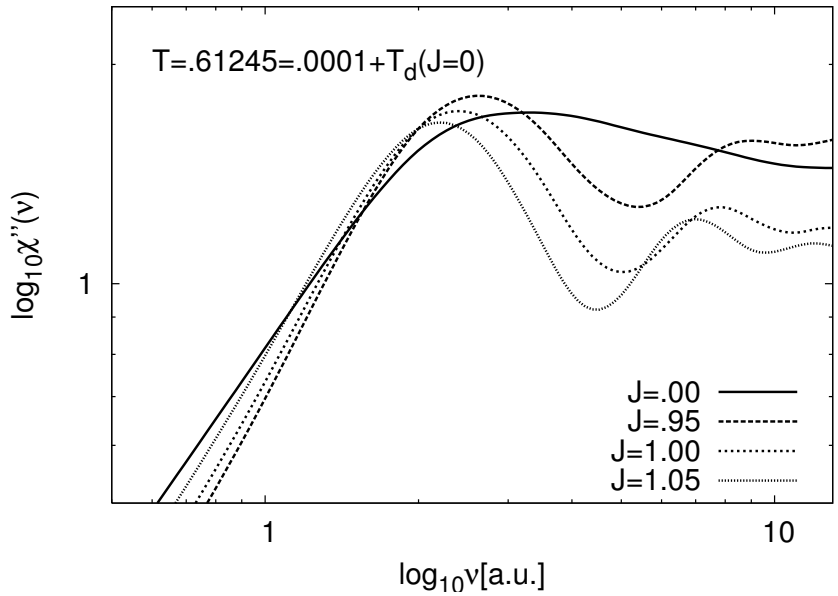

Figure 2.12: Susceptibility loss in frequency ω at constant temperature $T = 0.0001 + T_d(J_{16} = 0)$ and different values of J_{16}/J_3.

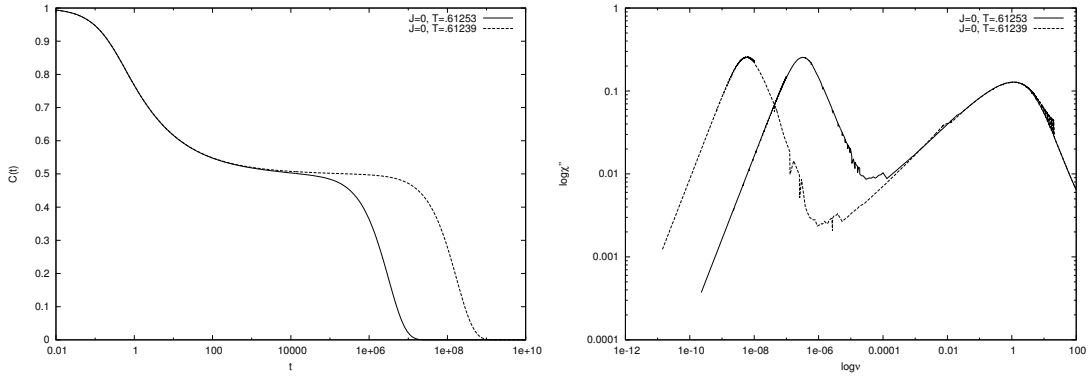

Figure 2.13: Susceptibility loss in frequency (right panel) and corresponding correlation function (left panel) at different temperatures and $J = 0$ (p-spin model).

2.5 Relation between relaxation times

From the characteristic decorrelation times each for well separated-plateau we can investigate the possibility of a functional relationship among them. In Ngai's Coupling Model [143, 144], the evidence of a deep relation between secondary and structural processes is connected, e. g., to a strong stretch in the exponential

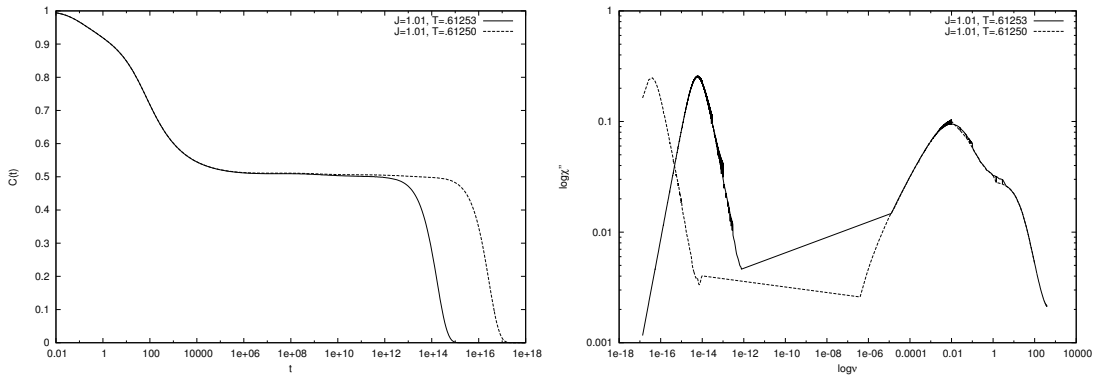

Figure 2.14: Susceptibility loss in frequency (right panel) and corresponding correlation function (left panel) at different temperatures and $J = 1.01$.

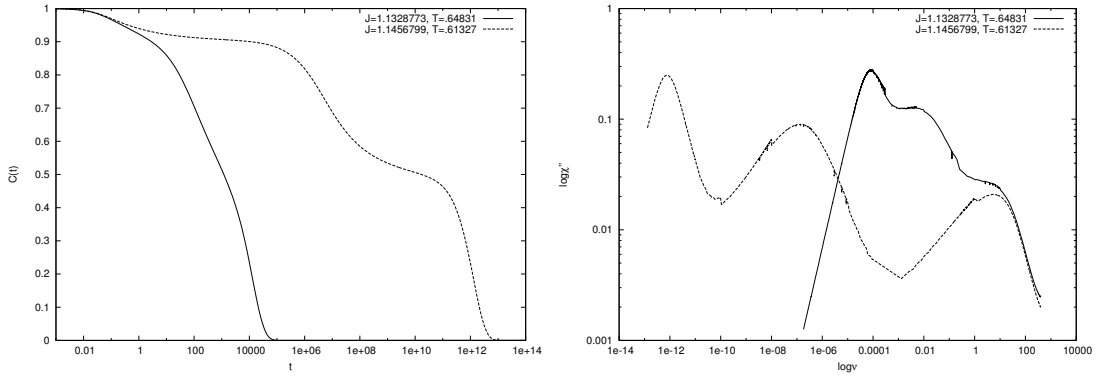

Figure 2.15: Susceptibility loss in frequency (right panel) and corresponding correlation function (left panel) at different temperatures varying J near the tricritical point.

relaxation to equilibrium in supercooled liquids [145][146]

$$C_{KWW}(t) = \exp\left[-\left(\frac{t}{\tau}\right)^{1-n}\right] \tag{2.181}$$

by the law

$$\tau_\alpha = [t_c^{-n}\tau_\beta]^{1/(1-n)}; \quad 0 < n < 1, \tag{2.182}$$

with t_c the time at which fast Maxwell-Debye exponential relaxation matches KWW relaxation. The larger is n, the stronger the peak at high frequency (short times) is pronounced. When n is small no peak related to secondary processes may

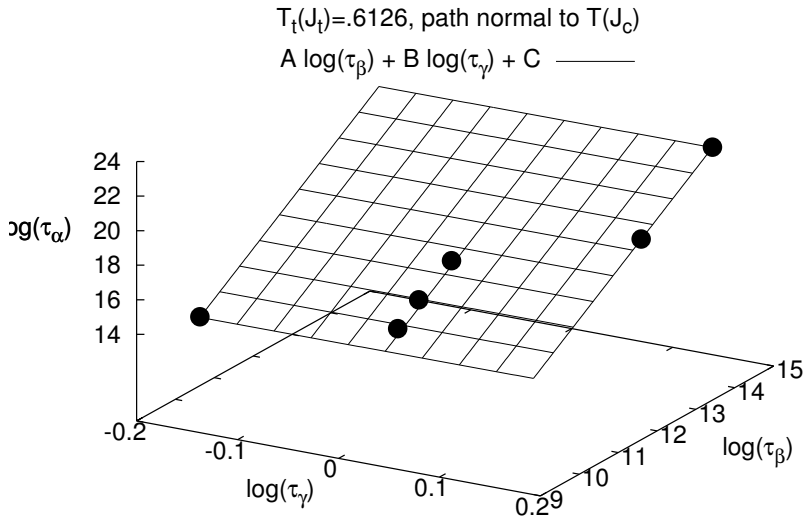

Figure 2.16: Relation between the characteristic relaxation times of the fast (γ), Johari-Goldstein (β) and fully cooperative (α) processes.

be seen.

In our model, the structural relaxation to equilibrium turns out to be purely exponential also very near to the dynamic transition temperature. However, the relaxation at time scales larger than τ_β (decay from the highest plateau) does exhibit a non exponential behaviour containing, on top of the final fully cooperative relaxation at τ_α, also the relaxation to the lowest plateau (where β processes are thermalized and α are completely stuck) and the decay from it, that follows the von Schweidler law, cf. eq. (2.172)[3]. In this respect, the stretched exponential might still be recovered and considered as an uneducated guess for the actual multi-time-scale dynamics. An alternative estimate of n would then support that conjecture. As a matter of fact, the relation between fast, secondary and structural processes appears to follow qualitatively Ngai's law, eq. (2.182) in a general form:

$$\log \tau_\alpha = \beta_0 \log \tau_\beta + \gamma_0 \log \tau_\gamma \tag{2.183}$$

[3]In MCT, it is, actually, common that stretched exponential relaxation only occurs at high wave numbers. In our model we do not implement the wave-number dependence, since we operate in the long distance limit.

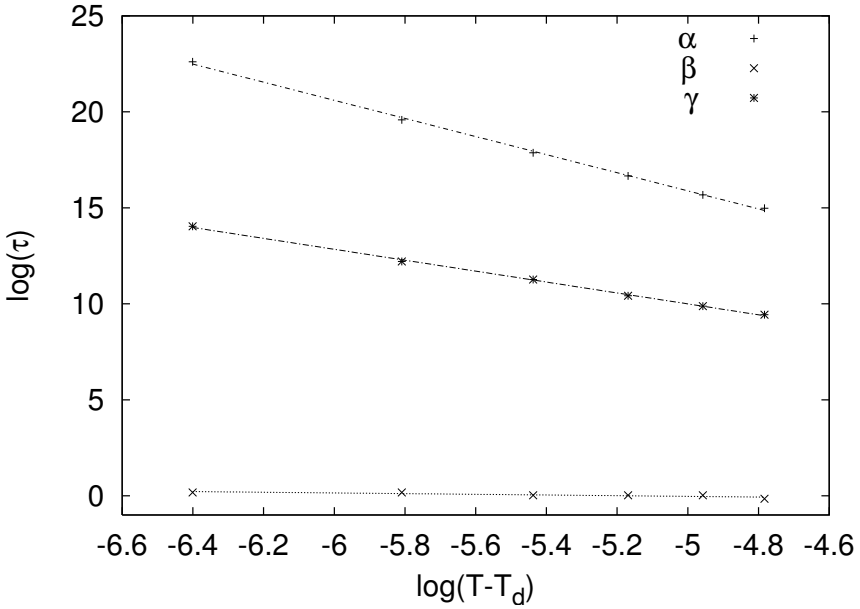

Figure 2.17: Behaviour of τ_α, τ_β and τ_γ vs $T - T_d^{(3c)}$ along the phase diagram path normal to the fluid/1RSB$_{II}$ dynamical transition line approaching the tricritical point.

In Fig. 2.16 we plot the inter-dependence of the relaxation times of separated processes and the dependence on $\log \tau_\alpha$ on $\log \tau_\beta$ and $\log \tau_\gamma$ turns out to lie on a plane (with $\log \tau_\gamma$ almost constant), confirming Eq. (2.183).

In our description the time scales over which one kind of process is active are well defined by characteristic times of relaxation to the plateaus. Cage rattling dynamics is thermalized already at the higher plateau of the correlation function and its equilibration time τ_γ does not depend on the distance from the dynamical critical point, (cf. Fig. 2.17).

Slower JG processes of intermolecular origin [115][147] take place when structural relaxation is completely stuck and are strongly correlated off equilibrium for a time such that $C(t) \simeq q_2$. Their characteristic time grows several order of magnitude, yet remaining several order of magnitudes smaller than τ_α, cf., Fig. 2.17. After that, they relax to equilibrium on the characteristic time τ_β and the total correlation decreases to a second plateau q_1 where the longest processes, the cooperative α processes, remain off equilibrium until $C(t) \simeq q_1$. Eventually, structural

relaxation goes towards equilibrium, on the characteristic time scale τ_α.

2.6 Dynamic scaling equation near plateaus

When we have discussed MCT equations, we have defined the MCT exponents, denoted a, b, which characterize the power law of $\phi(t)$ near the plateau. In particular, it is possible to write a relation between the two exponents. This relation can be generalized for a system which displays several plateaus.

Let us define the function $\bar{r}(q)$ as

$$\bar{r}(q) \;=\; \frac{1}{1-q} - \Lambda(q) \tag{2.184}$$

where Λ is defined in eq. (2.170), related to the solution $q = \lim_{t\to\infty} C(t)$ of (2.168) through

$$\bar{r}(q) = \bar{r}\;. \tag{2.185}$$

The solution to the above equation corresponds to a minimum of $\bar{r}(q)$ ($\bar{r}'(q) = 0$). Derivatives of $\bar{r}(q)$ take the form

$$\frac{d^m \bar{r}(q)}{dq^m} \;=\; \frac{m!}{(1-q)^{m+1}} - \frac{d^m \Lambda(q)}{dq^m}\,. \tag{2.186}$$

The phase diagram of the dynamical transition can be study through $\bar{r}(q)$. At the transition line the following relations hold

$$\left.\frac{d\bar{r}(q)}{dq}\right|_{q_t} = \left.\frac{d^2\bar{r}(q)}{dq^2}\right|_{q_t} = 0 \tag{2.187}$$

while at the tricritial point it is

$$\bar{r}(q_{tr}) = \left.\frac{d\bar{r}(q)}{dq}\right|_{q_{tr}} = \left.\frac{d^2\bar{r}(q)}{dq^2}\right|_{q_{tr}} = 0\,. \tag{2.188}$$

The function $\bar{r}(q)$ —introduced by Crisanti-Horner-Sommers [88]— is the dynamical counterpart of Franz-Parisi potential [148] (FPP). FPP is a function of the overlap q and develops a minimum near the glassy transition. In fig. (2.6) the

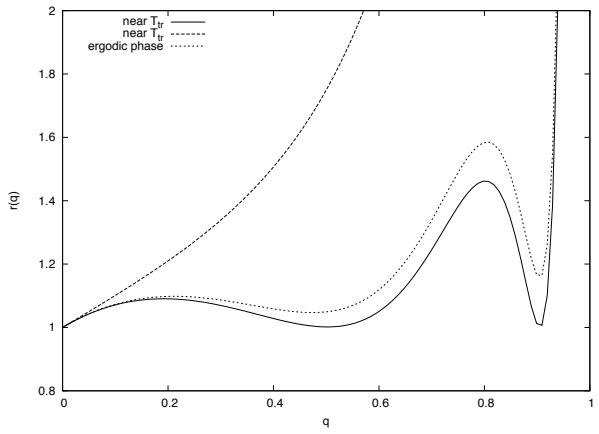

Figure 2.18: Near the tricritical point the function $\bar{r}(q)$ develops two minima at the values of q where $C(t)$ develops the plateau. The function $\bar{r}(q)$, introduced by Crisanti-Horner-Sommers [88] in order to study the dynamics of the $p-$spin, plays the same role of the Franz-Parisi potential [148] in the statics.

behaviour of $\bar{r}(q)$ near the tricritical point (for $s = 3$ and $p = 16$) is shown. As we can see $\bar{r}(q)$ develops two minima at the values q_i, where $i = 1, 2$, corresponding to the values of the plateaus of $C(t)$.

Writing $C(t) = q + \phi(t)$ we can expand $\Lambda[C(t)]$ near q, for small ϕ:

$$\Lambda(q + \phi) = \sum_{m=0}^{\infty} \frac{\Lambda^{(m)}(q)}{m!} \phi^m \tag{2.189}$$

where

$$\Lambda^{(m)} \equiv \frac{d^m \Lambda(q)}{dq^m} \tag{2.190}$$

We can, thus, rewrite the integral in eq. (2.168) in the form:

$$\int_0^t dt' \Lambda[C(t-t')]\partial_{t'}\phi(t') = -(1-q)\Lambda(q) + \sum_{m=1}^{\infty}\left[\frac{\Lambda^{m-1}(q)}{(m-1)!} - (1-q)\frac{\Lambda^m(q)}{m!}\right]\phi^m(t) + \sum_{m=1}^{\infty}\frac{\Lambda^m(q)}{m!}I_m(t)\,, \tag{2.191}$$

$$I_m(t) \equiv \int_0^t dt' \left[\phi^m(t-t') - \phi^m(t)\right]\partial_{t'}\phi(t')\,, \tag{2.192}$$

where $I_m(t) = O(\phi^{m-1}(t))$.

Expanding equation (2.168) in powers of $\phi(t)$ and using eq. (2.191), after some algebra we obtain

$$\Gamma_0^{-1}\partial_t\phi(t) + \left[\bar{r} + \Lambda(q) - (1-q)\Lambda^{(1)}(q)\right]\phi(t) + \sum_{m=2}^{\infty}\left[\frac{\Lambda^{(m-1)}}{(m-1)!} - (1-q)\frac{\Lambda^{(m)}(q)}{m!}\right]\phi^m(t) + \sum_{m=1}^{\infty}\frac{\Lambda^{(m)}(q)}{m!}I_m(t) = (1-q)\left[\bar{r} + \Lambda(q)\right] - 1\,. \tag{2.193}$$

From (2.186), by defining γ_m and δ_m as follows:

$$\begin{aligned}\gamma_m &\equiv \frac{1}{(1-q)^{m-2}} \\ \delta_m &\equiv \frac{(1-q)^3}{m!}\frac{d^m}{dq^m}\left[\bar{r}(q) - r\right]\,,\end{aligned} \tag{2.194}$$

we can write

$$\frac{\Lambda^{(m)}(q)}{m!} = \frac{1}{(1-q)^3}\left(\gamma_m - \delta_m\right)\,. \tag{2.195}$$

Substituting Eq. (2.195) into Eq. (2.193), we find

$$\Gamma_0^{-1}\partial_t\phi(t) + \frac{1}{(1-q)^3}\sum_{m=1}\left[-\delta_{m+1}\ (1-q)\delta_m\right]\phi^m(t)$$
$$+\frac{1}{(1-q)^3}\sum_{m=1}\left[\gamma_m-\delta_m\right]I_m(t) = -\frac{\delta_0}{(1-q)^2}\,. \tag{2.196}$$

This, at the order ϕ^2, becomes

$$\Gamma_0^{-1}\partial_t\phi(t) + \frac{1}{(1-q)^3}\left[-\delta_0+(1-q)\delta_1\right]\phi(t) \tag{2.197}$$
$$+\frac{1}{(1-q)^3}\left[-\delta_1+(1-q)\delta_2\right]\phi^2(t)$$
$$+\frac{1}{(1-q)^3}(\gamma_1-\delta_1)I_1(t) + o(\phi^3) = -\frac{\delta_0}{(1-q)^2}\ .$$

If $\bar{r}(q)$ develops a local minimum we have

$$\bar{r}'(q) = \delta_1 = 0 \tag{2.198}$$

near the minimum $\bar{r}(q) - \bar{r} \ll 1$. Consequently we define the small quantity

$$\sigma \equiv \delta_0 = (1-q)^3\left[\bar{r}(q)-\bar{r}\right] \ll 1\,. \tag{2.199}$$

Defining the quantity

$$\overline{m} \equiv \frac{(1-q)^3}{2}\Lambda''(q)\,, \tag{2.200}$$

we can than write

$$\delta_2 = 1-\overline{m}\,, \tag{2.201}$$

and rewrite Eq. (2.197) as follows:

$$\Gamma_0^{-1}\partial_t\phi(t) - \frac{\sigma}{(1-q)^3}\phi(t) \tag{2.202}$$
$$+\frac{1}{(1-q)^2}\left[(1-\overline{m})\phi^2(t)+I_1(t)\right] + o(\phi^3) = -\frac{\sigma}{(1-q)^2}\,.$$

When $\sigma \to 0$ the solution of Eq. (2.202) has the form

$$\phi(t) = \sigma^{1/2} g(\tau)\,, \quad \tau = t/t_\sigma = o(1)\,, \tag{2.203}$$

where $g(\tau)$ is the solution of the scaling equation:

$$(1-\overline{m})g^2(t) + \int_0^\tau d\tau' \left[g(\tau-\tau') - g(\tau)\right] \partial_\tau g(\tau') = -1.$$

If the dynamical equation develops a solution with two plateaus at the values q_κ (with $\kappa = 1, 2$), we can fix two rescaled time scales τ_κ where $t/t_{\sigma_\kappa} = o(1)$ and than generalize Eq. (2.204) to Eq. (2.174)

$$(1-\overline{m_\kappa})g_\kappa^2(t) + \int_0^\tau d\tau' \left[g_\kappa(\tau_\kappa-\tau') - g_\kappa(\tau_\kappa)\right] \partial_{\tau'} g_\kappa(\tau') = -1.$$

2.7 Conclusions

Glassy behaviour is a peculiar multi-scale problem. It is due to a bifurcation of the characteristic time scales of the dynamics. In this chapter we have suggested a model which can describe the emerging of secondary processes in glasses and glass formers. The model discussed is a generalization of the p-spin model with quenched disorder that reproduces some general features of structural glasses and has a dynamics leading to the MCT equation in the so-called Schematic Theory. I have studied in particular the equilibrium dynamics, solving numericcally the MCT-ST equation in regions of the phase diagram where we know that there is a dynamics evolving over three well separated time scales. Finally, I have generalized the relations between the MCT exponents for models which shows a multistep relaxation behaviour.

Chapter 3

Molecular Dynamics and Continuum Mechanics

In this chapter we will study the coupling between continuum and atomistic mechanics. The Andersen-Parrinello-Rahman method [14, 15, 16] is based on an extended Lagrangian allowing the MD cell to change both volume and shape during the simulation, its dynamics being governed by an externally applied stress, as well as by the internal particle dynamics. The APR method is well established and widely used [149]. However, some foundational issues remained unexplored until recently, since the Lagrangian introduced by Andersen [14] and generalized by Parrinello and Rahman [15, 16] has always been considered just as an expedient trick for generating the desired particle statistics. We assume a different standpoint: to us, APR-like Lagrangians embody the coupling between atomistic and continuum degrees of freedom. So, we are interested in the dynamics of the deforming computational cell per se, wishing to identify it with the body element of a Cauchy continuum. On this basis, we plan to construct atomistically informed approximations to a continuum by means of an array of interacting APR-like cells [150].

Continuum mechanics provides a set of partial differential equations governing the evolution of physical observables. Such observables are densities of, e. g., momentum, energy, mass, represented by macroscopic fields of different nature (i. e., scalar, vectorial or tensorial fields) evolving over a time and space scales

much larger than the microscopic scales. From the macroscopic point of view, determing the evolution of the system requires boundary and initial conditions, and constitutive relations. Moreover, in a mechanical system, a constitutive relation is a relation between the stress tensor (e. g., the pressure) and the deformation (e. g., change in the volume) of the material. Constitutive relations encode the mechanical properties of the medium (e. g., the response of a system to an external perturbation). Within continuum mechanics, constitutive relations have to be given phenomenologically. We can expect that a constitutive relation for a given material can be computed by a microscopic theory.

This chapter aims to build a multiscale algorithm which allows information to be exchanged between the microscopic time scales, governed by the atomistic mechanics (i. e., molecular dynamics in a numerical simulation) and the macroscopic time scale appropriate to continuum mechanics.

From the microscopic point of view, in order to obtain a constitutive relation we have to simulate the behaviour of a system at constant values of pressure, temperature and number of particles (i. e., in the (P, T, N) ensemble).

It is well known from the statistical mechanics that, when a thermodynamical variable is fixed, the conjugate variable fluctuates (e. g., in order to fix temperature energy fluctuations are to be allowed). Therefore, to fix the external pressure (or deformation), we have to allow to the system to change its volume (or the internal pressure), in order to reach equilibrium with the external environment. This can be done through the APR method.

In the following sections, after an introduction to the statistical ensemble in molecular dynamics, we will discuss the properties of the Nosè-Hoover, Andersen and Parrinello-Rahman algorithm and the representation of stress in molecular dynamics. Finally, we introduce a new method to couple continuum mechanics and molecular dynamics.

3.1 Statistical ensembles

In order to study through numerical simulations the dynamical and thermodynamical properties of a particle system, the simplest numerical experiment is the integration of Newton's equation [151, 99]. Since all the observables will be functions

defined over the phase space, the thermodynamical (i. e., macroscopic) observables will be averaged over the measure time τ much larger than the characteristic microscopic times

$$\overline{\mathcal{O}(t_0)} \equiv \lim_{\tau\to\infty} \frac{1}{\tau} \int_{t_0}^{\tau} dt\, \mathcal{O}(p(t), q(t))\,. \tag{3.1}$$

If the system is in an ergodic phase (i.e., a phase where it is reasonable to assume that the ergodic hypothesis holds), the equilibrium properties do not depend on the initial conditions

$$\overline{\mathcal{O}(t_0)} = \overline{\mathcal{O}} \tag{3.2}$$

and averaging $\mathcal{O}$ over time is equivalent to averaging it over the phase space with a suitable distribution function $\mathcal{P}[\Gamma]$

$$\overline{\mathcal{O}} = \langle \mathcal{O} \rangle = \int d\Gamma\, \mathcal{P}[\Gamma]\mathcal{O}[\Gamma] = \int d\mu(\Gamma) \tag{3.3}$$

where $d\Gamma$ is shorthand for $\prod_i \frac{d\mathbf{q_i} d\mathbf{p_i}}{h^{3N} N!}$, where $\Gamma = (p_i, q_i)$. For a Hamiltonian system, the natural *ensemble* to average the observables is the microcanonical one: $\mathcal{P}_{micro}[\Gamma]$ is an uniform distribution concentrated on a $3N-1$ hypersurface in the phase space (i.e., the surface corresponding to the fixed energy of the system). Therefore, a microcanonical measure over the system is a measure carried out at fixed values of (E, V, N).

From statistical mechanics, it is known that the distribution function for a system at thermal equilibrium with a fixed value of particles N in a volume V, is the *canonical distribution*, (i.e., the partition function defined by $1 = \int d\Gamma\, \mathcal{P}_{can}[\Gamma]$)

$$\mathcal{P}_{can}[\Gamma] = \frac{e^{-\beta\mathcal{H}}}{Z} \tag{3.4}$$

where Z is the mass of the distribution. In the Thermodynamic Limit (TL) (i.e., $N, V \to \infty$ with fixed $v = \frac{V}{N}$), the free energy per particle is

$$f(\beta, v) = \lim_{N,V\to\infty} \left[-\frac{1}{\beta} \log Z \right] \tag{3.5}$$

Therefore, the integration of the equations of motion allows us to study an isolated system in which energy, volume and number of particles are fixed. In order

to study the molecular dynamics of a system at fixed temperature something has to be changed.

To introduce a thermostat in a MD simulation Nosé and Hoover [152, 153] suggested the following Lagrangian

$$L(\mathbf{q}, \dot{\mathbf{q}}, s, \dot{s}) = \frac{1}{2}\sum_i m\dot{\mathbf{q}_\mathbf{i}}^2 s^2 - \frac{1}{2}Q\dot{s}^2 - \phi(q) - \frac{g}{\beta}\log s \tag{3.6}$$

where s is a *slow variable* which describes the coupling between the system and the thermostat. From the Lagrangian we obtain the Hamiltonian

$$\mathcal{H}_{NH}(\mathbf{p}, \mathbf{q}, s, p_s) = \sum_i \frac{{\mathbf{p}_\mathbf{i}}^2}{2ms^2} + \frac{p_s^2}{2Q} + \phi(q) + \frac{g}{\beta}\log s\ . \tag{3.7}$$

It is easy to prove that the equation of motions deriving from eq. (3.7) leads to a canonical measure in the phase space in the rescaling variables $\mathbf{p'_i} = \mathbf{p_i}/s$ [151].

Let us compute the microcanonical measure of (3.7)

$$\mathcal{Z}_{micro}(E, N, V, \beta) = \int \prod_i \frac{d\mathbf{p_i} d\mathbf{q_i} dp_s ds}{h^{3N} N!} \delta\left(\mathcal{H}_{NH} - E\right)\ . \tag{3.8}$$

In terms of the variable $\mathbf{p'_i}$, defining $\mathcal{H}'$ as

$$\mathcal{H}' = \sum_i \frac{{\mathbf{p'_i}}^2}{2m} + \phi(q) \tag{3.9}$$

we obtain

$$\mathcal{Z}_{micro}(E, N, V, \beta) = \int \prod_i \frac{d\mathbf{p'_i} d\mathbf{q_i} dp_s ds}{h^{3N} N!} s^{3N} \delta\left(\mathcal{H}' + \frac{p_s^2}{2Q} + \frac{g}{\beta}\log s - E\right)\ . \tag{3.10}$$

Using the property of the delta function

$$\begin{aligned} \delta[f(x)] &= \frac{\delta(x - x_0)}{f'(x_0)} \\ f(x_0) &= 0 \end{aligned} \tag{3.11}$$

and integrating over s, it follows that

$$\begin{aligned} \mathcal{Z}_{micro}(E,N,V,\beta) &= \frac{\beta e^{\beta\frac{E(3N+1)}{g}}}{g}\int dp_s e^{-\beta\frac{3N+1}{g}\frac{p_s^2}{2Q}}\int\prod_i d\mathbf{p_i'}d\mathbf{q_i}e^{-\beta\frac{3N+1}{g}\mathcal{H}'} = \\ &= const\int d\Gamma' e^{-\beta\mathcal{H}'} \end{aligned} \tag{3.12}$$

where the last term in eq. (3.12) is obtained by choosing $g = 3N + 1$ and $d\Gamma' \equiv \prod_i \frac{d\mathbf{p_i'}d\mathbf{q_i}}{h^{3N}N!}$. In conclusion, the microcanonical measure (i. e., a numerical integration of the equations of motion) with the Nosé-Hoover Hamiltonian is equivalent to the canonical measure with the Hamiltonian $\mathcal{H}'$.

From the point of view of MD, a thermostat is an object that rescales the momenta of the system in order to allow energy fluctuations. In NH, the temperature is fixed by an adjoint slow degree of freedom: the parameter s with the coniugate momentum p_s. This addition allows energy to fluctuate and preserves the volume of the phase space, according to Liouville Theorem [154]. Therefore, the resulting algorithm is time-reversible and the dynamics is well defined. The main effects of NH thermostat is a rescaling of the momenta of particles. In general, in order to obtain a correct value of the temperature, we can rescale the momenta without introducing a NH thermostat, but the algorithm obtained is not time-reversible and so the Liouville Theorem does not hold. In fig. (3.1) the thermalization of a system of $N = 108$ in a simulation box of side $L = 5$ interacting via Lennard-Jones potential at $T = 11.1$ (fluid) is shown. From a Lagrangian point of view, it is hard to obtain the expression (3.6) from first principle. Moreover, we can build a simple toy model which leads to a Hamiltonian quite similar to (3.7) based on the rescaling of the momenta.

Firstly we note that, in order to thermalize a system, we have to put it in contact with a thermal bath. In the NH the thermal bath is represented by the slow degree of freedom s. The program is the following: starting from a general Hamiltonian we want to integrate over some microsopic degrees of freedom in order to obtain an effective Hamiltonian. The idea is that the integration, after a suitable choice of the interaction, generates an effective potential that thermalizes the system. Following the two-temperature formalism developed to study structural glasses [84], we can define a Hamiltonian that depends on slow (ϕ) and fast (ψ) degrees

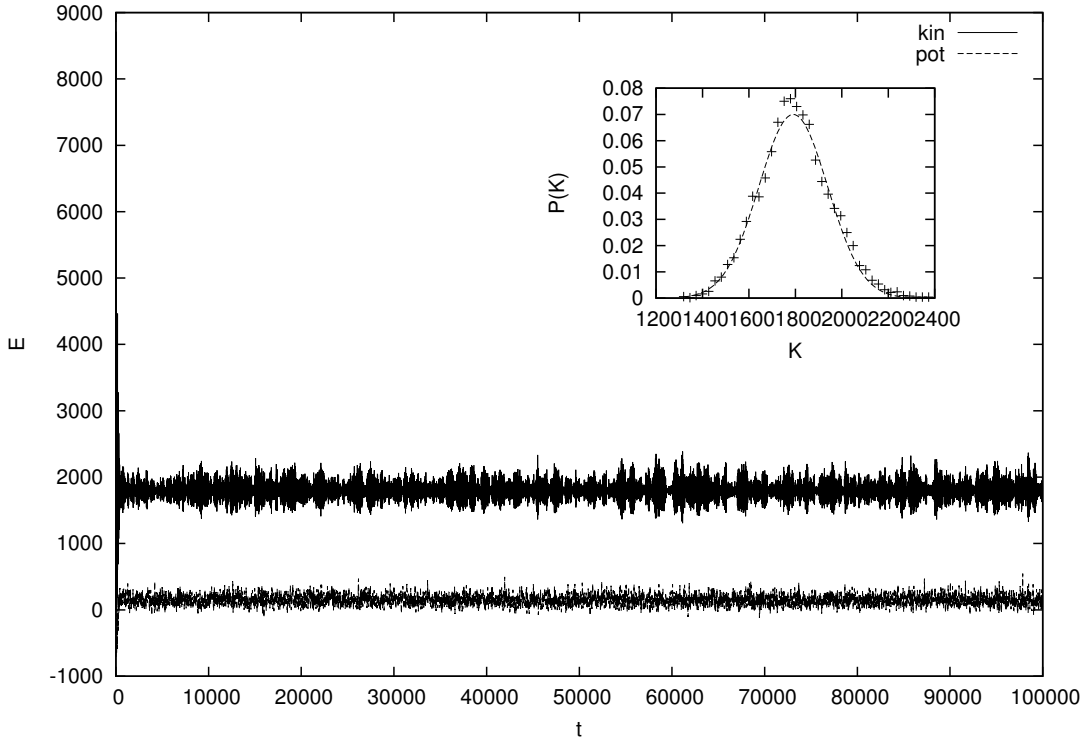

Figure 3.1: Energy and kinetic energy distribution in a Lennard-Jones fluid, $T = 11.1$, $N = 108$, $L = 5$

of freedom

$$\mathcal{H}[\phi, \psi] = \mathcal{H}_0[\phi] + \mathcal{H}_1[\psi] + \mathcal{H}_{int}[\phi, \psi] \,. \tag{3.13}$$

We can than define a partition function that depends on the slow variables ϕ

$$\mathcal{Z}_\beta[\phi] = \int d\psi \, e^{-\beta\mathcal{H}[\phi,\psi]} = e^{-\beta\mathcal{H}_0[\phi]} \int d\psi \, e^{-\beta\mathcal{H}[\psi]-\beta\mathcal{H}_{int}[\phi,\psi]} \,. \tag{3.14}$$

From this partition function, we can also define an effective Hamiltonian

$$\mathcal{H}_{\text{eff}}[\phi] = -\frac{1}{\beta} \log \mathcal{Z}_\beta[\phi] \,. \tag{3.15}$$

We note that, if $\mathcal{H}_{int} = 0$, the effective Hamiltonian is

$$\mathcal{H}_{\text{eff}}[\phi] = \mathcal{H}_0[\phi] - \frac{1}{\beta} \log \mathcal{Z}_\beta^\psi = \mathcal{H}_0[\phi] + f^\psi(\beta) \,. \tag{3.16}$$

Using $\mathcal{H}_{\text{eff}}$ to write the equation of motion for the variables ϕ, e. g., choosing $\phi = (\mathbf{p}, \mathbf{q})$, the effective Hamiltonia reads

$$\mathcal{H}_{\text{eff}}[\mathbf{p}, \mathbf{q}] = -\frac{1}{\beta} \log \mathcal{Z}_\beta[\mathbf{p}, \mathbf{q}] \,, \tag{3.17}$$

since the free energy $f^\psi(\beta)$ is indipendent of $(\mathbf{p}, \mathbf{q})$, we obtain the same dynamics of the Hamiltonian $\mathcal{H}(\mathbf{p}, \mathbf{q}, \psi)$.

Now we can try to study the evolution of $\mathcal{H}_{\text{eff}}[\mathbf{p}, \mathbf{q}]$ through the Hamilton equations. From statistical mechanics, we are able to compute the partition function only for few systems. Whereas, using the mean field (MF) approximation, we can to compute the partition function of many models. Starting from the following Hamiltonian

$$\begin{aligned} \mathcal{H}[\mathbf{p}, \mathbf{q}, \psi] &= \mathcal{H}_0[\mathbf{p}, \mathbf{q}] + \varphi_2(\mathbf{p}, \mathbf{q}, \psi) \,, \\ \mathcal{H}_0[\mathbf{p}, \mathbf{q}] &\equiv \sum_i \frac{\mathbf{p_i}^2}{2m} + \varphi_1(\mathbf{q}) \,, \end{aligned} \tag{3.18}$$

we can write an effective Hamiltonian that contains an effective interaction between the variables left by the integration over ψ

$$\mathcal{H}_{\text{eff}}[\mathbf{p}, \mathbf{q}] = \sum_i \frac{\mathbf{p_i}^2}{2m} + \varphi_1(\mathbf{q}) - \frac{1}{\beta} \log \int \mathcal{D}\psi \, e^{-\beta \varphi_2(\mathbf{p}, \mathbf{q}, \psi)} = \mathcal{H}_0[\mathbf{p}, \mathbf{q}] - \frac{1}{\beta} \varphi_{\text{eff}}(\mathbf{p}, \mathbf{q}) \,. \tag{3.19}$$

The equations of motion are

$$\begin{aligned} \dot{\mathbf{q}}_i &= \frac{\mathbf{p}_i}{m} - \frac{1}{\beta} \frac{\partial \varphi_{\text{eff}}(\mathbf{p}, \mathbf{q})}{\partial \mathbf{p}_i} \\ \dot{\mathbf{p}}_i &= -\left(\frac{\partial \varphi(\mathbf{q}_i)}{\partial \mathbf{q}_i} - \frac{1}{\beta} \frac{\partial \varphi_{\text{eff}}(\mathbf{p}, \mathbf{q})}{\partial \mathbf{q}_i} \right) \end{aligned} \tag{3.20}$$

choosing a mean-field interaction between fast and slow variables it is

$$\varphi_2(\mathbf{p}, \mathbf{q}, \psi) = \varphi_{MF}(\mathbf{p}, \mathbf{q}, \psi) \,, \tag{3.21}$$

and one gets

$$-\frac{1}{\beta}\log\int\mathcal{D}\psi\, e^{-\beta\varphi_{MF}(\mathbf{p},\mathbf{q},\psi)} \simeq -\frac{Ng(\psi_{SP},\mathbf{p},\mathbf{q})}{\beta} \tag{3.22}$$
$$\psi_{SP}\ :\quad \left.\frac{\delta g(\psi,\mathbf{p},\mathbf{q})}{\delta\psi}\right|_{SP}=0 \Longrightarrow \psi_{SP}=\psi(\mathbf{p},\mathbf{q})$$

where we can change $\simeq$ with $=$ at the thermodynamic limit (i. e., we think to work in a system with a finite number of particles but large enough to allow for a saddle-point approximation). The effective Hamiltonian reads as

$$\mathcal{H}_{\text{eff}}[\mathbf{p},\mathbf{q}]=\mathcal{H}_0[\mathbf{p},\mathbf{q}]+\frac{Ng(\psi_{SP},\mathbf{p},\mathbf{q})}{\beta} \tag{3.23}$$

with the following equations of motion

$$\begin{aligned}\dot{\mathbf{q}}_i &= \frac{\partial\mathcal{H}_0[\mathbf{p},\mathbf{q}]}{\partial\mathbf{p}_i}+\frac{\partial Ng(\psi_{SP},\mathbf{p},\mathbf{q})}{\partial\beta\mathbf{p}_i}+\frac{\partial Ng(\psi_{SP},\mathbf{p},\mathbf{q})}{\partial\beta\psi}\frac{\partial\psi}{\partial\mathbf{p}_i} \\ \dot{\mathbf{p}}_i &= -\left(\frac{\partial\mathcal{H}_0[\mathbf{p},\mathbf{q}]}{\partial\mathbf{q}_i}+\frac{\partial Ng(\psi_{SP},\mathbf{p},\mathbf{q})}{\partial\beta\mathbf{q}_i}+\frac{\partial Ng(\psi_{SP},\mathbf{p},\mathbf{q})}{\partial\beta\psi}\frac{\partial\psi}{\partial\mathbf{q}_i}\right).\end{aligned} \tag{3.24}$$

Which, using eq. (3.22) may be rewritten as

$$\begin{aligned}\dot{\mathbf{q}}_i &= \frac{\partial\mathcal{H}_0[\mathbf{p},\mathbf{q}]}{\partial\mathbf{p}_i}+\frac{\partial Ng(\psi_{SP},\mathbf{p},\mathbf{q})}{\partial\beta\mathbf{p}_i} \\ \dot{\mathbf{p}}_i &= -\left(\frac{\partial\mathcal{H}_0[\mathbf{p},\mathbf{q}]}{\partial\mathbf{q}_i}+\frac{\partial Ng(\psi_{SP},\mathbf{p},\mathbf{q})}{\partial\beta\mathbf{q}_i}\right).\end{aligned} \tag{3.25}$$

Integrating a set of variables with the Boltzmann measure is the first step to study the static properties of such set of variables. Indeed, through the partition function we study the properties of the variables at equilibium with a thermal bath at the inverse temperature β (i. e., through integration, variables ψ thermalizes). If the thermalized variables have an interaction (weak or strong) with other variables, the second one will be subjected to the effect of the thermal bath. In particular, we can think that the dynamics of eq. (3.22) is an equilibrium dynamics at fixed temperature.

Therefore, we can try to write a Hamiltonian with generalized momenta and coordinate which interact with a set of fast variables. The nature of the fast

variables is not important, since we expect that the thermalization of a system is indipendent of the nature of the thermostat. In order to make the calculation simple, we choose a fluid interacting weakly through a long-range potential with a bath of soft and spherical spins. The Hamiltonian of the system is

$$\begin{aligned} \mathcal{H}[\mathbf{p},\mathbf{q},\mathbf{s}] &= \sum_i \frac{\mathbf{p_i}^2}{2m} - A\sum_i \mathbf{s_i}\cdot\mathbf{p_i} + \varphi(\mathbf{q}) \\ \sum_i \mathbf{s_i}^2 &= 3N \end{aligned} \tag{3.26}$$

where we have chosen an interaction between spins and momenta. The partition function is

$$\begin{aligned} \mathcal{Z}_\beta[\mathbf{p},\mathbf{q}] &= e^{-\beta\sum_i \frac{\mathbf{p_i}^2}{2m} - \beta\varphi(\mathbf{q})} \int_{-\infty}^{+\infty} \prod_{i,\alpha}^{3N} ds_i^\alpha\, \delta\left(\sum_k^{3N} s_k^2 - 3N\right) e^{\beta A\sum_{i,\alpha}^{3N} s_i^\alpha p_i^\alpha} = \\ &= e^{-\beta\sum_i \frac{\mathbf{p_i}^2}{2m} - \beta\varphi(\mathbf{q})} X_\beta(\mathbf{p}) \\ X_\beta(\mathbf{p}) &\equiv \int_{-\infty}^{+\infty} \prod_{i,\alpha}^{3N} ds_i^\alpha\, \delta\left(\sum_{i,\alpha}(s_i^\alpha)^2 - 3N\right) e^{\beta A\sum_{i,\alpha}^{3N} s_i^\alpha p_i^\alpha} \end{aligned} \tag{3.27}$$

from which the effective Hamiltonian follows

$$\mathcal{H}_{eff}[\mathbf{p},\mathbf{q}] = \sum_i \frac{\mathbf{p_i}^2}{2m} + \varphi(\mathbf{q}) - \frac{1}{\beta}\log X_\beta(\mathbf{p}) \tag{3.28}$$

The delta distribution that encodes the spherical constraint, can be expressed through an auxiliary Lagrange multiplier λ, $M = 3N$

$$X_\beta(\mathbf{p}) = \int_{-\infty}^{+\infty} \prod_{i,\alpha}^{M} ds_i^\alpha \frac{d\lambda}{2\pi i} \exp\left\{-\lambda\sum_{i,\alpha}(s_i^\alpha)^2 + M\lambda + \beta A\sum_{i,\alpha}^{M} s_i^\alpha p_i^\alpha\right\}. \tag{3.29}$$

After a Gaussian integration, one gets

$$\begin{aligned} X_\beta(\mathbf{p}) &= \int_{-\infty}^{+\infty} \frac{d\lambda}{2\pi i}\, e^{-Mg(\mathbf{p},\lambda)} \\ g(\mathbf{p},\lambda) &\equiv -\frac{\beta^2 A^2}{4M}\sum_i \frac{\mathbf{p_i}^2}{\lambda} - \lambda + \frac{1}{2}\log\lambda\,. \end{aligned} \tag{3.30}$$

For reasons that will be clear later we define the funcion

$$\epsilon(p) \equiv \frac{1}{M} \sum_i \frac{\mathbf{p_i}^2}{2m} \tag{3.31}$$

where p is a shorthand for $(|\mathbf{p_i}|)_{i=1}^N$. Solving the integral with the saddle-point method we obtain a self-consistency equation for λ

$$\lambda_{SP} \; : \quad \lambda_{SP}^2 - \frac{1}{2}\lambda_{SP} - \frac{\beta^2 A^2 m}{2}\epsilon = 0 \, . \tag{3.32}$$

Finally, we obtain an effective Hamiltonian by choosing $\lambda_{SP}^+ = \lambda(p)$

$$\mathcal{H}_{\text{eff}}[\mathbf{p}, \mathbf{q}, \lambda(p)] = \sum_i \frac{\mathbf{p_i}^2}{2m}\left(1 - \frac{m\beta A^2}{2\lambda}\right) + \varphi(\mathbf{q}) - \frac{3N\lambda}{\beta} + \frac{3N}{2\beta}\log\lambda \, . \tag{3.33}$$

Since a self-consistency relation for λ holds, the equations of motion will be

$$\begin{aligned} \dot{\mathbf{q}}_i &= \frac{\mathbf{p}_i}{m}\left(1 - \frac{m\beta A^2}{2\lambda}\right) \\ \dot{\mathbf{p}}_i &= -\frac{\partial\varphi(\mathbf{q})}{\partial \mathbf{q}_i} \end{aligned} \tag{3.34}$$

where the coupling costant A is a free parameter of the model. We can fix A self-consistently by imposing the equipartition for a perfect monoatomic gas. Equipartition reads

$$\epsilon(p) = \frac{1}{2\beta} \, . \tag{3.35}$$

From this, it follows that

$$1 - \frac{m\beta A^2}{2\lambda} = \pm 1 \, . \tag{3.36}$$

The case $+1$ is trivial, since thus $A = 0$. Choosing -1, the solution is

$$A = \pm\sqrt{\frac{6}{m\beta}} \tag{3.37}$$

we note that A is in the right units, being $1/[mass]/[energy] = [momentum]^{-1}$. Moreover the thermalization is indipendent of the type of interaction, i. e., attractive or repulsive.

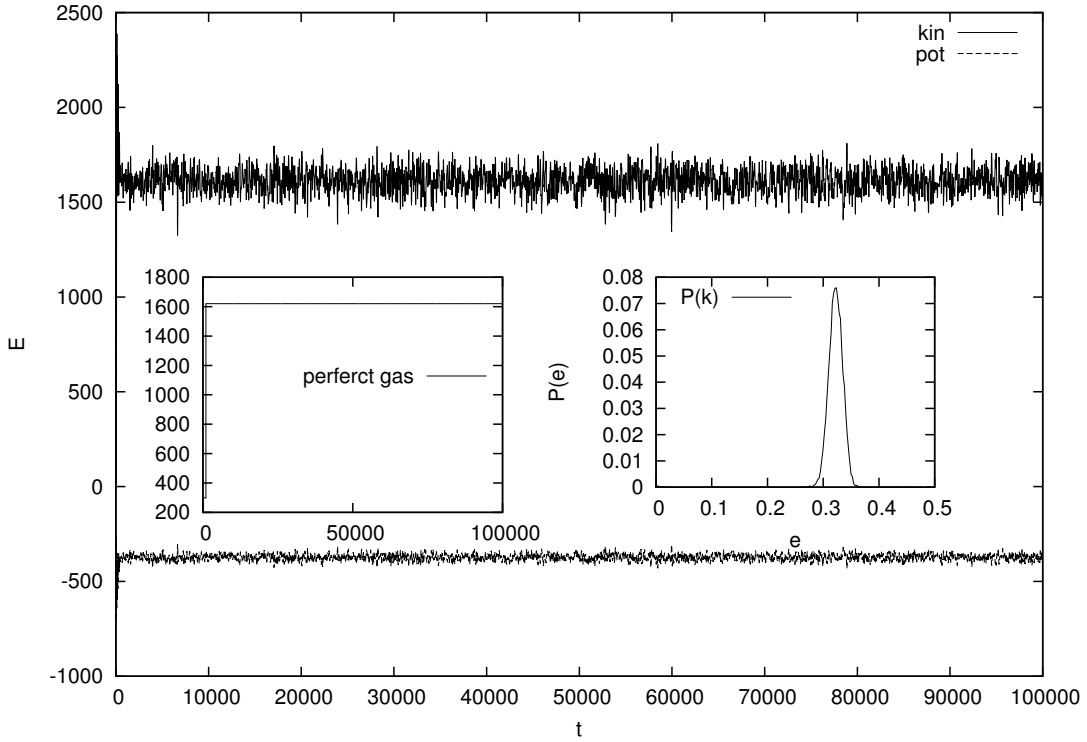

Figure 3.2: Perfect Gas and Lennard-Jones fluid simulated through algorithm (3.1), $N = 108$, $T = 11.1$ and $L = 5$.

I have numerically simulated the dynamics generated by eq. (3.1) in a gas and Lennard-Jones fluid (see fig. (3.2)). Choosing A according to eq. (3.1) we have the right thermalization. On the other hand we need to fine-tuning A to thermalize the Lennard-Jones fluid. In fig. (3.3) a comparison with NH is shown.

3.1.1 Liouvillians in MD

In the previous chapter we have used the Liouvillian formulation to write the MC equations. Now, starting from the well known expression for the evolution of an

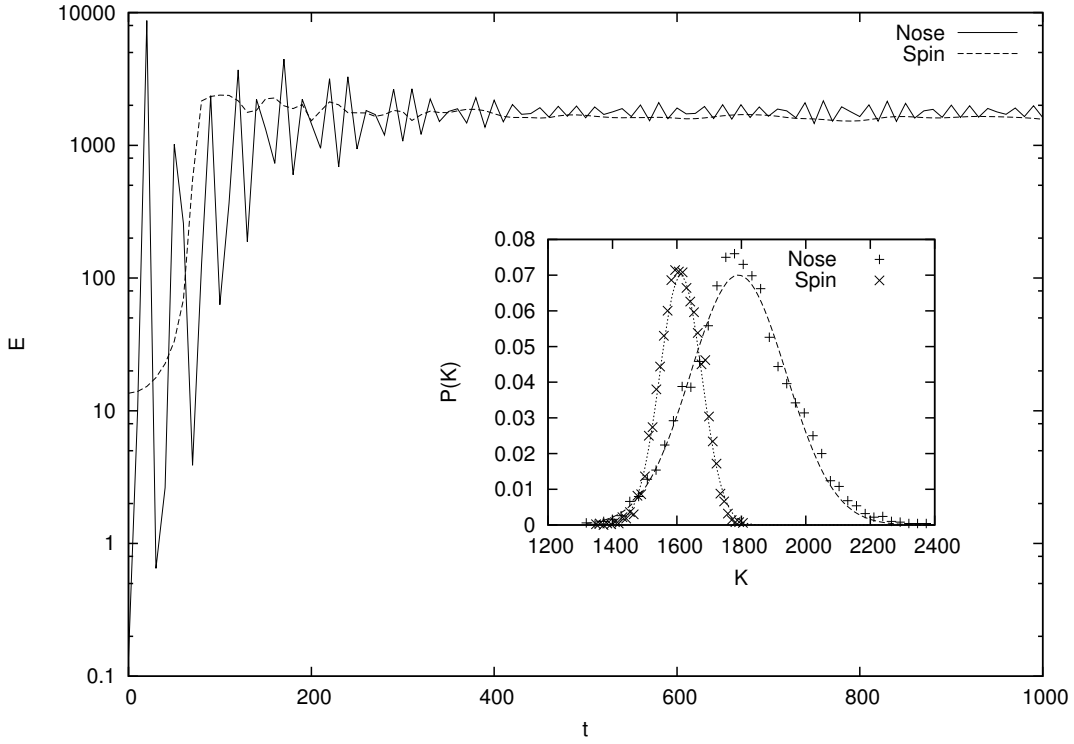

Figure 3.3: Comparison between NH and algorithm (3.1) in a Lennard-Jones fluid, $N = 108$, $T = 11.1$ and $L = 5$.

observable ($\partial_t \mathcal{O}(t) = 0$)

$$\begin{aligned} \frac{d\mathcal{O}}{dt}(p(t), q(t)) &= \sum_i \left(\frac{\partial \mathcal{O}}{\partial p_i} \dot{p}_i + \frac{\partial \mathcal{O}}{\partial q_i} \dot{q}_i \right) \\ i\mathcal{L} &\equiv \sum_i \left(\dot{p}_i \frac{\partial}{\partial p_i} + \dot{q}_i \frac{\partial}{\partial q_i} \right) \\ \mathcal{O}(t) &= e^{i\mathcal{L}t} \mathcal{O}(0) \,, \end{aligned} \tag{3.38}$$

in order to build an algorithm to integrate the equation of motion, we will give eq. (3.38) less formally.

Starting from the Hamilton equations

$$\dot{q}_i = \frac{\partial \mathcal{H}(p,q)}{\partial p_i} \,, \qquad \dot{p}_i = -\frac{\partial \mathcal{H}(p,q)}{\partial q_i} \,, \tag{3.39}$$

with no loss in generality, we study the case of only two degrees of freedom

$$\mathcal{H}(p,q) = \frac{p^2}{2m} + \phi(q) \tag{3.40}$$

defining the generalized force $f_q \equiv -\frac{\partial \phi}{\partial q}$ we can write the Liouvillian as

$$i\mathcal{L} = \frac{p}{m}\frac{\partial}{\partial q} + f_q \frac{\partial}{\partial p} \equiv A + B\,. \tag{3.41}$$

Choosing

$$\begin{aligned} A &\equiv \frac{p}{m}\frac{\partial}{\partial q} \\ B &\equiv f_q \frac{\partial}{\partial p}\,, \end{aligned} \tag{3.42}$$

we can compute the commutator between A and B

$$[A,B] = \frac{p}{m}\frac{\partial f_q}{\partial q}\frac{\partial}{\partial p} - \frac{f_q}{m}\frac{\partial}{\partial q}\,, \tag{3.43}$$

Since $[A,B] \neq 0$, we can not factorize the exponential of the Liouvillian:

$$e^{A+B} \neq e^A\, e^B\,. \tag{3.44}$$

However, through the Trotter Formula [155] we can write the follows identity

$$e^{(A+B)t} = \lim_{n\to\infty}\left(e^{\frac{At}{2n}}\, e^{\frac{Bt}{n}}\, e^{\frac{At}{2n}}\right)^n\,. \tag{3.45}$$

Introducing $\Delta t \equiv \frac{t}{n}$ and using eq. (3.45) [156, 157], one gets

$$e^{(A+B)\Delta t} = e^{\frac{A\Delta t}{2}}\, e^{B\Delta t}\, e^{\frac{A\Delta t}{2}} + o(\Delta t^3)\,. \tag{3.46}$$

Eq. (3.46) suggests a scheme to integrate numerically the equations of motion. We recall a remarkable property of the Liouvillian formulation: since the evolution is

expressed by unitary operator $U(t)$,

$$\begin{aligned} U(t) &= e^{i\mathcal{L}t} = \sum_n \frac{(i\mathcal{L}t)^n}{n!} \\ U(-t) &= e^{-i\mathcal{L}t} = U(t)^T \\ U(t)U(t)^T &= U(t)^T U(t) = 1 \end{aligned} \tag{3.47}$$

the evolution is time-reversal invariant and preserves the phase space volume. Indeed, the algorithm (3.46), which involves an error of order Δt^3, is time-reversible

$$\left(e^{\frac{A\Delta t}{2}}\, e^{B\Delta t}\, e^{\frac{A\Delta t}{2}}\right)\left(e^{\frac{A\Delta t}{2}}\, e^{B\Delta t}\, e^{\frac{A\Delta t}{2}}\right)^T = 1\,. \tag{3.48}$$

The operators that appear in the dynamics are of the type $a\partial_x$ or $x\partial_x$, where a is a constant while x is a generalized coordinate. These operators act on a general function $f(x)$ defined over the phase space as follows:

$$\begin{aligned} e^{a\partial_x} f(x) &= f(x+a) \\ e^{ax\partial_x} f(x) &= f(xe^a)\,. \end{aligned} \tag{3.49}$$

Relations (3.49) can be easily computed from the following representation of the exponential operator

$$e^{\beta\partial_z} = \sum_n \frac{(\beta\partial_z)^n}{n!}\,. \tag{3.50}$$

The action of (3.50) over a function $f(z) = \sum_i \alpha_i z^i$ reads

$$e^{\beta z} f(z) = \left(\sum_n \frac{(\partial_z)^n}{n!}\right)\left(\sum_i \alpha_i z^i\right) = f(z+a)\,. \tag{3.51}$$

From eq. (3.51), taking $z = ax$ we obtain the first relation (3.49); choosing $z = \log x$ we obtain the second one.

If the dynamics is generated by the Hamiltonian (3.40), the action of operator

A and B on a general observable $\mathcal{O}(p,q)$ reads

$$\begin{aligned} e^{\frac{p}{m}\frac{\partial}{\partial q}\Delta t}\mathcal{O}(p,q) &= \mathcal{O}(p,q+\frac{p}{m}\Delta t) \\ e^{f_q\frac{\partial}{\partial p}\Delta t}\mathcal{O}(p,q) &= \mathcal{O}(p+f_q\Delta t,q) \end{aligned} \tag{3.52}$$

For f(p,q)=(p,q) and $A = f_q\frac{\partial}{\partial p}$, $B = \frac{p}{m}\frac{\partial}{\partial q}$ we obtain the Velocity-Verlet algorithm[158, 151]

$$e^{\frac{A\Delta t}{2}}\, e^{B\Delta t}\, e^{\frac{A\Delta t}{2}}(p,q) = \left(p + \left\{ f_q(0) + f(\frac{\Delta t}{2}) \right\} \frac{\Delta t}{2}\,, q + \frac{p}{m}\Delta t \right) \tag{3.53}$$

Nosé-Hoover dynamics: Liouvillian formulation

Via the Liouvillian formulation of the dynamics, we can easily build a class of numerical alghoritms which preserve the volume of the phase space during the simulation. We can apply such procedure to integrate the Nosè-Hoover equations.

We start from the Hamiltonian (3.7). Performing the change of variables

$$\begin{aligned} \xi &= \log s \\ \mathbf{p}_i &\equiv \mathbf{p}'_i = \mathbf{p}_i e^{2\xi} \\ \mathbf{q}_i &= \mathbf{r}_i\,, \end{aligned} \tag{3.54}$$

the Hamiltonian reads

$$\mathcal{H}_{N.H}[\mathbf{p},\mathbf{r},\xi,p_\xi] = \sum_i \frac{\mathbf{p}_i^2}{2m} + \phi(\mathbf{r}) + \frac{p_\xi^2}{2Q} + \frac{g}{\beta}\xi \tag{3.55}$$

and we can write the Liouvillian operator as

$$\begin{aligned} i\mathcal{L} &= \mathcal{O}_{\mathbf{r}} + \mathcal{O}_{\mathbf{p}_1} + \mathcal{O}_{\mathbf{p}_2} + \mathcal{O}_{\xi} + \mathcal{O}_{p_\xi} \\ \mathcal{O}_{\mathbf{r}} &\equiv \sum_i \frac{\mathbf{p}_i}{m}\partial_{\mathbf{r}_i} \\ \mathcal{O}_{\mathbf{p}_1} &\equiv -\sum_i \frac{\partial\phi(\mathbf{r})}{\partial\mathbf{r}_i}\partial_{\mathbf{p}_i} \\ \mathcal{O}_{\mathbf{p}_2} &\equiv -\sum_i 2\dot{\xi}\mathbf{p}_i\partial_{\mathbf{p}_i} = -\sum_i 2\frac{p_\xi}{Q}\mathbf{p}_i \\ \mathcal{O}_{\xi} &\equiv C\partial_{p_\xi} \\ \mathcal{O}_{p_\xi} &\equiv \frac{p_\xi}{Q}\partial_\xi \\ C &\equiv \sum_i \frac{\mathbf{p}_i^2}{m} - \frac{g}{\beta}\,. \end{aligned} \tag{3.56}$$

According to the Trotter formula (3.45), we can choose the following split

$$e^{i\mathcal{L}\Delta t} \sim e^{\mathcal{O}_{p_\xi}\frac{\Delta t}{2}}\, e^{\mathcal{O}_{\xi}\frac{\Delta t}{2}}\, e^{\mathcal{O}_{\mathbf{p}_1}\frac{\Delta t}{2}}\, e^{\mathcal{O}_{\mathbf{p}_2}\frac{\Delta t}{2}}\, e^{\mathcal{O}_{\mathbf{r}}\Delta t}\, e^{\mathcal{O}_{\mathbf{p}_2}\frac{\Delta t}{2}}\, e^{\mathcal{O}_{\mathbf{p}_1}\frac{\Delta t}{2}}\, e^{\mathcal{O}_{\xi}\frac{\Delta t}{2}}\, e^{\mathcal{O}_{p_\xi}\frac{\Delta t}{2}}\,. \tag{3.57}$$

In order to obtain a numerical algorithm many other choices can be done, such as

$$\begin{aligned} e^{i\mathcal{L}\Delta t} &\sim \mathcal{U} e^{\mathcal{O}_{\mathbf{r}}\Delta t}\mathcal{U}^T \\ \mathcal{U} &\equiv e^{\mathcal{O}_{\mathbf{p}_2}\frac{\Delta t}{4}}\, e^{\mathcal{O}_{p_\xi}\frac{\Delta t}{4}}\, e^{\mathcal{O}_{\mathbf{p}_1}\frac{\Delta t}{4}}\, e^{\mathcal{O}_{\xi}\frac{\Delta t}{2}}\, e^{\mathcal{O}_{\mathbf{p}_1}\frac{\Delta t}{4}}\, e^{\mathcal{O}_{p_\xi}\frac{\Delta t}{4}}\, e^{\mathcal{O}_{\mathbf{p}_2}\frac{\Delta t}{4}} \\ \mathcal{U}^T &\equiv e^{\mathcal{O}_{\mathbf{p}_1}\frac{\Delta t}{4}}\, e^{\mathcal{O}_{p_\xi}\frac{\Delta t}{4}}\, e^{\mathcal{O}_{\mathbf{p}_2}\frac{\Delta t}{4}}\, e^{\mathcal{O}_{\xi}\frac{\Delta t}{2}}\, e^{\mathcal{O}_{\mathbf{p}_2}\frac{\Delta t}{4}}\, e^{\mathcal{O}_{p_\xi}\frac{\Delta t}{4}}\, e^{\mathcal{O}_{\mathbf{p}_1}\frac{\Delta t}{4}}\,. \end{aligned} \tag{3.58}$$

In order to check the code used to perform the MD simulations, we have implemented both algorithms (3.57) and (3.58). The results are reported in Fig. (). As can be seen, the kinetic energy obtained from different algorithms fluctuates around the same average value.

3.2 Strain and stress

In the previous chapter we have introduced the notion of stress and strain in order to study a link between the charcteristic time-scales and the response of a material

to deformation.

Now we adopt the standard notation in continuum mechanics [159]. Imagine to have a body, thought of as a continuum, deformed with respect to a given reference configuration. We will denote with $\mathbf{F}$ the deformation. For instance, giving a body $\mathcal{B}$ defined in a regular region of Euclidean space $\mathcal{E}$, denoting with $\mathbf{X} \in \mathcal{B}$ a point of the body. We can define a deformed configuration through a map $\phi : \mathcal{B} \to \mathcal{E}$ (ϕ is assumed to be a diffeomorphism between its domain $\mathcal{B}$ and its image $\phi(\mathcal{B})$)

$$\mathbf{x} = \phi(\mathbf{X}) \tag{3.59}$$

where $\mathbf{x}$ is a general point of the deformed body. The deformation is defined as

$$\mathbf{F} = \nabla_{\mathbf{X}}\phi \tag{3.60}$$

If a system of forces f acts on the body, introducing the Cauchy stress tensor σ, the equation of motion (i. e., equation of the balance for the forces) reads

$$\nabla \cdot \sigma + \mathbf{f} = \rho\dot{\mathbf{v}} \tag{3.61}$$

where $\mathbf{v} = \dot{\mathbf{X}}$ is the velocity. In order to extend the discussion to thermo-mechanical systems, we introduce the temperature T considering the themodynamic equilibrium. Relation between the deformation $\mathbf{F}$ and the Cauchy stress tensor σ reads

$$\sigma(T, \mathbf{F}) = \frac{1}{\det \mathbf{F}}(\nabla_{\mathbf{F}}\psi) \cdot \mathbf{F}^T \,, \tag{3.62}$$

$\mathbf{F}^T$ being for the transpose of $\mathbf{F}$ and $\cdot$ the inner product. We have called ψ the free energy to distinguish it to the forces. The Cauchy stress is measured in the deformed configuration, we can also define another stress tensor called Piola stress $\mathbf{S}$ wich is measured in a reference configuration $\mathbf{F}_0$

$$\mathbf{S} = \det \mathbf{F}\sigma\mathbf{F}^{-T} \,. \tag{3.63}$$

A microscopical representation of the Cauchy stress can be found as follows[160]. Since a deformation can change the metric properties of the space where the body

is defined, we adopt the following notation

$$\begin{aligned} \mathbf{p_i}^2 &= \mathbf{p_i}^T \cdot \mathbf{p_i} = \mathbf{p_i C p_i} \\ \mathbf{C} &= \mathbf{F}^T\mathbf{F} \end{aligned} \tag{3.64}$$

where C is the metric tensor and vector $\mathbf{p_i}^T$ is the transpose of vector $\mathbf{p_i}$. If we have the following Hamiltonian of a particle system

$$\mathcal{H}[\mathbf{p},\mathbf{q}] = \sum_i \frac{\mathbf{p_i}^T \cdot \mathbf{p_i}}{2m} + \varphi(\mathbf{q}) \tag{3.65}$$

Performing a canonical transformation generated by

$$G(\mathbf{P},\mathbf{Q}) = -\sum_i \mathbf{P}_i \cdot (\mathbf{F}\mathbf{Q}_i) \tag{3.66}$$

where we have introduced the deformed generalized coordinates

$$\begin{aligned} \mathbf{q}_i &= \mathbf{F}\mathbf{Q}_i \\ \mathbf{P}_i &= \mathbf{F}^T\mathbf{p}_i\,. \end{aligned} \tag{3.67}$$

The relation between the old and the new Hamiltonian reads

$$\widetilde{\mathcal{H}} = \mathcal{H} + \frac{\partial G}{\partial t} \tag{3.68}$$

since $\frac{\partial G}{\partial t} = 0$, the Hamiltonian becomes

$$\widetilde{\mathcal{H}}[\mathbf{P},\mathbf{Q}] = \mathcal{H} = \sum_i \frac{(\mathbf{F}^{-T}\mathbf{P_i})\cdot(\mathbf{F}^{-T}\mathbf{P_i})}{2m} + \varphi(\mathbf{F}\mathbf{Q})\,. \tag{3.69}$$

The free energy for a fixed deformation $\mathbf{F}$ reads

$$\sigma(T,\mathbf{F}) = -\frac{1}{\beta V_0}\log\mathcal{Z} = \frac{1}{V}\langle\nabla_{\mathbf{F}}\mathcal{H}[\mathbf{P},\mathbf{Q}]\rangle\mathbf{F}^T \tag{3.70}$$

V_0 being the reference volume and $V = (\det\mathbf{F})V_0$. Since the operator $\nabla_{\mathbf{F}}$ acts

linearly on a generical function $\mathbf{g}$ of $\mathbf{F}$, at first order in ϵ we can write

$$\nabla_{\mathbf{F}}\,\mathbf{g}\,\mathbf{Q} = (\mathbf{g} + \epsilon\,\mathbf{L})\,\mathbf{g}\,\mathbf{Q} - \mathbf{g}\,\mathbf{Q} = \epsilon\,\mathbf{L}\,\mathbf{g}\,\mathbf{Q} \tag{3.71}$$

where $\mathbf{L}$ is a linear operator. If $\mathbf{q} = \mathbf{F}$ one has

$$\nabla_{\mathbf{F}}(\mathbf{F}\mathbf{Q}) :\ \mathbf{L} \mapsto \mathbf{L}\,\mathbf{Q}\,. \tag{3.72}$$

If $\mathbf{g} = \mathbf{F}^{-1}$ we note that

$$(\mathbf{F} + \epsilon\,\mathbf{L})(\mathbf{F} + \epsilon\,\mathbf{L})^{-1} = \mathbf{1}\,, \tag{3.73}$$

at first order in ϵ we can write

$$\begin{aligned} (\mathbf{F} + \epsilon\,\mathbf{L})^{-1} &= (\mathbf{A} + \epsilon\,\mathbf{B})^{-1} \\ \mathbf{A} = \mathbf{F}^{-1}\,, \quad \mathbf{B} &= -\mathbf{F}^{-1}\,\mathbf{L}\,\mathbf{F}^{-1}\,. \end{aligned} \tag{3.74}$$

Introducing the diadic product $\otimes$, we finally obtain the following expression for the Cauchy stress

$$\sigma(T,\mathbf{F}) = -\frac{1}{V}\sum_i \left\langle \frac{\mathbf{p}_i \otimes \mathbf{F}^{-1}\mathbf{p}_i}{m} + f_{\mathbf{q}_i} \otimes \mathbf{Q}_i \right\rangle \mathbf{F}^T = -\frac{1}{V}\sum_i \left\langle \frac{\mathbf{p}_i \otimes \mathbf{p}_i}{m} + f_{\mathbf{q}_i} \otimes \mathbf{q}_i \right\rangle \tag{3.75}$$

where we have defined the generalized force $f_{\mathbf{q}_i}$ as

$$f_{\mathbf{q}_i} \equiv \frac{\partial\varphi(\mathbf{q})}{\partial \mathbf{q}_i}\,. \tag{3.76}$$

The r.h.s of Eq. (3.75), which is one of the relations of Irving&Kirkwood [161], is a microscopic picture of the Cauchy-stress.

Therefore, using the continuum mechanics formalism, we can obtain a microscopical interpretation of the stress tensor through a simple canonical transformation. Since the transformation is canonical, the Liouville theorem holds, i. e., the thermal average in eq. (3.75) can be done with respect to the new or the old canonical variables and the measure on the phase space does not change.

The same expression for the Cauchy stress can be obtained starting directly

from Statistical Mechanics [162, 163]. The procedure to obtain such expression is quite similar to the method used in quantum field theory to obtain the Ward-Takahashi (WT) identity [162, 68].

Imagine to have a theory depending by a multiplet of fields $(\phi(\mathbf{x})_i) = \phi(x)$, $i = 0, .., n$ in $d-$dimensions and assume that the action $\mathcal{A}_0[\phi(x)]$ is invariant under the action of a symmetry group $O(n)$. The action of the group over the fields ϕ, for an infinitesimal transformation of the fields, reads [1]

$$\delta\phi_i = \alpha_a \lambda^a_{ij} \phi_j \tag{3.77}$$

where the matrices λ^a define the Lie algebra of the group and α is a parameter. We can define the current

$$j^a_\mu(\mathbf{x}) = \partial_\mu \phi_i \lambda^a_{ij} \phi_j \tag{3.78}$$

where μ runs over the spatial coordinates. The generating functional it is

$$Z[h] = \int \mathcal{D}\phi(\mathbf{x}) e^{-\mathcal{A}_0[\phi] + \int d\mathbf{x} h_i(\mathbf{x})\phi_i(\mathbf{x})} = \int \mathcal{D}\phi(\mathbf{x}) e^{-\mathcal{A}_0[\phi, \mathbf{h}(x)]} \,, \tag{3.79}$$

where $h_i(\mathbf{x})$ is the multiplet of external fields (sources) coupled with the fields. If we perform a variable shift

$$\phi_i(\mathbf{x}) = \phi'_i(\mathbf{x}) + \alpha_a(\mathbf{x}) \lambda^a_{ij} \phi_j(\mathbf{x}) \,, \tag{3.80}$$

the generataing functional becomes

$$Z[h] = \int \mathcal{D}\phi(\mathbf{x}) e^{-\mathcal{A}[\phi, \mathbf{h}(x)]} \left(1 - \int d\mathbf{x} \partial_\mu \alpha^a(\mathbf{x}) j^a_\mu(\mathbf{x}) + \int d\mathbf{x} h_i(\mathbf{x}) \alpha^a(\mathbf{x}) \lambda^a_{ij} \phi_j(\mathbf{x}) \right) . \tag{3.81}$$

Since the measure is invariant under the variable shift (3.80), taking a functional derivative with respect the external source $h_j(\mathbf{y})$ and satting to zero the external fields we obtain the WT identity

$$\partial_\mu \left\langle j^a_\mu(\mathbf{x}) \phi_j(\mathbf{y}) \right\rangle + \delta_{ij} \delta^{(d)}(\mathbf{x} - \mathbf{y}) \lambda^a_{ik} \left\langle \phi_k(\mathbf{x}) \right\rangle = 0 \tag{3.82}$$

[1] We adopt Einstein's summation convention.

where $\delta^{(d)}(\mathbf{x}-\mathbf{y})$ is the Dirac distribution in $d-$dimension.

We now consider a particle system described thorough the Hamiltonian given in eq. (3.65). Acting with a *diffeomorphism*, an infinitesimal point transformation over the generalized coordinates, which brings $\mathbf{q} \to \mathbf{q}'$ we can write [162]

$$\mathbf{q}'_i = \mathbf{q}_i + \epsilon(\mathbf{q}_i)\,. \tag{3.83}$$

The vector function $\epsilon(\mathbf{q}_i)$ satisfies appropriate boundariy condition, according to the boundary conditions of the particle system. We note that the diffeomorphism expressed by $\epsilon(\mathbf{q}_i)$ is a local transformation. Otherwise, the canonical transformation introduced through the deformation tensor $\mathbf{F}$ is a global transformation. We can define a local deformation $\mathbf{F}(\mathbf{q})$ as follows. Acting a local deformation the relative distance between two particles becomes

$$\begin{aligned} \mathbf{q}'_i - \mathbf{q}'_j &= [\mathbf{1} + \mathbf{F}(\mathbf{q}_i)]\,\mathbf{q}_{ij} \\ \mathbf{q}_{ij} &\equiv \mathbf{q}_i - \mathbf{q}_j \\ \mathbf{F}_{ab}(\mathbf{q}_i) &\equiv \partial_b \epsilon^a(\mathbf{q})|_{\mathbf{q}_i}\,, \end{aligned} \tag{3.84}$$

where the indices a, b runs over the coordinate of the space. In order to make the transformation canonical, we have to perfom the follows transformation on the momenta

$$\mathbf{p}_i = [\mathbf{1} + \mathbf{F}(\mathbf{q}_i)]\,\mathbf{p}'_i\,. \tag{3.85}$$

Since the measure of phase space is invariant under canonical transformations, the partition function will be still expressed as an integral over the undeformed momenta and coordinates. The new partition function, adding an external potential source $\varphi(\mathbf{q})$, reads

$$\begin{aligned} \mathcal{Z}' &= \int d\Gamma e^{-\beta\mathcal{H}'} \\ \mathcal{H}' &\equiv \mathcal{H}[\mathbf{p}', \mathbf{q}'] + \varphi_{ext}(\mathbf{q}')\,. \end{aligned} \tag{3.86}$$

The invariance of $\mathcal{Z}$ becomes

$$\left.\frac{\delta \log \mathcal{Z}'}{\delta \mathbf{F}(\mathbf{x})}\right|_{\mathbf{F}(\mathbf{x})} = 0 \tag{3.87}$$

The eq. (3.87) leads to the following identity

$$\nabla \cdot \left\langle \sum_i \delta(\mathbf{x}-\mathbf{q}_i) \left(\frac{\mathbf{p}_i \otimes \mathbf{p}_i}{m} + \mathbf{q}_i \otimes f_{\mathbf{q}_i} \right) \right\rangle - \left\langle \sum_i \delta(\mathbf{x}-\mathbf{q}_i) \mathbf{f}_i^{ext}(\mathbf{q}) \right\rangle = 0\,, \tag{3.88}$$

where we have defined the external force

$$\mathbf{f}_i^{ext}(\mathbf{q}) \equiv \frac{\partial \varphi(\mathbf{q})}{\partial \mathbf{q}_i}\,. \tag{3.89}$$

As we can see, we can define a stress tensor $\tilde{\sigma}$ and a bulk (macroscopic) force $\mathbf{f}$ such that

$$\begin{aligned} 0 &= \nabla \cdot \tilde{\sigma} + \mathbf{f} \\ \tilde{\sigma} &\equiv \left\langle \sum_i \delta(\mathbf{x}-\mathbf{q}_i) \left(\frac{\mathbf{p}_i \otimes \mathbf{p}_i}{m} + \mathbf{q}_i \otimes f_{\mathbf{q}_i} \right) \right\rangle \\ \mathbf{f} &\equiv -\left\langle \sum_i \delta(\mathbf{x}-\mathbf{q}_i) \mathbf{f}_i^{ext}(\mathbf{q}) \right\rangle . \end{aligned} \tag{3.90}$$

These expressions, integrated over the body, are consistent with the papers [161, 164, 165, 166, 167, 168].

Therefore, through a molecular dynamics simulation we can compute the Cauchy stress. As we can read in eq. (3.75) and (3.90), there are two contributed to the stress tensor: one kinetic and the other due to the interaction between the particles. We have use such expression to compute the internal pressure of the system when a deformation of the simulation box is enforced.

In the next section we will discuss the details to perform a numerical simulation under given external pressure or deformation.

3.3 Andersen Dynamics

In Section 3.1 we have introduced the concept of a thermostat in MD. In order to preserve the dynamical properties of the system, to thermalize it we can not simply rescale the momenta, but we have to reproduce the correct statistical ensemble. We could build, for instance, some model which heuristically reproduce a thermostat, also starting from general models, but such a trick does not reproduce the dynamics towards equilibrium.

Now we want to study model where we fix the pressure or, more general, by the strain. The applied stress causes a deformation of the material. The material responds to the external stress through an internal stress.

As we have seen for the temperature, from the statistical mechanics point of view, fixing the pressure implies volume fluctuations: this is a geneal effect of the thermodynamical Legendre transformation on statistical mechanics. We restrict our study to *linear transformations* and, in particular, to spherical dilations. We will consider a system of N particles in a cell (i. e., the simulation box) of side L, assuming that it is possible to apply an external pressure on the box. Such external stress is represented by a spherical tensor.

We call $\mathbf{s_i}$ the coordinate of the particle i in box units.

$$\mathbf{r}_i = L\mathbf{s_i} \tag{3.91}$$

$$\mathbf{s_i} = \frac{\mathbf{r_i}}{L} \tag{3.92}$$

If we allow the simulation box to fluctuate we can substitute L with a parameter $0\lambda L$ depending on time

$$\mathbf{s_i} = \frac{\mathbf{r_i}}{\lambda}\,, \tag{3.93}$$

hence

$$\dot{\mathbf{r_i}} = \lambda\dot{\mathbf{s}}_\mathbf{i} + \dot{\lambda}\mathbf{s_i}\,. \tag{3.94}$$

In order to introduce the pressure, we can try to make a canonical transformation on the Lagrangian changing the variable V with its thermodynamically coniugate π. Now we discuss the case with only one particle in a d-dimensional cell and

external pressure π

$$\begin{aligned} L(s,\lambda,\dot{s},\dot{\lambda};\pi) &= L(r,\lambda) - \pi\lambda^d = K - V \\ K &= \frac{1}{2}m\left(\lambda^2\dot{s}^2 + \dot{\lambda}^2 s^2 + 2\lambda\dot{\lambda}s\dot{s}\right) \\ V &= \phi(\lambda s) + \pi\lambda^2 \end{aligned} \tag{3.95}$$

In order to obtain a Hamiltonian which leads to the right ensemble average, Andersen suggested [14] that the dynamics be governed by the following Lagrangian

$$L_A[\lambda,\dot{\lambda},\mathbf{s},\dot{\mathbf{s}}] = \frac{1}{2}\sum_i m\lambda^2\dot{\mathbf{s}}_\mathbf{i}^T\cdot\dot{\mathbf{s}}_\mathbf{i} + \frac{1}{2}Wd\dot{\lambda}^2 - \phi(\lambda s) - \pi\lambda^2\,. \tag{3.96}$$

As we can see, the Lagrangian proposed by Andersen differes from (3.95). However, with an appropiate hypothesis, we can recover (3.96) from (3.95). If we assume that the dynamics has two well-separated time scales, one microscopic τ and another mesoscopic t, related through

$$t = n\tau, \quad \frac{d\lambda}{d\tau} = n\frac{d\lambda}{dt} \tag{3.97}$$

and we average the Lagrangian (3.95) over a time T much larger than τ but much smaller than t, we obtain

$$\overline{K} = \frac{1}{2}m\lambda\overline{\dot{s}^2} + \frac{1}{2}\overline{ms^2}\dot{\lambda}^2 + \lambda n\frac{d\lambda}{dt}\left(\frac{s^2(t) - s^2(0)}{T}\right) \tag{3.98}$$

since $0 \le s(t) \le 1$ for all t, the last term in the r.h.s of eq. (3.98) is negligible.

If particles interact through a two-body potential it is

$$\begin{aligned} \phi(\lambda s) &= \phi(\mathbf{r}) = \sum_{i<j}\phi(r_{ij}) \\ r_{ij} &= |\mathbf{r_i} - \mathbf{r_j}| \end{aligned} \tag{3.99}$$

differentianting the potential w.r.t $\mathbf{r}_i$ and recalling that $\mathbf{s}_i$ and $\mathbf{r}_i$ are collinear, it follows that

$$\frac{\partial\phi(\mathbf{r})}{\partial\mathbf{r}_i} = \sum_{i<j}\frac{\partial\phi(r_{ij})}{\partial r_{ij}}\hat{\mathbf{s}}_\mathbf{i} \equiv -\lambda^{-1}\mathbf{f_i}\,, \tag{3.100}$$

where $\mathbf{f}_i$ is the total force acting on the particle.

The Lagrangian equations of motion are

$$\begin{aligned} \ddot{\mathbf{s}}_\mathbf{i} &= \frac{1}{\lambda}\left(\mathbf{f}_\mathbf{i} - \dot{\lambda}\dot{\mathbf{s}}_\mathbf{i}\right) \\ W\ddot{\lambda} &= \lambda\left(\sum_i \dot{\mathbf{s}}_\mathbf{i}^T \cdot \mathbf{s}_\mathbf{i} + \mathbf{f}_\mathbf{i}\right) - d\pi\lambda^{d-1}\,. \end{aligned} \tag{3.101}$$

Introducing the momenta $\mathbf{p}_{\mathbf{s}_\mathbf{i}}$ and p_λ,

$$\begin{aligned} \mathbf{p}_{\mathbf{s}_\mathbf{i}} &= \lambda^2\dot{\mathbf{s}}_\mathbf{i} \\ p_\lambda &= W\dot{\lambda}\,, \end{aligned} \tag{3.102}$$

and using a shorthand for the potential, we can write the Andersen Hamiltonian as follows

$$\mathcal{H}_A[\mathbf{p}_\mathbf{s}, \mathbf{s}, p_\lambda, \lambda] = \sum_i \frac{{\mathbf{p}_{\mathbf{s}_\mathbf{i}}}^T \cdot \mathbf{p}_{\mathbf{s}_\mathbf{i}}}{2m\lambda^2} + \frac{p_\lambda^2}{2W} + \phi(\lambda\mathbf{s}) + \pi\lambda^d\,. \tag{3.103}$$

The Hamilton equations ensue:

$$\begin{aligned} \dot{\mathbf{s}}_\mathbf{i} &= \frac{\mathbf{p}_{\mathbf{s}_\mathbf{i}}}{\lambda^2 m}\,, \\ \dot{\mathbf{p}}_{\mathbf{s}_\mathbf{i}} &= \frac{1}{\lambda}\mathbf{f}_\mathbf{i}\,, \\ \dot{\lambda} &= \frac{p_\lambda}{W}\,, \\ \dot{p}_\lambda &= \lambda\sum_i \frac{{\mathbf{p}_{\mathbf{s}_\mathbf{i}}}^T \cdot \mathbf{p}_{\mathbf{s}_\mathbf{i}}}{m\lambda^4} + \lambda\mathbf{f}_\mathbf{i} - d\pi\lambda^{d-1}\,. \end{aligned} \tag{3.104}$$

In order to numerically integrate eqs. (3.104), we introduce the rescaled momenta

$$\mathbf{p}'_\mathbf{i} = \lambda\mathbf{p}_{\mathbf{s}_\mathbf{i}} \tag{3.105}$$

and rewrite eqs. (3.104) as follows:

$$\begin{aligned}
\dot{\mathbf{s}}_\mathbf{i} &= \frac{\mathbf{p}'_\mathbf{i}}{m}\,, \\
\dot{\mathbf{p}}'_\mathbf{i} &= \frac{1}{\lambda}\mathbf{f}_\mathbf{i}\,, \\
\dot{\lambda} &= \frac{p_\lambda}{W}\,, \\
\dot{p}_\lambda &= \sum_i \frac{{\mathbf{p}'_\mathbf{i}}^T \cdot \mathbf{p}'_\mathbf{i}}{\lambda m} + \lambda \mathbf{f}_\mathbf{i} - d\pi\lambda^{d-1}\,.
\end{aligned} \tag{3.106}$$

Andersen dynamics: Liouvillian formulation

In order to implement numerically the Andersen dynamics (coupled with a Nosé-Hoover thermal bath), we need the Liouvillian operator associated with the following Hamiltonian:

$$\begin{aligned}
\mathcal{H}_{A-N.H}[\mathbf{p_s}, \mathbf{s}, p_\lambda, \lambda, \xi, p_\xi] &= \sum_i \frac{{\mathbf{p}_{\mathbf{s}_\mathbf{i}}}^T \cdot \mathbf{p}_{\mathbf{s}_\mathbf{i}}}{2m\lambda^2} + \frac{p_\lambda^2}{2W} + \phi(\lambda\mathbf{s}) + \pi\lambda^d + \frac{p_\xi^2}{2Q} + \frac{g}{\beta}\xi \\
\mathbf{p}_{\mathbf{s}_\mathbf{i}} &\equiv {\mathbf{p}_{\mathbf{s}_\mathbf{i}}}' = \mathbf{p}_{\mathbf{s}_\mathbf{i}} e^{2\xi}\,, \\
p_\lambda &\equiv p'_\lambda = p_\lambda e^{2\xi}\,.
\end{aligned} \tag{3.107}$$

Redefining the momenta

$$\mathbf{p_i} = \lambda \mathbf{p}_{\mathbf{s}_\mathbf{i}}\,, \tag{3.108}$$

we can rewrite (3.107) as follows:

$$\mathcal{H}_{A-N.H}[\mathbf{p_s}, \mathbf{s}, p_\lambda, \lambda, \xi, p_\xi] = \sum_i \frac{{\mathbf{p_i}}^T \cdot \mathbf{p_i}}{2m} + \frac{p_\lambda^2}{2W} + \phi(\lambda\mathbf{s}) + \pi\lambda^d + \frac{p_\xi^2}{2Q} + \frac{g}{\beta}\xi \tag{3.109}$$

and finally obtain the Liouvillian

$$
\begin{aligned}
i\mathcal{L} &= \mathcal{O}_{\mathbf{s}} + \mathcal{O}_{\mathbf{p}} + \mathcal{O}_{\lambda} + \mathcal{O}_{p_\lambda} + \mathcal{O}_{\xi} + \mathcal{O}_{p_\xi} \qquad (3.110)\\
\mathcal{O}_{\mathbf{s}} &\equiv \sum_i \frac{\mathbf{p_i}}{m}\partial_{\mathbf{s_i}}\\
\mathcal{O}_{\mathbf{p}} &\equiv \left(\frac{\mathbf{f_i}}{\lambda} + A + B\right)\partial_{\mathbf{p_i}}\\
A &\equiv \frac{p_\xi}{Q}\mathbf{p_i}\\
B &\equiv \frac{p_\lambda}{W}\mathbf{p_i}\\
\mathcal{O}_{\lambda} &\equiv \frac{p_\lambda}{W}\partial_\lambda\\
\mathcal{O}_{p_\lambda} &\equiv \left[\sum_i \left(\frac{\mathbf{p_i}^T\cdot\mathbf{p_i}}{m\lambda} + \mathbf{s_i}\cdot\mathbf{f_i}\right) - d\pi\lambda^{d-1}\right]\partial_{p_\lambda}\\
\mathcal{O}_{\xi} &\equiv \frac{p_\xi}{Q}\partial_\xi\\
\mathcal{O}_{p_\xi} &\equiv \left(\sum_i \frac{\mathbf{p_i}^T\cdot\mathbf{p_i}}{m} + \frac{p_\lambda^2}{W} - \frac{g}{\beta}\xi\right)\partial_{p_\xi}
\end{aligned}
$$

3.4 Parrinello-Rahman method

In order to allow the shape of the simulation box to change, we have to extend the Andersen Lagrangian to a general linear transformation:

$$\mathbf{r_i} = \mathbf{F}\mathbf{s_i}\,. \qquad (3.111)$$

The deformation $\mathbf{F}$ encodes all the degrees of freedom of an affine box, i. e., in three dimension is a 3×3 matrix. For a cubic cell the columns of the matrix of $\mathbf{F}$ represent the box edges. Parrinello and Rahman (PR) suggested [15, 16] the following Hamiltonian

$$L_{APR}(\mathbf{s},\dot{\mathbf{s}},\mathbf{F},\dot{\mathbf{F}}) = \frac{1}{2}\sum_i m_i\mathbf{F}^T\dot{\mathbf{s}}_\mathbf{i}\cdot\mathbf{F}\dot{\mathbf{s}}_\mathbf{i} + \frac{1}{2}W\mathrm{Tr}\left(\dot{\mathbf{F}}^T\cdot\dot{\mathbf{F}}\right) - \phi(\mathbf{F}^{-1}\mathbf{s}) - \pi\det\mathbf{F} \qquad (3.112)$$

where π is the external pressure. As in Andersen dynamics, substituting eq. (3.111) in a Lagrangian which describes a particle system does not lead to eq. (3.112). In fact, assuming $\mathbf{F}$ as a dynamical variable one has

$$\dot{\mathbf{r}}_\mathbf{i} = \dot{\mathbf{F}}\mathbf{s}_\mathbf{i} + \mathbf{F}\dot{\mathbf{s}}_\mathbf{i}\,. \tag{3.113}$$

The kinetic term of a Lagrangian contains several terms

$$K = \frac{1}{2}\sum_i m_i \mathbf{F}^T\dot{\mathbf{s}}_\mathbf{i}\cdot\mathbf{F}\dot{\mathbf{s}}_\mathbf{i} + \frac{1}{2}\sum_i m_i \mathbf{s}_\mathbf{i}\otimes\mathbf{s}_\mathbf{i}\mathrm{Tr}\,\dot{\mathbf{F}}^T\cdot\dot{\mathbf{F}} + \sum_i m_i\mathbf{F}^T\dot{\mathbf{F}}\mathbf{s}_\mathbf{i}\otimes\dot{\mathbf{s}}_\mathbf{i}\,. \tag{3.114}$$

It is possible to recover eq. (3.112) from eq.(3.114) through the following assumptions[169]

$$\begin{aligned}\sum_i m_i\mathbf{s}_i\otimes\mathbf{s}_i &= Const. \equiv W\mathbf{I} \qquad (3.115)\\ \sum_i m_i\mathbf{F}^T\dot{\mathbf{F}}\mathbf{s}_i\otimes\dot{\mathbf{s}}_i &= 0\,.\end{aligned}$$

The first equation (3.115) is satisfied when the inertia tensor of the particles system is stationary and spherical: under the hypothesis that the first is satisfied the second is satisfied if the angular velocity of the cell is negligible.

The generalized momenta of the Lagrangian (3.112) are

$$\begin{aligned}\mathbf{p}_\mathbf{i} &= m_i\mathbf{F}^T\mathbf{F}\dot{\mathbf{s}}_i \qquad (3.116)\\ \mathbf{p}_\mathbf{F} &= W\dot{\mathbf{F}}\,.\end{aligned}$$

Introducing the metric tensor $\mathbf{G} = \mathbf{F}^T\mathbf{F}$, we can write the following Hamiltonian:

$$\mathcal{H}(\mathbf{p},\mathbf{p}_\mathbf{F},\mathbf{s},\mathbf{F}) = \sum_i \frac{\mathbf{p}_\mathbf{i}\,\mathbf{G}^{-1}\,\mathbf{p}_\mathbf{i}}{2m_i} + \frac{\mathrm{Tr}\,\mathbf{p}_\mathbf{F}{}^T\cdot\mathbf{p}_\mathbf{F}}{2W} + \phi(\mathbf{F}^{-1}\mathbf{s}) + \pi\det\mathbf{F} \tag{3.117}$$

defining the rescaled momenta $\mathbf{p_{s_i}} = \mathbf{G}^{-1}\mathbf{p_i}$, the equations of motion read

$$\begin{aligned}
\dot{\mathbf{p}}_{\mathbf{s_i}} &= \mathbf{F}^{-1}\mathbf{f}_{\mathbf{s_i}} - \mathbf{G}^{-1}\dot{\mathbf{G}}\mathbf{p}_{\mathbf{s_i}} \\
\dot{\mathbf{p}}_{\mathbf{F}} &= \left(\sum_i \mathbf{f}_{\mathbf{s_i}}\mathbf{s_i}^T + \sum_i \mathbf{F}\dot{\mathbf{s}}_\mathbf{i}\dot{\mathbf{s}}_\mathbf{i}^T - \pi\mathbf{F}^{-1}\det\mathbf{F}\right) \\
\dot{\mathbf{s}}_\mathbf{i} &= \frac{\mathbf{p}_{\mathbf{s_i}}}{m_i} \\
\dot{\mathbf{F}} &= \frac{\mathbf{p}_\mathbf{F}}{W}
\end{aligned} \tag{3.118}$$

The Hamiltonian conserved by the eq.(3.118) is

$$\mathcal{H}(\mathbf{p}, \mathbf{p_F}, \mathbf{s}, \mathbf{F}) = \sum_i \frac{\mathbf{p_{s_i}}\,\mathbf{G}\,\mathbf{p_{s_i}}}{2m_i} + \frac{\mathrm{Tr}\,\mathbf{p_F}^T\mathbf{p_h}}{2W} + \phi(\mathbf{F}^{-1}\mathbf{s}) + \pi\det\mathbf{F} \tag{3.119}$$

In order to numerically integrate eq.(3.118), we consider the Liouvillian

$$i\mathcal{L} = \sum_i \left\{\dot{\mathbf{s}}_\mathbf{i}\partial_{\mathbf{s_i}} + \dot{\mathbf{p}}_{\mathbf{s_i}}\partial_{\mathbf{p_{s_i}}}\right\} + \dot{\mathbf{F}}\partial_\mathbf{F} + \dot{\mathbf{p}}_\mathbf{F}\partial_{\mathbf{p_F}} \equiv A + B + C + D\,, \tag{3.120}$$

choosing the operators as follows

$$\begin{aligned}
A &\equiv \frac{\mathbf{p}_\mathbf{F}}{W}\partial_\mathbf{F} \\
B &\equiv \sum_i \frac{\mathbf{p_{s_i}}}{m_i}\partial_{\mathbf{s_i}} \\
C &\equiv \left[\mathcal{V} + \mathcal{K} - \pi\mathbf{F}^{-1}\det\mathbf{F}\right]\partial_{\mathbf{p_F}} \\
D &\equiv \left[\mathbf{F}^{-1}\mathbf{f}_{\mathbf{s_i}} - \mathbf{G}^{-1}\dot{\mathbf{G}}\mathbf{p}_{\mathbf{s_i}}\right]\partial_{\mathbf{p_{s_i}}} = D_1 + D_2\,,
\end{aligned} \tag{3.121}$$

where we have defined the potential and kinetic virials

$$\mathcal{V} = \sum_i \mathbf{f}_{\mathbf{s_i}}\mathbf{s_i}^T\,, \quad \mathcal{K} = \sum_i \mathbf{F}\dot{\mathbf{s}}_\mathbf{i}\dot{\mathbf{s}}_\mathbf{i}^T\,, \tag{3.122}$$

while

$$D_1 \equiv \mathbf{F}^{-1}\mathbf{f}_{\mathbf{s_i}} \quad D_2 \equiv -\mathbf{G}^{-1}\dot{\mathbf{G}}\mathbf{p}_{\mathbf{s_i}}\,. \tag{3.123}$$

The Trotter formula reads

$$e^{i\mathcal{L}\Delta t} \simeq e^{\frac{A}{4}\Delta t} e^{\frac{B}{2}\Delta t} e^{\frac{A}{4}\Delta t} e^{\frac{C}{2}\Delta t} e^{\frac{D_1}{2}\Delta t} e^{D_2\Delta t} e^{\frac{D_1}{2}\Delta t} e^{\frac{C}{2}\Delta t} e^{\frac{A}{4}\Delta t} e^{\frac{B}{2}\Delta t} e^{\frac{A}{4}\Delta t} , \tag{3.124}$$

and the evolution of D_2 is given by

$$e^{-\mathbf{G}^{-1}\dot{\mathbf{G}}\partial_{\mathbf{p_{s_i}}}\Delta t} f(\mathbf{p_{s_i}}) = f(e^{-\mathbf{G}^{-1}\dot{\mathbf{G}}\Delta t}\mathbf{p_{s_i}}) \tag{3.125}$$

We have performed numerical simulations using the operators (3.121). In order to allow the thermalization of the system, we have coupled the APR Hamiltonian to a Nosè-Hoover thermostat.

For a given value of the external pressure, startig from a cubic box, we have equilibrated the system at a fixed temperature. After the thermalization, we have let the system evolve according to the APR equations of motion. The Liouvillian formulation allows to separate the time scales of the microscopic (fast) degrees of freedom $\mathbf{s}_i$ and the mesoscopic (slow) $\mathbf{F}$. The evolution of the fast degrees of freedom is done with a time-scale Δt, whereas the evolution of slow degrees of freedom is done with a time step $\Delta t' = n\Delta t$.

The numerical simulations are perfomed using Argon interacting via Lennard-Jones potential in reduced variables [151]

$$\phi(r) = 4\epsilon \left[\left(\frac{\sigma}{r}\right)^{12} - \left(\frac{\sigma}{r}\right)^{6} \right] . \tag{3.126}$$

In order to check the code we have simulated an fcc crystal ($N = 256$, $T = 0.17$ and $p_{ext} = 1.62$) near the transition to bcc [15, 16] (cf. fig. (3.4)).

3.5 APR-based multiscale algorithm

The Lagrangian introduced by Andersen and extended by Parrinello and Rahman, can be used to couple continuum and atomistic mechanics. In fact, in the equations of motion (3.118) both continuum and atomistic degrees of freedom appear: through a Molecular Dynamics simulation we can compute the evolution of $\mathbf{F}$ and

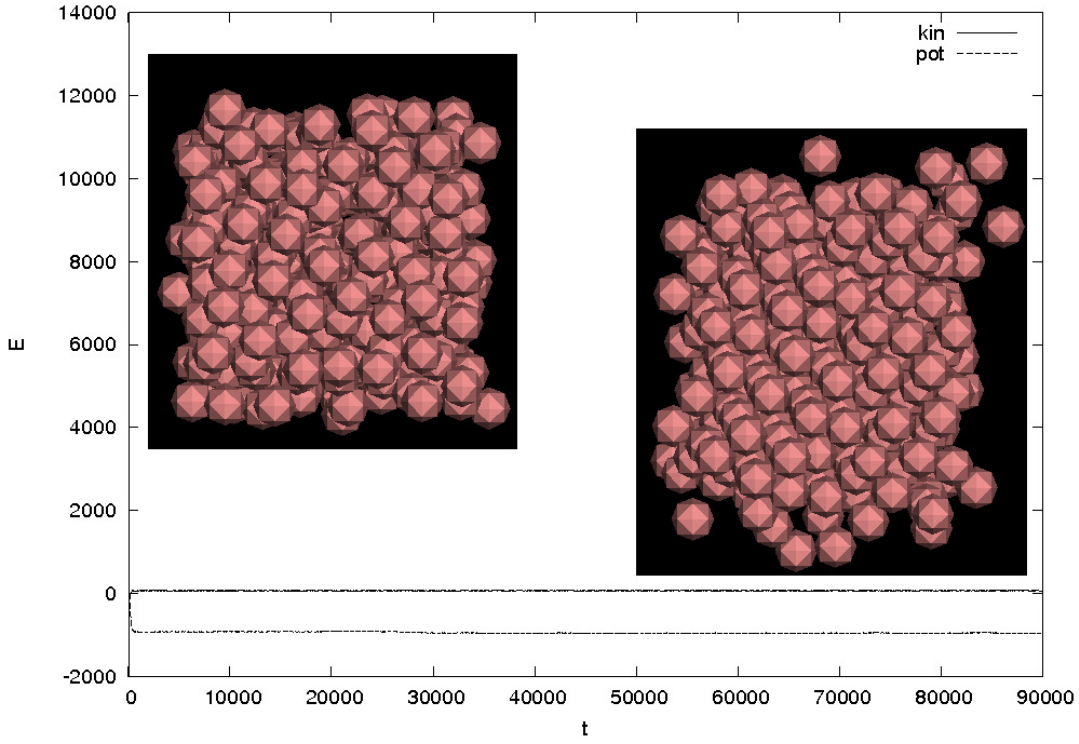

Figure 3.4: Transition between fcc to bcc $N = 256$, $T = 0.17$ and $p_{ext} = 1.62$.

$\mathbf{s_i}$:

$$\begin{aligned} \ddot{\mathbf{F}} &= \frac{1}{W}\left(\mathcal{V}+\mathcal{K}-\pi\mathbf{F}\det\mathbf{F}\right) \\ \ddot{\mathbf{s}}_\mathbf{i} &= \frac{1}{m_i}\left(\mathbf{F}^{-1}\mathbf{f}_{\mathbf{s_i}}-\mathbf{G}^{-1}\dot{\mathbf{G}}\dot{\mathbf{s}}_\mathbf{i}m_i\right). \end{aligned} \tag{3.127}$$

As we can see, $\mathbf{F}$ depends by the atomistic dynamic variables $(\mathbf{s_i}\,,\,\dot{\mathbf{s}}_\mathbf{i})$. Since we can fix the external pressure π, the simulation box will fluctuate: this fact is expressed by the first equation in (3.127). Now we can think of performing a MD simulation at zero pressure. If the particle system is in equilibrium during the simulation $\mathbf{F}$ does not change. On the other hand, if initially the box is not in an equilibrium configuration, $\mathbf{F}$ evolves.

If the box is thought of as an element of an array, where the array samples a macroscopic medium, we can simulate many boxes, each of which is representative of a microscopic point of the material.

From the macroscopic point of view, the evolution of the deformation is governed by the balance equation (3.61), if the external force is zero, it reads

$$\nabla\cdot\sigma(\mathbf{F})=\rho\ddot{\mathbf{u}} \tag{3.128}$$

where $\mathbf{u}=\mathbf{u}(\mathbf{x},t)$ is the macroscopic displacement at the point $\mathbf{x}$ and time t, while ρ is the macroscopic (homogeneous) density of the material. For equation (3.128) we have choosen periodic boundary conditions and the initial condition on the deformation is such that

$$\oint d\mathbf{x}\,\mathbf{u}(\mathbf{x},0)=0 \tag{3.129}$$

From the microsopic point of view, the continuum variable $\mathbf{x}$ is replaced by the discrete index l of the box $\mathcal{B}_l$ (see fig. (3.5)). Eq. (3.128) gives a set of deformations $\mathbf{F}_l$ for the array of boxes: these deformations constitute the initial condition for the microscopic simulations driven by the APR algorithm expressed by eq. (3.127) at zero external pressure. From the MD simulation we obtain a new set of internal pressures which will evolve through eq. (3.128). The key feature of this approach is that we dispense with phenomenological constitutive relations since implicitly recovered from the physical properties of the particle system. Indeed, imposing an

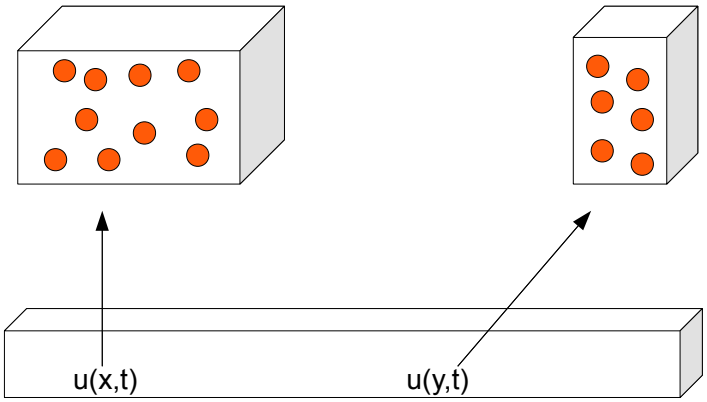

Figure 3.5: Schematics of the multiscale algorithm. At each point $\mathbf{x}$ at the (macroscopic) time t of a medium $\mathbf{u}(\mathbf{x}, t)$, modelled as a continuum, we associate a simulation box $\mathcal{B}_l$. The evolution of $\mathbf{u}$ is governed by the balance equation (3.128): the deformation $\mathbf{u}(\mathbf{x}, t + dt)$ it is the input of the molecular dynamics simulation.

initial box deformation away from equilibrium, according to

$$\mathbf{h}_l \equiv \mathbf{h}(\mathbf{x}, t + dt) = \mathbf{h}_0 + \mathbf{u}(\mathbf{x}, t + dt) \tag{3.130}$$

$$\mathbf{F}_l \equiv \mathbf{F}(\mathbf{x}, t + dt) = \mathbf{h}(\mathbf{x}, t + dt)^T \mathbf{h}(\mathbf{x}, t + dt)$$

$$\sigma(\mathbf{F}_l) = \frac{1}{V}\langle \mathcal{K} + \mathcal{V} \rangle \tag{3.131}$$

where $\mathbf{h}_0$ is the box in a referenced configuration and $\mathbf{u}(\mathbf{x}, t + dt)$ is given by the solution of (3.128). Since the microscopic dynamics evolves over a time scale much shorter than the macroscopic time scale t, the rearrangement of the particles in the boxes will be instantaneous with respect the continuum time scale.

In fig. (3.6) the evolution of $\mathbf{u}$ is shown. The spatial evolution is along $\mathbf{x}$. I have simulated 16 APR-cell, each one with $N = 108$ Argon molecules interacting via Lennard-Jones potential at $T = 0.7$ and zero external pressure. In fig. (3.7) the thermalization of the cell is checked.

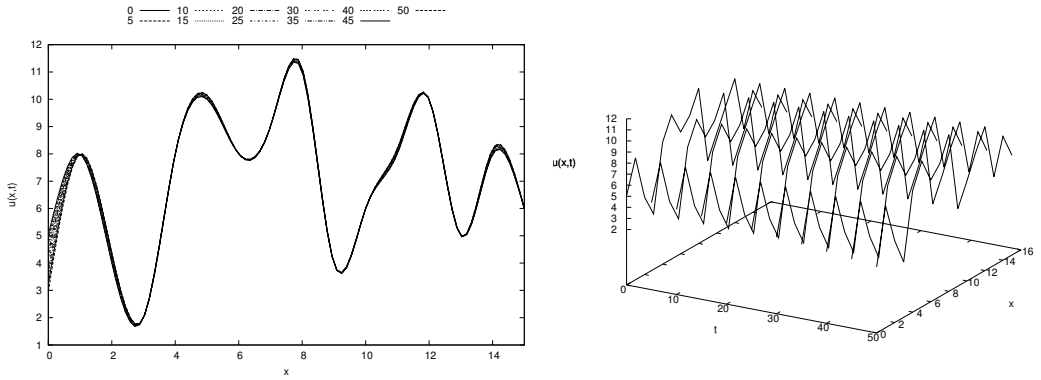

Figure 3.6: Evolution of $\mathbf{u}(\mathbf{x}, t)$ for an array of 16 APR-cell (along the $\mathbf{x}$ direction) and $N_t = 50$ macroscopical time-steps.

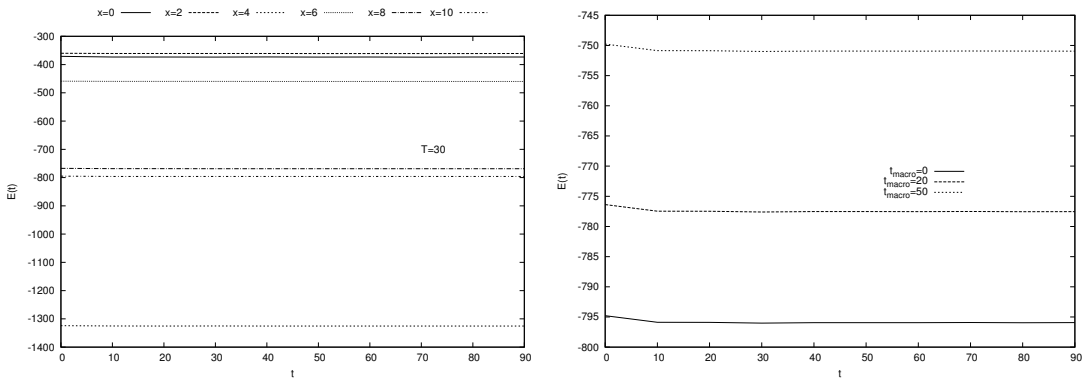

Figure 3.7: APR-cell energy behaviour at fixed macroscopical time (left panel) and for different macroscopical times (right).

3.6 Conclusions

In the last chapter of this Thesis we have introduced algorithm which allows to couple continuum mechanics and molecular dynamics. We have introduced the stress tensor in statistical mechanics: from the microscopic point of view, the stress tensor is a well-defined observable, related with the total virial of the system. In order to perform numerical simulation in (N, P, T) ensemble we have studied molecular dynamics algorithms that allow to fix the temperature and the pressure.

Reconsidering the Nosé-Hoover thermostat, we have suggested a class of algorithm to rescale systematically the velocity of the particles in order to obtain the right average of the kinetic energy. We are not able to prove whether this algorithm samples a canonical mesure over the phase space. However the scheme suggested is time reversible, i. e., we can implement the equations of motion through a Liouvillian formulation obtaining a stable algorithm (indipendently of the order of the operators). Moreover, we have defined the thermostat through a simple toy-model: a spherical-spin bath used to thermalize the system. In this model only one free parameter appears, i. e., the coupling costant between spins and particles. For the perfect gas the coupling can be exactly fixed imposing equipartition. When studying interacting systems, the coupling can be fixed by studying the behaviour of the temperature in function of the coupling itself and of the size of the system.

Finally, discussing the Andersen-Parrinello-Rahman algorithm, we have pointed out that a time-scale separation between slow and fast degrees of freedom underlie these schemes. The degrees of freedom of the simulation box evolve on a time scale slower than that of the particles. The main results of this chapter is the definition of a numerical algorithm to exchange information between the microscopic dynamics, driven by an equilibrium dynamics by means of the APR method, and a macroscopic dynamics governed by the balance equation of continuum mechanics. In other terms, we can close the set of partial differential equations for the stress and the deformation without guessing any constitutive relation.

Conclusions

Analytical and numerical techniques play an important role to understand complex system, amorphous materials and, in general, models whose dynamics involves many interacting degrees of freedom. In this Thesis I have studied three different kinds of multiscale problems in thermodynamics, in equilibrium dynamics and in molecular dynamics.

In the first chapter an intensive study of the Blume-Capel model with quenched disorder in three dimensions has performed by means of Monte Carlo simulations through Parallel Tempering techinque. The simulations have confirmed the mean-field phase diagram. The criticality is studied through quotient method and it has been possible to compute the critical exponents of the theory. In this analysis, we have carefully checked finite size effects. Moreover, the second-order transition belongs to the same universality class of Edwards-Anderson model.

The first-order transition line has the property of displaying inverse freezing: an IT takes place between SG phase and PM phase and latent heat is exchanged. The low-temperature phase is paramagnetic and the system freezes into a spin-glass phase as temperature is increased. To conclude, in lattice gas model with quenched disorder, in order to have an IT the key-role is played by the interplay between active and neutral component.

Since glassy behaviour is a peculiar multi-scale problem, in the second chapter, a study about the secondary processes in the framework of random firs order theory has been presented. In particular, I suggested a mean-field theory to describe a glass former which relaxes over three time-scale. The model is a generalization of the p-spin model with quenched disorder whose dynamics leads to the mode-coupling equation in the so-called schematic theory.

The mean-field equation has been solved numerically and the spectrum has

been studied. Approaching the tricritical point —where the thermodynamics is stabilized by a two-step replica symmetry breaking solution— susceptibility loss shows a distinct secondary peak. The interrelation between relaxation times is studied comparing the results with the Ngai's coupling model.

Finally, I generalized analytically the relations between the mode coupling exponents for models which are characterized by a multistep relaxation behaviour.

In last chapter I have proposed a possible coupling between continuum mechanics and molecular dynamics. Firstly, I have reconsidered the Nosé-Hoover thermostat suggesting a class of algorithm to rescale systematically the velocity of the particles. In this model only one free parameter appears. For a perfect gas the coupling can be exactly fixed imposing the equipartition. For interacting system the coupling has to be tuned in function of the temperature and the size of the system.

The main result of the third chapter has been the definition of a numerical algorithm to exchange information between the microscopic dynamics —performed by means of Andersen-Parrinello-Rahman method— and a macroscopic dynamics governed by the balance equation of continuum mechanics. In particular, from the equations of the molecular dynamics we can compute the constitutive relation closing the balance equations.

Acknowledgment

During my Ph. D., I felt free to investigate in different directions: I wish to thank my supervisor Antonio di Carlo, who, through many discussions, gave me a lot of useful suggestions. Moreover, He also gave me the opportuinity to understand some aspects of continuum mechanics which have deeply improved my knowledge.

Most of this work has done in collaboration with Andrea Crisanti and Luca Leuzzi: it has been a pleasure to discuss statistical mechanics and disordered systems with them and only thanks to their collaboration I reached some of the results presented in this Thesis.

I wish to thank the referee of this Ph. D. Thesis Walter Kob, his detailed review and his suggestions have been crucial to finalize the manuscript.

I wish to thank all my colleagues at La.M.S of Roma Tre University, the colleagues at Physics departements of Roma Tre University and Sapienza University and the researchers of IPCF-CNR in Rome.

Last but not least, I wish to thank my family and the people who shared with me these last months: without their understanding and patience I would never have accomplished this work.

Bibliography

[1] M. Paoluzzi, L. Leuzzi, and A. Crisanti. Thermodynamic first order transition and inverse freezing in a 3d spin glass. *Phys. Rev. Lett.*, **104**:120602, 2010.

[2] M. Paoluzzi, L. Leuzzi, and A. Crisanti. The overlap parameter across an inverse first-order phase transition in a 3d spin-glass. *Phil. Mag.*, **91**:1966, 2011.

[3] L. Leuzzi, M Paoluzzi, and A. Crisanti. Random blume-capel model on a cubic lattice: First-order inverse freezing in a three-dimensional spin-glass system. *Phys. Rev. B*, **83**:014107, 2011.

[4] M. Blume, V. J. Emery, and R. B. Griffiths. Ising model for the λ transition and phase separation in he^3-he^4 mixtures. *Phys. Rev. A*, **4**:1071, 1971.

[5] H. W. Capel. On the possibility of first-order phase transitions in ising systems of triplet ions with zero-field splitting. *Physica*, **32**:966, 1966.

[6] S. K. Ghatak and D. Sherrington. Crystal field effects in a general s ising spin glass. *J. Phys. C: Solid State Phys.*, **10**:3149, 1977.

[7] A. Crisanti and L. Leuzzi. Stable solution of the simplest spin model for inverse freezing. *Phys, Rev. Lett.*, **95**:087201, 2005.

[8] N. Schupper and N. M. Shnerb. Spin model for inverse melting and inverse glass transition. *Phys. Rev. Lett.*, **93**:037202, 2004.

[9] L. Berthier and G. Biroli. Theoretical perspective on the glass transition and amorphous materials. *Rev. Mod. Phys.*, **83**:587, 2011.

[10] A. Crisanti, L. Leuzzi, and M. Paoluzzi. Statistical mechanical approach to secondary processes and structural relaxation in glasses and glass formers. *Eur. Phys. J. E*, **34**:98, 2011.

[11] B. Deridda. Random-energy model: Limit of a family of disordered models. *Phys. Rev. Lett.*, **45**:79, 1980.

[12] A. Crisanti and H.J. Sommers. The spherical p-spin interaction spin glass model: The statics. *Z. Phys. B*, **87**:341, 1992.

[13] T. R. Kirkpatrick and P. G. Wolynes. Stable and metastable states in mean-field potts and structural glasses. *Phys. Rev. B*, **36**:8552, 1987.

[14] H. C. Andersen. Molecular dynamics simulations at constant pressure and/or temperature. *J. Chem. Phys.*, **72**:2384, 1980.

[15] M. Parrinello and A. Rahman. Crystal structure and pair potentials: A molecular-dynamics study. *Phys. Rev. Lett.*, **45**:1196, 1980.

[16] M. Parrinello and A. Rahman. Polymorphic transitions in single crystals: A new molecular dynamics method. *J. Appl. Phys.*, **52**:7182, 1981.

[17] J. Wilks and D.S. Betts. *An Introduction to Liquid Helium.* Oxford University Press (USA), 2007.

[18] G. Tammann. Kristallisieren und schmelzen. *Metzger und Wittig, Leipzig*, 1903.

[19] F. H. Stillinger, P. G. Debenedetti, and T. M. Truskett. The kauzmann paradox revisited. *J. Phys. Chem. B*, **105**:11809, 2001.

[20] G.W.H. Rastogi, S. Höhne and A. Keller. Unusual pressure-induced phase behavior in crystalline poly(4-methylpentene-1):? calorimetric and spectroscopic results and further implications. *Macromolecules*, **32**:8897, 1999.

[21] N.J.L. van Ruth and S. Rastogi. Nonlinear changes in specific volume. a route to resolve an entropy crisis. *Macromolecules*, **37**:8191, 2004.

[22] A.L. Greer. Too hot to melt. *Nature*, **404**:134, 2000.

[23] R. Angelini, G. Ruocco, and S. De Panfilis. Reply to comment on phase diagram of a solution undergoing inverse melting. *Phys. Rev. E*, **79**:053502, 2009.

[24] M. Plazanet, M.R. Johnson, and H. P. Trommsdorff. Comment on phase diagram of a solution undergoing inverse melting. *Phys. Rev. E*, **79**:053501, 2009.

[25] R. Angelini, G. Salvi, and G. Ruocco. Shear thickening in a solution undergoing inverse melting. *Phil. Mag.*, **88**:4109, 2008.

[26] R. Angelini, G. Ruocco, and S. De Panfilis. Phase diagram of a solution undergoing inverse melting. *Phys. Rev. E*, **78**:020502, 2008.

[27] C. Ferrari, E. Tombari, C. Salvetti, and G. P. Johari. Composition dependence and the nature of endothermic freezing and exothermic melting. *J. Chem. Phys.*, **126**:124506, 2007.

[28] R. Angelini and G. Ruocco. Viscosity measurements in a solution undergoing inverse melting. *Phil. Mag.*, **87**:553, 2007.

[29] M. Plazanet, M. R. Johnson, R. Schweins, and H.P. Trommsdorff. Inverse freezing in ?-cyclodextrin solutions probed by quasi elastic neutron scattering. *Chem. Phys.*, **331**:35, 2006.

[30] M. Plazanet, M. Dean, M. Merlini, A. Huller, H. Emerich, C. Meneghini, M. R. Johnson, and H. P. Trommsdorff. Crystallization on heating and complex phase behavior of ?-cyclodextrin solutions. *J. Chem. Phys.*, **125**:154504, 2006.

[31] E. Tombari, C. Ferrari, G. Salvetti, and G. P. Johari. Endothermic freezing on heating and exothermic melting on cooling. *J. Chem. Phys.*, **123**:051104, 2005.

[32] M. Plazanet, C. Floare, M. R. Johnson, R. Schweins, and H. P. Trommsdorff. Freezing on heating of liquid solutions. *J. Chem. Phys.*, **121**:5031, 2004.

[33] C. Chevillard and M.A.V. Axelos. Phase separation of aqueous solution of methylcellulose. *Colloid. Polym. Sci.*, **275**:537, 1997.

[34] M. Hirrien and *et al.* Thermogelation of methylcelluloses: new evidence for understanding the gelation mechanism. *Polymer*, **39**:6251, 1998.

[35] A. Haque and E. R. Morris. Thermogelation of methylcellulose. part i: molecular structures and processes. *Carb. Pol.*, **22**:161, 1993.

[36] N. Avraham, B. Khaykovich, Y. Myasoedov, M. Rappaport, H. Shtrikman, D. E. Feldman, T. Tamegai, P. H. Kes, M. Li, Konczykowski6 M., and E. van der Beek, K.and Zeldov. 'inverse' melting of a vortex lattice. *Nature*, **411**:451, 2001.

[37] M. Greiner, O. Mandel, T. Esslinger, T. W. Hänsch, and I. Bloch. Quantum phase transition from a superfluid to a mott insulator in a gas of ultracold atoms. *Nature*, **415**:39, 2002.

[38] B. Donnio, P. Garcia-Vázquez, J.-L. Gallani, D. Guillon, and E. Terazzi. Dendronized ferromagnetic gold nanoparticles self-organized in a thermotropic cubic phase. *Adv. Mater.*, **19**:3534, 2007.

[39] B. Donnio, A. Derory, E. Terazzi, M. Drillon, D. Guillon, and J.-L. Gallani. Very slow high-temperature relaxation of the remnant magnetic moment in 2 nm mesomorphic gold nanoparticles. *Soft Matter*, **6**:965, 2010.

[40] N. Schupper and N. M. Shnerb. Inverse melting and inverse freezing: A spin model. *Phys. Rev. E*, **72**:046107, 2005.

[41] D. Bagchi, A. Kumar, and R. Menon. Ion-induced multiply reentrant liquid-liquid transitions and the nature of criticality in ethanol-water mixture. *J. Chem. Phys.*, **125**:034511, 2006.

[42] H. Verbeek, G. J. Nieuwenhuys, H. Stocker, and J.A. Mydosh. Evidence for a ferromagnet–spin-glass transition in pdfemn. *Phys. Rev. Lett.*, **40**:586, 1978.

[43] Y. Yeshurun, M.B. Salamon, K.V. Rao, and H.S. Chen. Spin-glass-ferromagnetic critical line in amorphous fe-mn alloys. *Phys. Rev. Lett.*, **45**:1366, 1980.

[44] F. H. Stillinger and P. G. Debenedetti. Phase transitions, kauzmann curves, and inverse melting. *Biophys. Chem.*, **105**:211, 2003.

[45] M. R. Feeney., P. G. Debenedetti, and F. H. Stillinger. A statistical mechanical model for inverse melting. *J. Chem. Phys.*, **119**:4582, 2003.

[46] S. Prestipino. Inverse melting in lattice-gas models. *Phys. Rev. E*, **75**:011107, 2007.

[47] A. Crisanti and L. Leuzzi. Stable solution of the simplest spin model for inverse freezing. *Phys. Rev. Lett.*, **95**:08720170, 2005.

[48] M. Sellitto. Inverse freezing in mean-field models of fragile glasses. *Phys. Rev. B*, **73**:180202, 2006.

[49] M. Sellitto and J. Kurchan. Shear-thickening and entropy-driven reentrance. *Phys. Rev. Lett.*, **95**:236001, 2005.

[50] A. Allahverdyan and Petrosyan. Anomalous latent heat in nonequilibrium phase transitions. *Phys. Rev. Lett.*, **96**:065701, 2006.

[51] L. Leuzzi. Spin-glass model for inverse freezing. *Phil. Mag.*, **87**:543, 2006.

[52] G. Parisi. Toward a mean field theory for spin glasses. *Phys. Lett. A*, **73**:203, 1979.

[53] G. Parisi. A sequence of approximated solutions to the s-k model for spin glasses. *J. Phys. A*, **13**:L115, 1980.

[54] G. Parisi. Order parameter for spin-glasses. *Phys. Rev. Lett.*, **50**:1946, 1983.

[55] M. Mèzard, G. Parisi, and M. A. Virasoro. *Spin glass theory and beyond.* Word Scientific, Singapore, 1987.

[56] D. Sherrington and S. Kirkpatrick. Solvable model of a spin-glass. *Phys. Rev. Lett.*, **35**:1792, 1975.

[57] S. F. Edwards and P. W. Anderson. Theory of spin glasses. *J. Phys. F: Metal Phys.*, **5**:965, 1975.

[58] S. Caracciolo and *et al.* Wolff-type embedding algorithms for general non-linear σ-models. *Nucl. Phys. B*, **403**:475, 1993.

[59] M. Palassini and S. Caracciolo. Universal finite-size scaling functions in the 3d ising spin glass. *Phys. Rev. Lett.*, **82**:5128, 1999.

[60] H. G. Ballesteros, A. Cruz, L. A. Fernandez, V. Martin-Mayor, J. Pech, J. J. Ruiz-Lorenzo, A. Tarancon, P. Tellez, C. L. Ullod, and C. Ungiland. Critical behavior of the three-dimensional ising spin glass. *Phys. Rev. B*, **62**:14237, 2000.

[61] C. Itzykson and J.-M. Drouffe. *Statistical Field Theory vol. 2.* Cambridge, UP, 1990.

[62] K. Binder and D. W. Heerman. *Monte Carlo Simulation in Statistical Physics.* Springer, 2002.

[63] W. Kauzmann. The nature of the glassy state and the behavior of liquids at low temperatures. *Chem. Rev.*, **43**:219, 1948.

[64] T. H. Hill. Thermodynamics of Small Systems. Dover, 2002.

[65] R. S. Andrist, H. G. Katzgraber, H. Bombin, and M.A. Martin-Delgadoand. Topological color codes on union jack lattices: a stable implementation of the whole clifford group. *Phys. Rev. A*, **81**:012319, 2010.

[66] A. Crisanti and L. Leuzzi. First-order phase transition and phase coexistence in a spin-glass model. *Phys. Rev. Lett.*, **89**:237104, 2002.

[67] E. K. Riedel and F. J. Wegner. Tricritical exponents and scaling fields. *Phys. Rev. Lett.*, **29**:349, 1972.

[68] J. Zinn-Justin. *Quantum Field Theory and Critical Phenomena.* 1989.

[69] T. Jörg. Critical behavior of the three-dimensional bond-diluted ising spin glass: Finite-size scaling functions and universality. *Phys. Rev. B*, **73**:224431, 2006.

[70] F. Belletti, M. , Cotallo, A. Cruz, L.A. Fernandez, A. Gordillo-Guerrero, M. Guidetti, A. Maiorano, F. Mantovani, E. Marinari, V Martin-Mayor, A. Munoz Sudupe, D. Navarro, G. Parisi, S. Perez-Gaviro, J. J. Ruiz-Lorenzo, S. F. Schifano, D. Sciretti, A. Tarancon, R. Tripiccione, J. L. Velasco, and D. Yllanes. Nonequilibrium spin-glass dynamics from picoseconds to a tenth of a second. *Phys. Rev. Lett.*, **101**:157201, 2008.

[71] M. Hasenbusch, F. P. Toldin, A. Pellissetto, and E. Vicari. Critical behavior of the three-dimensional ±j ising model at the paramagnetic-ferromagnetic transition line. *Phys. Rev. B*, **76**:094402, 2007.

[72] T. Jorg and H. G. Katzgraber. Evidence for universal scaling in the spin-glass phase. *Phys. Rev. Lett.*, **77**:214426, 2008.

[73] M. Hasenbusch, A. Pelissetto, and E. Vicari. The critical behavior of 3d ising spin glass models: universality and scaling corrections. *J. Stat. Mech.*, page L02001, 2008.

[74] H. Katzgraber, M Korner, and A.P. Young. Universality in three-dimensional ising spin glasses: A monte carlo study. *Phys. Rev. B*, **73**:224432, 2006.

[75] E. Marinari, G. Parisi, and J. J. Ruiz-Lorenzo. Phase structure of the three-dimensional edwards-anderson spin glass. *Phys. Rev. B*, **58**:14852, 1998.

[76] A. Crisanti and L. Leuzzi. Thermodynamic properties of a full-replica-symmetry-breaking ising spin glass on lattice gas: The random blume-emery-griffiths-capel model. *Phys. Rev. B*, **70**:014409, 2004.

[77] D. S. Fisher and D. A. Huse. Ordered phase of short-range ising spin-glasses. *Phys. Rev. Lett.*, **56**:1601, 1986.

[78] D. S Fischer and D. A. Huse. Nonequilibrium dynamics of spin glasses. *Phys. Rev. B*, **38**:373, 1998.

[79] F. Krzakala and O. C. Martin. Spin and link overlaps in three-dimensional spin glasses. *Phys. Rev. Lett.*, **85**:3013, 2000.

[80] E. Marinari, G. Parisi, F. Ritort, and J.J. Ruiz-Lorenzo. Off-equilibrium dynamics at very low temperatures in three-dimensional spin glasses. *J. Phys. A*, **33**:2373, 2000.

[81] P. Contucci, C. Giardiná, C. Giberti, G. Parisi, and C. Vernia. Ultrametricity in the edwards-anderson model. *Phys. Rev. Lett.*, **99**:057206, 2007.

[82] L. Leuzzi, G. Parisi, F. Ricci-Tersenghi, and J.J. Ruiz-Lorenzo. Dilute one-dimensional spin glasses with power law decaying interactions. *Phys. Rev. Lett.*, **101**:107203, 2008.

[83] S. Kullback and R. A. Leibler. On information and sufficiency. *Ann. Math. Stat.*, **22**:79, 1951.

[84] L. Leuzzi and T.M. Nieuwenhuizen. *Thermodynamics of the glassy state.* Taylor & Francis, 2007.

[85] A. Cavagna. Supercooled liquids for pedestrians. *Phys. Rep.*, **476**:51, 2009.

[86] W. Kob. Supercooled liquids, the glass transition, and computer simulations. *arXiv:cond-mat/0212344*, 2002.

[87] T. R. Kirkpatrick and D. Thirumalai. Dynamics of the structural glass transition and the p-spin–interaction spin-glass model. *Phys. Rev. Lett.*, **58**:2091, 1987.

[88] A. Crisanti, H. Horner, and H.J. Sommers. The spherical p-spin interaction spin glass model: The dynamics. *Z. Phys. B*, **92**:257, 1993.

[89] W. Götze. *Complex Dynamics of glass forming liquids. A mode-coupling theory.* Oxford University Press (Oxford, UK), 2009.

[90] H. Nishimori and G. Ortiz. *Elements of phase transitions and critical phenomena.* Oxford University Press, 2011.

[91] J.-P. Bouchaud and G. Biroli. On the adam-gibbs-kirkpatrick-thirumalai-wolynes scenario for the viscosity increase in glasses. *J. Chem. Phys.*, **121**:7347, 2004.

[92] G. Biroli, J.-P. Bouchaud, A. Cavagna, T. Grigera, and P. Verrocchio. Thermodynamic signature of growing amorphous order in glass-forming liquids. *Nat. Phys.*, **4**:771, 2007.

[93] F. Sausset and G. Tarjus. Growing static and dynamic length scales in a glass-forming liquid. *Phys. Rev. Lett.*, **104**:065701, 2010.

[94] A. Montanari and G. Semerjian. Rigorous inequalities between length and time scales in glassy systems. *J. Stat. Phys.*, **125**:23, 2006.

[95] L. Berthier and W. Kob. Static point-to-set correlations in glass-forming liquids. *Phys. Rev. E*, **85**:011102, 2012.

[96] A. C. Angell, P. H. Poole, and J. Shao. Glass-forming liquids, anomalous liquids, and polyamorphism in liquids and biopolymers. *Nuovo Cimento D*, **16**:993, 1994.

[97] L. Landau and E. Lifsits. *Teoria dell'elasticità*. Editori Riuniti, 1979.

[98] R. Zwanzig. *Nonequilibrium Statistical Mechanics*. Oxford University Press, 2001.

[99] J. P. Hansen and I. R. McDonald. *Theory of simple liquids*. Academic Press, 2006.

[100] D. Reichman and P. Charbonneau. Mode-coupling theory. *J. Stat. Mech.*, **P05013**:P05013, 2005.

[101] H. Mori. Transport, collective motion, and brownian motion. *Prog. Theor. Phys.*, **33**:423, 1965.

[102] S. P. Das. Mode-coupling theory and the glass transition in supercooled liquids. *Rev. Mod. Phys.*, **76**:785, 2004.

[103] .E. Leutheusser. Dynamical model of the liquid-glass transition. *Phys. Rev. A*, **29**:2765, 1984.

[104] M. Talagrand. The parisi formula. *Ann. of Math.*, **163**:221, 2006.

[105] F. Guerra and F. L. Tonielli. The thermodynamic limit in mean field spin glass models. *Comm. Math. Phys.*, **230**:71, 2002.

[106] F. Guerra. Broken replica symmetry bounds in the mean field spin glass model. *Comm. Math. Phys.*, **233**:1, 2003.

[107] F. Guerra. Spin glasses. *arXiv:0507581*, 2008.

[108] A. Crisanti and L. Leuzzi. Amorphous-amorphous transition and the two-step replica symmetry breaking phase. *Phys. Rev. B*, **76**:184417, 2007.

[109] P.C. Martin, E.D. Siggia, and H.A. Rose. Statistical dynamics of classical systems. *Phys. Rev. A*, **8**:423–437, 1973.

[110] C. De Dominicis. Toward a mean field theory of spin glasses: The tap route revisited. *Physics Reports*, **67**:37 – 46, 1980.

[111] T. R. Kirkpatrick and D. Thirumalai. p-spin-interaction spin-glass models: Connections with the structural glass problem. *Phys. Rev. B*, **36**:5388, 1987.

[112] H. Sompolinsky. Time-dependent order parameters in spin-glasses. *Phys. Rev. Lett.*, **47**:935, 1981.

[113] T. Castellani and A. Cavagna. Spin-glass theory for pedestrians. *J. Stat. Mech.*, page P05012, 2005.

[114] M. Fuchs, W. G. Götze, I. Hofacker, and A. Latz. Comments on the α-peak shapes for relaxation in supercooled liquids. *J. Phys. Condens. Matter*, **3**:5047, 1991.

[115] G. Johari and M. Goldstein. Viscous liquids and the glass transition. ii. secondary relaxations in glasses of rigid molecules. *J. Chem. Phys.*, **53**:2372, 1970.

[116] G. Johari and M. Goldstein. Molecular mobility in simple glasses. *J. Phys. Chem.*, **74**:2034, 1970.

[117] G. Johari and M. Goldstein. Viscous liquids and the glass transition. iii. secondary relaxations in aliphatic alcohols and other nonrigid molecules. *J. Chem. Phys.*, **55**:4245, 1971.

[118] J. Wong and C. Agnell. Glass: structure by spectrocopy. 1974.

[119] S. Adichtchev, T. Blochowicz, C. Gainaru, V. N. Novikov, E. A. Rossler, and C. Tschirwitz. Evolution of the dynamic susceptibility of simple glass formers in the strongly supercooled regime. *Journal of Physics: Condensed Matter*, **15**:S835, 2003.

[120] T. Blochowicz, C. Tschirwitz, S. Benkhof, and E.A. Rössler. Susceptibility functions for slow relaxation processes in supercooled liquids and the search for universal relaxation patterns. *J. Chem. Phys.*, **118**:7544, 2003.

[121] S. Adichtchev, T. Blochowicz, C. Tschirwitz, V. N. Novikov, and E. A. Rossler. Reexamination of the evolution of the dynamic susceptibility of the glass former glycerol. *Phys. Rev. E*, **68**:011504, 2003.

[122] K. L. Ngai, P. Lunkenheimer, C. Leon, U. Schneider, L. A. Brand, and A. R. Loidl. Nature and properties of the johari–goldstein β-relaxation in the equilibrium liquid state of a class of glass-formers. *J. Chem. Phys.*, **115**:1405, 2001.

[123] K.L. Ngai and M. Paluch. Classification of secondary relaxation in glass-formers based on dynamic properties. *J. Chem. Phys.*, **120**:857, 2004.

[124] H.Z. Cummins. Dynamics of supercooled liquids: excess wings, β peaks, and rotation–translation coupling. *J. Phys.: Condens. Matter*, **17**:1457, 2005.

[125] W. Götze and M. Sperl. Nearly logarithmic decay of correlations in glass-forming liquids. *Phys. Rev. Lett.*, **92**:105701, 2004.

[126] J.D. Stevenson and P.G. Wolynes. A universal origin for secondary relaxations in supercooled liquids and structural glasses. *Nature Physics*, **6**:62, 2010.

[127] J. Wiedersich, T. Blochowicz, S. Benkhof, A. Kudlik, N.V. Surotsev, C. Tschirwitz, V.N. Novikov, and E. Rössler. Fast and slow relaxation processes in glasses. *J. Phys.: Condens. Matter*, **11**:A147, 1999.

[128] A. Kudlik, C. Tschirwitz, T. Blochowicz, S. Benkhof, and E. Rössler. Slow secondary relaxation in simple glass formers. *J. Non-Cryst. Solids*, **235-237**:406, 1999.

[129] R. Nozaki, D. Suzuki, S. Ozawa, and Y Shiozaki. The ? and the ? relaxation processes in supercooled sorbitol. *J. Non-Cryst. Solids*, **235-237**:393, 1998.

[130] P. Chaudhuri, L. Berthier, P. I. Hurtado, and W. Kob. When gel and glass meet: A mechanism for multistep relaxation. *Phys. Rev. E*, **81**:040502, 2010.

[131] P. Lunkenheimer, L. C. Pardo, M. Kohler, and A. R. Loidl. Broadband dielectric spectroscopy on benzophenone: α relaxation, β relaxation, and mode coupling theory. *Phys. Rev. E*, **77**:031506, 2008.

[132] V. Krakoviack. Comment on spherical 2+p spin-glass model: An analytically solvable model with a glass-to-glass transition. *Phys. Rev. B*, **76**:136401, 2007.

[133] A. Crisanti and L. Leuzzi. Reply to comment on spherical 2+p spin-glass model: An analytically solvable model with a glass-to-glass transition. *Phys. Rev. B*, **76**:136402, 2007.

[134] M. J. Greenall and M. E. Cates. Crossover behavior and multistep relaxation in a schematic model of the cut-off glass transition. *Phys. Rev. E*, **75**:051503, 2007.

[135] A. Crisanti and L. Leuzzi. Spherical 2+p spin-glass model: An exactly solvable model for glass to spin-glass transition. *Phys. Rev. Lett.*, **93**:217203, 2004.

[136] A. Crisanti and L. Leuzzi. Spherical 2+p spin-glass model: An analytically solvable model with a glass-to-glass transition. *Phys. Rev. B*, **73**:014412, 2006.

[137] T. R. Kirkpatrick, D. Thirumalai, and P. G. Wolynes. Scaling concepts for the dynamics of viscous liquids near an ideal glassy state. *Phys. Rev. A*, **40**:1045, 1989.

[138] L. Leuzzi. Static and dynamic glass-glass transitions: a mean-field study. *Philos. Mag.*, **88**:4015–4023, 2008.

[139] H. Sompolinsky and A. Zippelius. Relaxational dynamics of the edwards-anderson model and the mean-field theory of spin-glasses. *Phys. Rev. B*, **25**:6860, 1982.

[140] A. Crisanti. Long time limit of equilibrium glassy dynamics and replica calculation. *Nuclear Physics B*, **796**:425–456, 2008.

[141] J.-P. Bouchaud, J. Cugliandolo, L.F. an Kurchan, and M. Mézard. Mode-coupling approximations, glass theory and disordered systems. *Physica A*, **226**:243, 1996.

[142] E. Donth. *The Glass Transition.* Springer (Berlin), 2001.

[143] K. L. Ngai. An extended coupling model description of the evolution of dynamics with time in supercooled liquids and ionic conductors. *J. Phys. and Condens. Matter*, **15**:S1107–S1125, 2003.

[144] K.L. Ngai and S. Capaccioli. Relation between the activation energy of the johari-goldstein β relaxation and tg of glass formers. *Phys. Rev. E*, **69**:031501, 2004.

[145] R. Kohlrausch. Theorie des elektrischen ruckstandes in der leidner flasche. *Ann. Phys. (Leipzig)*, **12**:393, 1847.

[146] G. Williams and D.C. Watts. Non-symmetrical dielectric relaxation behaviour arising from a simple empirical decay function. *Trans. Faraday Soc.*, **66**:80, 1970.

[147] G. Johari. Intrinsic mobility of molecular glasses. *J. Chem. Phys.*, **58**:1766, 1973.

[148] S. Franz and G. Parisi. Phase diagram of coupled glassy systems: A mean-field study. *Phys. Rev. Lett.*, **79**:2486, 1997.

[149] M. Marchi and M. Procacci. Coordinates scaling and multiple time step algorithms for simulation of solvated proteins in the npt ensemble. *J. Chem. Phys.*, **109**:5194, 1998.

[150] A. Di Carlo, M. Minozzi, M. Paoluzzi, and M Ribezzi-Crivellari. *unpublished.*

[151] D. Frenkel and B. Smit. *Understanding molecular simulation.* Academic Press, INC, 2002.

[152] S. Nosé. A unified formulation of the constant temperature molecular dynamics methods. *J. Chem. Phys.*, **81**:511, 1984.

[153] W. G. Hoover. Canonical dynamics: Equilibrium phase-space distributions. *Phys. Rev. A*, **31**:1695, 1985.

[154] M. E. Tuckerman, B.J. Berne, and G.J. Martyna. Reversible multiple time scale molecular dynamics. *J. Chem. Phys.*, **97**:1990, 1992.

[155] H. F. Trotter. On the product of semi-groups of operators. *Proc. Math. Soc.*, **10**:545, 1959.

[156] H. de Raedt and B. de Raedt. Applications of the generalized trotter formula. *Phys. Rev. A*, **28**:3575, 1983.

[157] H. Yoshida. Construction of higher order symplectic integrators. *Phys. Rev. A*, **150**:262, 1990.

[158] W. C. Swope, H. C. Andersen, P. H. Berens, and K. R. Wilson. A computer simulation method for the calculation of equilibrium constants for the formation of physical clusters of molecules: Application to small water clusters. *J. Chem. Phys.*, **76**:637, 1982.

[159] M. E. Gurtin. *An introduction to Continuum Mechanics*. Academic Press, INC, 1981.

[160] N. C. Admal and E. B. Tadmor. A unified interpretation of stress in molecular systems. *J. Elast.*, **100**:63, 2010.

[161] J. H. Irving and J. G. Kirkwood. The statistical mechanical theory of transport processes. iv. the equations of hydrodynamics. *J. Chem. Phys.*, **18**:817, 1950.

[162] S. Morante, C. G. Rossi, and M. Testa. The stress tensor of a molecular system: An exercise in statistical mechanics. *J. Chem. Phys.*, **123**:034101, 2006.

[163] C. G. Rossi and M. Testa. The stress tensor in thermodynamics and statistical mechanics. *arXiv:0904.2283*, 2009.

[164] D. J. Tildesley, J. P. R. B. Walton, and J. S. Rowlinson. The pressure tensor at the planar surface of a liquid. *Mol. Phys.*, **48**:1357, 1983.

[165] D. J. Tildesley, J. P. R. B. Walton, and J. S. Rowlinson. erratum. *Mol. Phys.*, **58**:1013, 1986.

[166] J. J. Erpenbeck. Einstein-kubo-helfand and mcquarrie relations for transport coefficients. *Phys. Rev. E*, **51**:4296, 1995.

[167] D. H. Tsai. The virial theorem and stress calculation in molecular dynamics. *J. Chem. Phys.*, **70**:1375, 1979.

[168] R. G. Winkler, H. Morawitz, and D. Y. Toon. Novel molecular dynamics simulations at constant pressure. *Mol. Phys.*, **75**:669, 1992.

[169] P. Podio-Guidugli. On (andersen–)parrinello–rahman molecular dynamics, the related metadynamics, and the use of the cauchy–born rule. *J. Elast.*, **100**:145, 2010.